

DISS. ETH NO. 17195

**PHYSICAL AND CHEMICAL FUNCTIONALIZATION OF  
POLYMERS**

A dissertation submitted to

**ETH ZURICH**

for the degree of

**Doctor of Sciences**

presented by

**STEFAN LOHER**

Dipl. Masch.-Ing. ETH

born 10.07.1979

citizen of Oberriet-Montlingen SG, Switzerland

Accepted on the recommendation of

Prof. Dr. W. J. Stark, examiner  
Prof. Dr. M. Fussenegger, co-examiner

2007



## Acknowledgements

I would like to express my deepest gratitude to Prof. Wendelin J. Stark who supervised my PhD and contributed much to the success with his continuous motivation and encouragement. The valuable education I enjoyed has not only been limited to develop “scientific skills” but also to improve in soft skills which I truly appreciate.

Many thanks are addressed to my co-examiner Prof. Martin Fussenegger for his interest in my work.

This project has been carried out in strong collaboration with Perlen Converting AG (PECO), a Swiss film finishing company. Special thanks are addressed to Ulrich Frauchiger (PECO), Wolfgang Grimm (PECO), and Dr. Stefan Bokorny (PECO) for making the project possible and for giving me the opportunity to work within this very interesting field of coating technology. Their valuable comments and continuous encouragement have been very conducive to the progress of the project. I also would like to cordially thank Tobias Maienfisch (PECO) for the help in product development and the subsequent implementation into lab-scale and production-scale processes at Perlen Converting AG. I am also very grateful for the help from all the involved employees at Perlen Converting AG, who were on site during large-scale production. Further thank is addressed to Dr. Moritz Braun (Zeochem AG), Dr. Armin Pfenninger (Zeochem AG), Dr. Sonja Odolo-Hitz (Zeochem AG), Martina Christiansen (PECO), Stephan Rätzer (PECO) and Dr. Hartmut Weyda (Zeochem AG) for their valuable comments and the fruitful discussions.

This work would not have been possible without the contributions by Valentine Reboul, Stephanie Streather, Roland Fuhrer, Oliver Schneider, and Norman Luechinger within different “Projekt-” and “Masterarbeiten” or as a Hifsassistent/In. A special thank belongs to my colleagues Robert, Neil, Tobias, Ludwig, Samuel, Evangelos, and Oliver in Prof. Stark’s group. I experienced that the work mentality is strongly influenced by the work environment. All these people have greatly contributed to the optimal premises and often helped me with a useful piece of advice.

Many thanks go to the employees of the mechanical and electronic workshop of the Institute for Chemical- and Bioengineering (ETH Zurich) for their inventive solutions and their excellent work building up new equipment.

Special thank goes to Marc Simonet (Institute of Polymer Technology, ETH Zurich) for help in polymer processing and Dr. Frank Krumeich (Laboratory of Inorganic Chemistry, ETH Zurich) for electron microscopy.

I cordially thank Prof. H. P. Merkle and Dr. Lorenz Uebersax (Institute of Pharmaceutical Sciences, ETH Zurich) for introducing me into the fundamentals of cell biology and for their help in cell culture experiments.

I would like to thank Dr. Patrick R. Schmidlin (Clinic of Preventive Dentistry, Periodontology and Cariology, University of Zurich) and Dr. Franz Weber (Department of Craniomaxillofacial Surgery, University of Zurich) for the interesting collaboration in the field of biomaterials in dentistry and for the vivid and helpful discussions.

I am deeply grateful for moral support from my family and friends.

Finally, I would like to acknowledge financial support by the Commission for Technology and Innovation (CTI project no. 7021.2).

## Contents

Acknowledgements	3
<b>Contents</b>	<b>5</b>
<b>Zusammenfassung</b>	<b>9</b>
<b>Summary</b>	<b>15</b>
<b>1. Functional polymers: The development of novel physical and chemical properties</b>	<b>21</b>
1.1 Introduction	21
1.2. Physical functionalization of polymers	22
1.3. Application of polymers as foils	23
1.4. Low adhesion coatings	23
1.5. Introducing catalytic functionality in polymers	24
1.6. The functionalization of polymeric biomaterials	25
1.7. References	25
<b>2. Rapid production of micro-patterned surfaces using a fluid dynamical instability</b>	<b>29</b>
2.1. Introduction	30
2.2. Experimental	35
2.2.1. Materials and surface coating method	35
2.2.2. Characterization methods	35
2.3 Results and Discussions	36
2.3.1. Rheology of the coating resin	36
2.3.2. Roll coating of a Herschel-Bulkley fluid	39
2.3.3. Adhesion properties	42
2.4. Conclusions	43
2.5. Acknowledgements	44
2.6. References	44
<b>3. Improved degradation and bioactivity of amorphous aerosol derived tricalcium phosphate nanoparticles in poly(lactide-co-glycolide)</b>	<b>47</b>
3.1. Introduction	48
3.2. Materials and methods	49
3.2.1. Preparation of PLGA/ATCP composites	49
3.2.2. Characterization of ATCP nanoparticles and PLGA/ATCP composites	50
3.2.3. Degradation protocol	51
3.2.4. Statistical methods	51
3.3. Results and Discussions	52

3.3.1. Tricalcium phosphate nanoparticle filler properties	52
3.3.2. Mechanical properties of PLGA/ATCP nanocomposites	53
3.3.3. Mass loss and water uptake	54
3.3.4. Surface properties	56
3.3.5. Thermal analysis	56
3.3.6. Surface composition of PLGA/ATCP composites	58
3.4. Conclusions	61
3.5. Acknowledgements	61
3.6. References	61
<b>4. Cotton wool-like nanocomposite biomaterials: In vitro biocompatibility and osteogenic differentiation of human mesenchymal stem cells</b>	<b>65</b>
4.1. Introduction	66
4.2. Materials and Methods	67
4.2.1. Preparation of ATCP particles	67
4.2.2. Particle characterization	68
4.2.3. Scaffold preparation	68
4.2.4. Scaffold characterization	69
4.2.5. Cell culture	69
4.2.6. Confocal laser scanning microscopy	70
4.2.7. Alkaline phosphatase activity, osteocalcin and DNA content	71
4.2.8. Statistical analysis	71
4.3. Results	71
4.3.1. Amorphous tricalcium phosphate nanoparticles	71
4.3.2. PLGA/ATCP nanocomposite scaffolds	72
4.3.3. Simulation of bone defect repair	75
4.3.4. Proliferation and osteogenic differentiation of hMSC	75
4.4. Discussion	77
4.5. Conclusions	79
4.6. Acknowledgements	79
4.7. References	79
<b>5. Homogeneous, catalytic absorption of ethene by a modified Wacker process incorporated into a polymeric coating</b>	<b>83</b>
5.1. Introduction	84
5.1.1. Passive methods	85
5.1.2. Active methods	85
5.2. Materials and Methods	87
5.2.1. Catalytic solution and film preparation	87
5.2.2. Characterization methods	88
5.3. Results and Discussions	88
5.3.1. Activity of the aqueous catalytic solution	88
5.3.2. Activity of the film material	91

---

5.4. Conclusions	95
5.5. Acknowledgements	96
5.6. References	96
<b>6. Silver-doped tricalcium phosphate nanoparticles as highly efficient antimicrobial agents in hydrophobic polymers</b>	<b>99</b>
6.1. Introduction	100
6.1.1. Release systems using ionic silver	100
6.1.2. Release systems using metallic silver	101
6.1.2.1. Materials having no carrier	101
6.1.2.2. Materials with inorganic carrier	101
6.2. Materials and Methods	104
6.2.1. Polymeric coating preparation	104
6.2.2. Characterization methods	105
6.3. Results and Discussion	106
6.3.1. Powder characteristics	106
6.3.2. Film characteristics	112
6.4. Conclusions	117
6.5. Acknowledgements	117
6.6. References	118
<b>7. Research Recommendations &amp; Outlook</b>	<b>119</b>
7.1. Further application fields of micro-structured coatings	119
7.2. Flame-made calcium phosphates for the preparation of polymeric nanocomposite biomaterials	121
<b>Curriculum Vitae</b>	<b>123</b>





## Zusammenfassung

Im Rahmen der vorliegenden Doktorarbeit soll die Implementierung von funktionellen Nanomaterialien in herkömmliche Kunststoffanwendungen untersucht werden. Diese Funktionalisierung erlaubt es, die physikalischen und chemischen Eigenschaften ausgewählter Nanomaterialien mit der einfachen Verarbeitung moderner Polymere zu kombinieren. Ein Teil dieser Arbeit geschah in enger Zusammenarbeit mit einem Industriepartner, Perlen Converting AG. Durch dieses Zusammenspiel konnte erfolgreich die Markteinführung eines der entwickelten Produkte hervorgebracht werden. Der biomedizinische Teil dieser Arbeit basiert auf der Zusammenarbeit mit zwei Gruppen des Universitätsspitals Zürich und dem Institut für Pharmazie sowie dem Institute für Polymertechnologie, beide der ETH Zürich angehörend. Die Arbeit ist aufgeteilt in sechs Kapitel, wobei mit einem allgemeinen Teil über die Funktionalisierung von Polymeren in das Thema eingeführt wird. Es folgen fünf Kapitel, die im Speziellen die physikalische und chemische Funktionalisierung von Kunststoffen mittels ausgewählten Nanomaterialien thematisieren. Die hier erläuterte Arbeit macht sich die gewonnenen Erkenntnisse aus der Diplomarbeit des Autors (Loher S et al., Chem. Mater., (2004), 17, 36-42) zu Nutzen.

Kapitel 1 gibt einen Überblick auf die heutigen Forschungsbestrebungen im Feld der Funktionalisierung von Kunststoffen. Das Augenmerk wurde vor allem auf die Verwendung spezieller Füllstoffe in Partikelform gerichtet und weniger auf den Ansatz des Polymerdesigns mittels organischer Chemie.

Kapitel 2 beinhaltet eine Untersuchung über den Gebrauch von kommerziellen Siliziumdioxid-Agglomeraten als Rheologiemodifikator zur direkten Appli einer strukturierten Beschichtung in einem Einzelschritt-Prozess. In diesem Kapitel wird stark auf die Fluidodynamik eingegangen und zugleich aufgezeigt, welches Potential die integrierte Produktentwicklung entfalten kann, bei der Lösung von gegenwärtigen Schwierigkeiten in der Produktion von Grossmengen an strukturierten Beschichtungen. Im hier diskutierten Fall wurde ein konventionelles Rollenbeschichtungsverfahren angewendet zur kontinuierlichen Applikation einer strukturierten Oberfläche auf ein Kunststofffilmsubstrat. Eine hohe

Maschinengeschwindigkeit (bis zu  $120 \text{ m min}^{-1}$ ) ermöglichte die grossflächige und kostengünstige Durchführung, was diesen Prozess äusserst attraktiv macht für die Serienproduktion. Die Oberflächen-Strukturierung konnte von 100 Mikrometer bis 2 Millimeter variiert werden. Eine detaillierte Analyse des Prozesses zeigte, dass die Strukturierung auf einer rheologischen Instabilität basiert, welche auch unter dem Namen "viscous fingering" bekannt ist. Hervorgerufen wird dieses Phänomen durch die hohen Scherkräfte beim Rollenbeschichtungsverfahren. Kommerzielles, pyrogenes Siliziumdioxid wurde einem flüssigen, ursprünglich Newtonschen Poly(Dimethylsiloxan)-Oligomer beigemischt, was in einer Bingham'schen Flüssigkeit mit strukturviskosem Verhalten (Herschel-Bulkley Flüssigkeit) resultierte. Somit blieb die noch unpolymersierte strukturierte Beschichtung nach dem Rollenauftrag erhalten, bis diese in einem späteren Prozessschritt thermisch ausgehärtet wurde. Die regelmässige Strukturierung wurde durch den gemittelten Rillenabstand charakterisiert und konnte durch die Anpassung der Rollengeschwindigkeit und der Rollenspaltbreite im Bereich von Mikro- bis Millimetern kontrolliert eingestellt werden. Durch das Messen der Haftkraft von verschiedenen Haftklebebändern, konnten die Hafteigenschaften der strukturierten Oberfläche mit denen der glatten Beschichtung verglichen werden. Für ein aggressives Gummi-basierendes Haftklebeband wurde eine 8-fache Verminderung der Haftkraft von strukturierten Beschichtungen im Vergleich zu der planen Referenz-Beschichtung festgestellt. Solche Beschichtungen mit stark reduzierten Hafteigenschaften finden zurzeit Anwendung in der Verpackungs- und Lebensmittelverarbeitungs-Industrie sowie für die Einkleidung von sanitären Anlagen. Die Produktion wurde vollständig auf den Grossmassstab übertragen und die Beschichtungen sind erwerbbar auf dem freien Markt.

Kapitel 3 beinhaltet ein Beispiel zur chemischen Funktionalisierung eines Kunststoffes durch das Einbringen eines biologisch abbaubaren Polymerfüllstoffes. Die Einführung von bioabbaubaren Kunststoffen im Grossmassstab (z. B. Frankreich verbietet den Gebrauch von klassischen Kunststoffbeuteln ab 2010), zieht die dringende Verwendung von Füllstoffen mit ähnlicher Abbaubarkeit nach sich. Als erstes wurde ein zurzeit industriell genutzter Flammensynthese-Prozess zur Herstellung von Siliziumdioxid-Füllmaterialien so modifiziert, dass bisher unzugängliche Stoffe wie amorphe Trikalziumphosphat-Nanopartikel (ATCP) und

Nano-Kalk verfügbar wurden. Durch die Verwendung eines ähnlichen Produktionsprozesses resultierte eine gleichartige Morphologie der bioabbaubaren Füllstoffe wie bei traditionell verwendeten Siliziumdioxiden. Das Einbringen solcher hoch agglomerierten ATCP-Nanopartikel in ein gebräuchliches, bioabbaubares Poly(Laktid-Co-Glykolid) (PLGA) wurde auf die resultierenden mechanischen Eigenschaften sowie die *in vitro* Biodegradation und Biomineralisation untersucht. PLGA-Filme mit einem Partikelgehalt von 0 bis 30 Gew.-% wurden mittels eines Lösungsmittel-Gussverfahrens hergestellt. Um zu beweisen, dass sowohl der Füllstoff wie auch der Kunststoff, biologisch abbaubar sind, wurde der Abbau über 42 Tage bei 37 °C unter sterilen Bedingungen in künstlicher Körperflüssigkeit quantitativ verfolgt. Dabei wurden Messungen mittels Ramanspektroskopie, Rasterelektronenmikroskopie (REM), thermische Analyse und Zugversuche durchgeführt. Die Einbindung von Nanopartikeln in die PLGA-Matrix hatte eine geringfügige Erhöhung des E-Moduls von bis zu 30% im Vergleich zum reinen Polymer zur Folge. Darüber hinaus zeigten die mit Nanopartikeln beladenen Filme eine signifikant erhöhte Abnahme der Polymermasse über die Abbaupzeit. Die Untersuchung mittels REM liess auf einen Abbau der PLGA-Matrix durch Korrosion schliessen, welche durch das vorhandene nanopartikuläre Kalziumphosphat unterstützt wurde. Die Ablagerung von ca. 10 nm grossen Hydroxyapatit-Kristallen wurde vorwiegend bei ATCP-haltigen Filmen beobachtet und konnte mittels Ramanspektroskopie und Röntgendiffraktometrie nachgewiesen werden. Die Kombination von erhöhter Hydroxyapatit-Bildung und erleichtertem Polymerabbau bringt eine Verwendung der ATCP-Kunststoff-Nanokomposite als nicht-tragende Knochenersatzmaterialien in Vorschlag.

In Kapitel 4 wird der ATCP-PLGA Komposit in eine klinisch anwendbare Form gebracht. Das Elektrosplein-Verfahren wurde verwendet um flexible, wolle-artige Nanokomposite zu produzieren. Im Vergleich zu konventionellen, granulösen Knochenersatzmaterialien ergeben sich ein einfaches Portionieren sowie die erleichterte Anwendung in komplexen Knochendefekten und die vorteilhafte Entfernung im Falle einer Fehlapplikation. Somit kann der Chirurg wesentlich an Zeit im Operationssaal sparen was sich positiv auf die Operationskosten für den Patienten auswirkt. Diese Hypothese wurde *in vitro* sowie in einer ersten Tierstudie am Universitätsspital Zürich getestet.

Eine Zellkulturstudie mit menschlichen, mesenchymalen Stammzellen (hMSC) ermöglichte es, die potentielle Anwendung des Materials als Knochenersatz zu evaluieren. ATCP-Pulver wurde mittels Flammenspraysynthese hergestellt was in Primärpartikelgrößen von 20-80 nm resultierte. Daraus wurden mittels Elektrosponning, Scaffolds bestehend aus PLGA und ATCP mit einem Nanopartikel-Gehalt von 0-40 Gew.-% angefertigt. Drei verschiedene Scaffolds wurden mit hMSC besiedelt. Eines bestand aus reinem PLGA, die anderen zwei waren mit 40 Gew.-% Nanopartikel beladen. Davon wurde eines ohne Behandlung verwendet und eines wurde vor dem Experiment 15 Stunden in künstliche Körperflüssigkeit getaucht, um einen allfälligen Kalziumionen-Ausbruch beim Besiedeln mit Zellen zu verhindern. Die Proben wurden anschliessend unter osteogenem Medium inkubiert und nach 4 Wochen wurden die Proliferation sowie die osteogene Differenzierung der Zellen bestimmt. Aus den konfokalen Laserrastermikroskopie-Bildern war ersichtlich, dass die Zellen bei allen Proben ordnungsgemäss an den Fasern anhafteten und keine ungewöhnliche morphologische Änderung der Zellstruktur eintrat. Es wurden bei der fluorometrischen Quantifizierung der dsDNA sowie bei der Alkaline Phosphatase-Aktivität keine statistisch signifikanten Unterschiede unter den Proben festgestellt. Daraus wurde geschlossen, dass durch die implementierten Nanopartikel keine akuten zytotoxischen Effekte hervorgerufen wurden. Der Osteocalcin-Gehalt war für alle Scaffolds zwischen 0.12 und 0.19 ng pro ng DNA, was die osteogene Differenzierung bestätigte.

Kapitel 5 beschreibt die komplexe Inkorporierung eines katalytischen Prozesses in eine Kunststoffbeschichtung zur Oxidation von Ethylen. Eine wässrige Poly(Styrolsulfonsäure)-Lösung und ein katalytisches System bestehend aus Palladiumchlorid (Katalysator) und einem Heteropolyanion (Co-Katalysator), genauer  $\text{Na}_3\text{H}_3\text{PMo}_9\text{V}_3\text{O}_{40}$ , wurden mittels eines Lösungsmittel-Beschichtungsverfahrens auf einen Polyester-Träger aufgebracht und unter Umgebungsbedingungen ausgehärtet. Verschiedene "Katalysator zu Co-Katalysator" Verhältnisse wurden auf ihre Leistung bei der Umsetzung von tiefen Ethylenkonzentrationen (100 ppm) über eine Zeit von drei Wochen und total sechs Beschickungen geprüft. Der Palladium-Gehalt in der Beschichtung wurde aus ökonomischen Gründen konstant tief, bei 5 mg/m<sup>2</sup> gehalten. Der Ethylenumsatz wurde mittels Gaschromatographie unter Verwendung eines Flammenionisationsdetektors (GC-FID) für bis

zu 200 Stunden verfolgt und aufgezeichnet. Während die katalytischen Beschichtungen zu Beginn eine Ethylenkonzentration von  $<5$  ppm innert einem Tag erreichten, ging die Aktivität nach 3 Wochen Testzeit und sechs Beschickungen mit 100 ppm Ethylen merklich zurück. Bei der sechsten Beschickung dauerte die Dezymierung auf  $<5$  ppm etwa 5 Tage. Das Verhältnis von "Katalysator zu Co-Katalysator" hatte nur geringen Einfluss auf die Aktivität. Zur Verhinderung von Migration der katalytischen Substanzen wurde in einem zusätzlichen Experiment eine Schutzbeschichtung aus Polystyrol auf die katalytische Schicht aufgetragen. Die geschützte Folie hatte nach einem Tag etwa 50 ppm Ethylen umgesetzt und nach 60 Stunden waren drei Viertel der anfänglich vorhandenen Ethylenkonzentration absorbiert. Aus den viel versprechenden Umsatzgeschwindigkeiten kann eine Anwendung der aktiven Folien zur Verpackung von ethylen-empfindlichen Frischprodukten wie Früchte, Gemüse oder Schnittblumen suggeriert werden.

In Kapitel 6 wird die Verwendung von Silber-dotiertem Trikalziumphosphat als antimikrobieller Zusatz in hydrophoben Polymerbeschichtungen evaluiert. Reines Trikalziumphosphat (TCP), Silber-dotiertes Trikalziumphosphat (Ag-TCP) mit Silbergehalten von 1 bis 10 Gew.-% und Silber-dotiertes Siliziumdioxid (Ag-SiO<sub>2</sub>) wurden mittels Flammenspraysynthese hergestellt. Die Eigenschaften der Pulver wurden mit kommerziell erhältlichen, antimikrobiellen Substanzen verglichen. Die Morphologie und Phasenzusammensetzung der verschiedenen Pulver wurde mittels Elektronenmikroskopie, Stickstoffadsorption, Röntgen-Zentrifugation und Röntgendiffraktometrie untersucht. Alle Flammen-synthetisierten Pulver und eines der kommerziellen Produkte bestanden aus einem nanopartikulären Trägermaterial auf dem Silberpartikel in der Grösse von  $<10$  nm fein dispergiert vorlagen. Die heutzutage am Meisten verwendete Substanz hingegen bestand aus vergleichbar riesigen,  $>1$   $\mu\text{m}$  grossen Partikeln auf denen kein metallisches Silber detektiert wurde. Zur Bestimmung der antimikrobiellen Wirkung wurden die Pulver in eine hydrophobe Silikon-Beschichtung eingearbeitet und folglich nach den standardisierten Methoden ASTM E2149-01 und ASTM E2180-01 untersucht. Alle Beschichtungen mit inkorporierten 20 Gew.-% Ag-TCP zeigten eine starke, 4- bis 6-log Reduktion von gramnegativen *E.coli* Bakterien in beiden Tests. Beschichtungen, die Ag-SiO<sub>2</sub> enthielten, wiesen in den gleichen Tests eine 2- bis 4-log Reduktion auf und waren gesamtheitlich betrachtet um mindestens einen Faktor 10

weniger wirksam als entsprechende Beschichtungen mit Ag-TCP. In einem direkten Vergleich von Ag-TCP Beschichtungen und beiden kommerziellen Produkten (HeiQ-Silver und Ionpure40) überragte die Wirksamkeit des phosphathaltigen Trägermaterials um einen Faktor 100 bis 5000. Darüber hinaus zeigte die Ag-TCP Beschichtung hohe Wirkung (4- bis 6-log Reduktion) gegen *P.aeruginosa* und *C.albicans*. Diese aussergewöhnliche antimikrobielle Aktivität schlägt eine Verwendung solcher Materialien in der Verpackung von Lebensmitteln und Pharmazeutika sowie für die Beschichtung von Oberflächen in sanitären Anlagen und Krankenhäusern vor.

In Kapitel 7 wird ein Ausblick in zukünftige Forschungsrichtungen aufgezeigt wobei Hauptgewicht auf die Anwendung der diskutierten Materialien gelegt wird.

## Summary

The scope of the present work is to implement functional nanomaterials into existing polymer applications. This functionalization allows a combination of the physical and chemical properties of specific nanomaterials with the easy processability of modern polymers. Part of this work was done in strong collaboration with an industrial partner, the Perlen Converting AG and resulted in the market introduction of a product developed within this thesis. The more biomedical part of this thesis has been made in collaborations with two medical groups from the University Hospital Zurich, the Institute of Pharmaceutical Sciences and the Institute of Polymer Technology both at ETHZ. The thesis is structured in six chapters starting with a general overview on the functionalization of polymers followed by five chapters discussing physical or chemical functionalization of polymers by the introduction of specific nanomaterials. The present work strongly uses knowledge on the preparation of flame-made nanoparticles arising from the Diploma thesis of the author (Loher S et al., *Chem. Mater.*, (2004), **17**, 36-42).

Chapter 1 gives an overview of the present research efforts on the functionalization of polymers. Emphasis was placed on the incorporation of special filler materials rather than on a design approach using organic chemistry to modify the polymer molecules themselves.

Chapter 2 investigates the use of specific silica agglomerates as rheological modifiers to directly prepare structured coatings in a single-step process. This chapter makes strong use of fluid dynamics and illustrates how an integrated process development can provide an elegant solution to the presently difficult large scale manufacturing of structured coatings. More specifically, conventional roll coating has been used to continuously apply a structured surface on a polymeric film substrate. High line speed (up to 120 m min<sup>-1</sup>) allowed for large area, low-cost structuring making it most attractive for series production and afforded patterning in the range of 100 micrometers to 2 millimeters. A detailed analysis showed that the process relied on a rheological instability, also called viscous fingering, related to high shear rates in the roll coating device. Commercial, fumed silica was added to a liquid, an

otherwise Newtonian poly(dimethylsiloxane) precursor to obtain a fluid with Bingham behavior and shear thinning properties (Herschel-Bulkley fluid). This facilitated the preservation of the wet, structured coating during the following thermal curing step. The highly regular pattern was characterized in terms of averaged branch width and could be controlled from micro- to millimeter size by adjusting coating roll velocity and roll gap distance. The adhesive properties of the structured coating were compared to unstructured conventional silicone coatings by measuring the release force of pressure sensitive adhesives. For rubber-based tape, the release force of patterned PDMS was reduced by a factor of up to eight if compared to smooth reference silicone. These ultra-low adhesive coatings are currently finding applications in packaging, food processing, and for covering sanitary surfaces. The materials are available on the free market and have been fully scaled up to multiton production.

Chapter 3 discusses the possibility to chemically functionalize a polymer by the introduction of a biodegradable polymer filler. With the introduction of biodegradable plastics on a large scale (e.g. France banned the use of classical plastic bags by 2010), fillers of similar degradation are urgently needed. First, the production of such hitherto unknown materials was made accessible by modifying the currently industrially used flame synthesis of silica polymer fillers as to access amorphous tricalcium phosphate (ATCP) nanoparticles or nano-limestone. The use of a similar process resulted in a comparable morphology of the biodegradable filler and the traditionally used silica. Doping of a prominent biodegradable plastic, poly(lactic-co-glycolic acid) (PLGA), with such highly agglomerated ATCP was investigated for mechanical properties, *in vitro* biodegradation and biomineralization. PLGA films with particle loadings ranging from 0 to 30 wt% were prepared by solvent casting. In order to proof that both filler and polymer were biodegradable, the degradation was quantitatively followed in simulated body fluid (SBF) at 37 °C under sterile conditions for up to 42 days by Raman spectroscopy, scanning electron microscopy (SEM), thermal analysis and tensile tests. The presence of nanoparticles in the PLGA matrix slightly increased the Young's modulus up to 30% compared to pure polymer reference materials. The nanoparticles doped films showed a significantly increased loss of polymer mass during degradation. Scanning electron microscopy images of doped films showed that the SBF



degraded the PLGA by corrosion as facilitated by the incorporation of nanoparticulate calcium phosphate. Raman spectroscopy and X-ray powder diffraction revealed that the deposition of about 10 nm sized hydroxyapatite crystallites on the surface of doped PLGA films was strongly increased by the addition of tricalcium phosphate fillers. The combination of increased hydroxyapatite formation and enhanced polymer degradation may suggest the use of such amorphous, aerosol derived ATCP fillers for applications in non-load-bearing bone implant sites.

In Chapter 4, the tricalcium phosphate/poly(lactide-co-glycolide) composite of chapter 3 was brought into a clinically applicable form. Electrospinning was used to obtain a flexible, cotton wool-like poly(lactide-co-glycolide) (PLGA)/amorphous tricalcium phosphate (ATCP) nanocomposite. The easy portioning, the facilitated application into complex bone defects, and the advantageous removal in case of misplacement compared to conventional granular bone substitute materials may result in a relevant time saving for the surgeon. Thus, the easy handling would not only facilitate the surgery but would also be cost-saving for the patient. This hypothesis was tested both in vitro and in a first animal study being done at the University Hospital Zurich.

A cell culture study with human mesenchymal stem cells (hMSC) allowed assessing the application of the material for potential use as a bone graft. ATCP powder was prepared by flame spray synthesis and exhibited a particle size between 20-80 nm. Scaffolds with nanoparticle loadings ranging from 0 to 40% (w/w) were prepared by electrospinning of a PLGA-based composite. Three different scaffolds, namely one containing no ATCP (reference) and two samples with 40% (w/w) ATCP in PLGA (as-prepared and pre-immersed in SBF for 15 hours) were seeded with hMSC. Proliferation and osteogenic differentiation were assessed by incubating cells in osteogenic medium for 4 weeks. Proper adhesion and an unaffected morphology of the cells were observed by confocal laser scanning microscopy (CLSM) for all samples. Fluorometric quantification of dsDNA and analysis of alkaline phosphatase (ALP) activity revealed no significant difference between the three scaffolds tested and excluded any acute cytotoxic effects of the nanoparticles. The osteocalcin content

for all scaffolds was 0.12 to 0.19 ng per ng DNA confirming osteogenic differentiation of human mesenchymal stem cells on these flexible bone implants.

Chapter 5 describes the more complex incorporation of a full catalytic process into a polymer film for ethylene oxidation. An aqueous solution of poly(styrenesulfonic acid) and a catalytic system consisting of palladium chloride (catalyst) and a heteropolyanion (co-catalyst), more specifically  $\text{Na}_3\text{H}_3\text{PMo}_9\text{V}_3\text{O}_{40}$ , were solution-coated onto a polyester carrier film and dried at ambient conditions. Different “catalyst to co-catalyst” ratios were evaluated for their performance in conversion of low ethene concentration (100 ppm) over an extended time period of three weeks and totally six loadings of 100 ppm ethene in synthetic air. The palladium content in the coating was kept constant at  $5 \text{ mg/m}^2$  because of considerations regarding the price of the final film. The ethene conversion was determined by gas chromatography using a flame ionization detector (GC-FID) and followed for up to 200 hours. While initially the catalytic films reached ethene levels of  $<5 \text{ ppm}$  within one day the activity drastically decreased after 3 weeks and six ethene loadings, where levels of  $<5 \text{ ppm}$  ethene were observed after about 5 days. The “catalyst to co-catalyst” ratio had only minor influence on the activity. Further an active coating was additionally covered with a polystyrene protection coating to prevent subsequent migration of the catalyst. The protected film converted roughly 50 ppm of ethene after 25 hours and three quarter of the initial  $\text{C}_2\text{H}_4$  concentration were absorbed after 60 hours. The promising ethene conversion rate suggests the use of such films for the packaging of ethene-sensitive fresh produce such as fruits, vegetables, or cut flowers.

In Chapter 6 silver-doped tricalcium phosphate was evaluated as antimicrobial agent for the use in hydrophobic polymer coatings. Pure tricalcium phosphate (TCP), silver-doped tricalcium phosphate (Ag-TCP) with silver contents ranging from 1wt% to 10wt% and silver-doped silica ( $\text{Ag-SiO}_2$ ) containing 1wt% and 5wt% silver were prepared by flame spray synthesis. The characteristics of the powders were compared to commercially available antimicrobial agents in powder form, namely HeiQ-Silver (silver-doped silica) and Ionpure40 (silver ion containing glass powder). The morphology and phase composition of the powders was accessed by electron microscopy, nitrogen adsorption, X-ray disc centrifugation and X-

ray powder diffraction. While all flame-made powders and sample HeiQ-Silver were composed of a nanoparticulate support carrying finely dispersed, <10 nm metallic silver particles Ionpure40 showed large, >1  $\mu\text{m}$  particles containing no detectable amounts of metallic silver. As to access the antimicrobial efficacy the powders were incorporated into a silicone elastomer film and evaluated according to ASTM E2149-01 and ASTM E2180-01. All films containing 20wt% of flame-made Ag-TCP showed a 4- to 6-log reduction of Gram-negative *E.coli* in both tests. Films containing flame-made Ag-SiO<sub>2</sub> showed only a 2- to 4-log reduction and were at least 10 fold less efficient as corresponding films with Ag-TCP. In a direct comparison of Ag-TCP films and both commercial products (HeiQ-Silver and Ionpure40) the efficiency of the phosphate containing carrier clearly excelled by a factor of 100 to 5000. The Ag-TCP film further exhibited high efficacy (4-log to 6-log reduction) against *P.aeruginosa* and *C.albicans*. This exceptional antimicrobial activity of Ag-TCP films suggests the use of such materials for the coating of surfaces in sanitary and hospital facilities and for the packaging of food and pharmaceuticals.

In Chapter 7 an outlook is given listing possible future research directions with emphasis on the application of the proposed materials.



# **1. Functional polymers: The development of novel physical and chemical properties**

## **1.1 Introduction**

Polymers are today the fastest growing materials sector and enable the manufacturing of numerous commodity products. These large variety of materials reflect a tremendous research effort mainly in organic chemistry. A variety of functionalized monomer and different polymerization approaches allow a fine tuning of both mechanical and chemical properties for a specific application. Such examples range from car tires to polymer packaging for food, contact lenses, degradable biomaterials and functional clothing. Limitations to this organic chemistry based approach are given mainly through the capacity of such molecules to enable change or to provide specific catalytic properties.

Recently, the availability of nanomaterials with specific physical or chemical properties has motivated the development of both mechanically improved or catalytically active polymer composites. Research done at ETH Zurich has most recently given access to a broad variety of chemically active materials, such as heterogeneous catalysts, degradable nanoparticles and materials for fine tuned optical properties. It was expected at the beginning of this thesis that incorporation of such advanced functional materials into existing polymers would allow to combine novel properties with the easy processing of the polymer.

The following chapter gives an overview of the state of the research today and starts with physically functionalized composites. In a second part, chemical functionalization of composites using the introduction of functional materials is discussed.

## 1.2. Physical functionalization of polymers

The addition of particles to a polymers dates back to the early development of polymer engineering in the thirties and forties [1-5]. Probably the largest application in terms of volume is the preparation of car tires. Abrasion resistance is introduced by the implementation of carbon in the form of carbon black [6-8]. This material today is manufactured at over 8 million tons annually by a flame aerosol process. In the fifties the introduction of silica into polymers has enabled the preparation of mechanically improved elastomers [9-11] and so-called green tires [12, 13], combinations of silica aerosols and rubber. Improved mechanical stability was further introduced by the use of glass fiber reinforced materials [14-16]. Today, both car and airplane manufacturing is largely based on the availability of these composites.

Mixing between the particulate and the polymer phase is typically done in the range of several micrometers up to a few millimeters and fibers often attain length scales in the area of one centimeter. It has been repeatedly speculated that a further reduction of the feature size may increase the homogeneity and allow even higher mechanical stability. Since the nineties numerous approaches with more complex inorganic dopants in the size range of nanometers were investigated and experimental proof on increased mechanical properties was given [17-22]. Today, most technically applied polymers contain a certain amount of particles (Figure 1-1) either to increase their strength [23, 24], stability against UV radiation [25] or processability [26, 27].

A second field of physical functionalization of polymers covers the incorporation of specific surface morphologies which entail novel properties. Regular micron-sized patterns enable specific wetting of surfaces [28] and in some cases even exhibit superhydrophobicity [29] or superoleophilicity [30]. Further application of patterned polymers may be found in integrated optics [31]. Such systems require highly regular features used as polymeric optical waveguides. Present techniques to achieve a structuring in the range of micrometers to several hundred micrometers are mainly based on multi-step processes such as lithographic methods [28, 29, 32, 33] or require complex tools carrying the negative structure. Latter is predominately applied either in a molding, casting or embossing process [34-37].

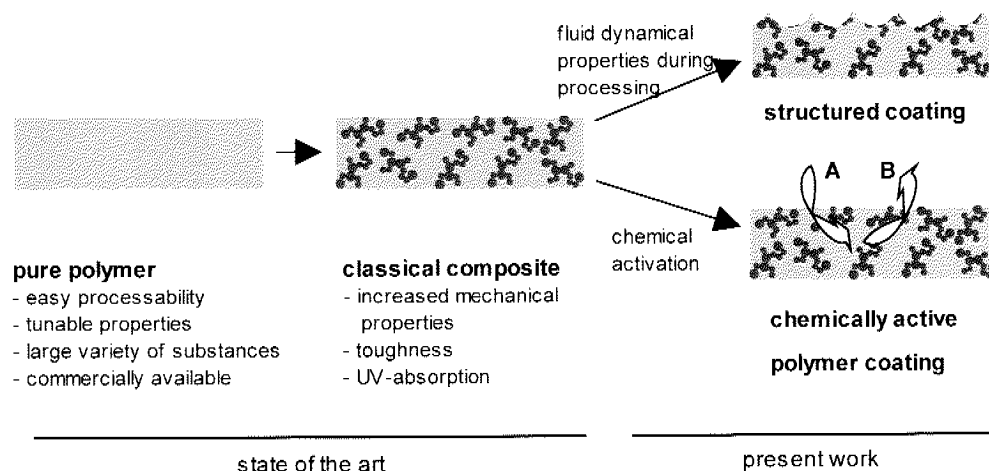


**Figure 1-1.** Schematic of the development in physical and chemical functionalization of polymers. Starting point is the pure polymer (left) which can be altered mainly in terms of physical properties with different filler materials (middle). Further functionality can be obtained by an implementation of surface structures during processing (right, top) or by the introduction of chemically active substances (right, bottom).

### 1.3. Application of polymers as foils

Packaging foils today constitute a major share of the polymer market. Mainly passive systems are used to block access to air, water, off-flavor and microbiological organisms to or from food, pharmaceuticals or consumer goods. Present polymer foils are made of single constituents or contain multi-layer sandwich constructions. Latter morphology allows a combination or stacking of different properties. Specific barrier functions are introduced by the combination of polymers either by lamination two rigid foils or by the application of a coating from a liquid polymer precursor (e.g. by roll coating).

### 1.4. Low adhesion coatings

For over fifty years, polydimethylsiloxane (PDMS) has preferably been used for low adhesion coatings, so-called release coatings, because of its relatively low cost and easy processing

[38]. The application of low adhesion surfaces or release coatings in combination with pressure sensitive adhesives, such as adhesive tapes, has become omnipresent in large scale manufacturing. Control on the peeling process and resulting forces are crucial for safe production [39]. Release coatings for high-end applications preferably consist of materials with very low surface energies ( $< 20 \text{ mN m}^{-1}$ ) such as fluoropolymers. Unfortunately, latter are economically less favorable and often difficult to process. Fluorine-modified siloxanes (e.g. poly(methylnonafluorohexylsiloxane), PMNFHS) offer a solution to achieve very low surface energy [38, 40] while maintaining the easy processing properties of siloxane polymers. At present, their application is still restricted to the use of low swelling coatings for applications in contact to organic solvents and for PDMS based pressure sensitive adhesives [38]. Several detailed studies on siloxanes were carried out by Gordon and co-workers [39, 41, 42] focusing on pressure sensitive adhesives and controlled release. For relatively low peel rates ( $0.005\text{-}0.17 \text{ m s}^{-1}$ ) controlled release could alternatively be achieved by high release additives (HRA, e.g. methyl silicate) which increase substrate adhesion.

## 1.5. Introducing catalytic functionality in polymers

Up to the present, the enhanced mechanical strength of composites has been a mainly physical improvement (Figure 1-1). In a next step the addition of chemical functionality to a polymer would be technically most intriguing. Combining a catalytic process or a chemical activity with the processability of the polymer would allow transferring chemical reactions out of industrial production settings to a consumer based market. Most everyday applications of polymers could benefit from additional activity next to a structural purpose. Early investigation on hydrogenations [43, 44] being carried out in polymers have shown that small nanoclusters or nanoparticles of noble metals retain very active catalytic properties. Another prominent area of examples includes anchoring heterogeneous catalysts on polymer supports or membranes [45-50]. Probably the largest focused approach has been done in the development of fuel cell membranes [51, 52] where an intimate mixture between the membrane itself and its electro-catalytically active constituents today enables an efficient conversion of hydrogen into electricity.



## 1.6. The functionalization of polymeric biomaterials

The efforts done in the field of biomaterials research nicely exemplifies once more the development towards more complex and functional materials. In the sixties and seventies a first generation of biomaterials was developed for use in human body. It was the absolute aim to achieve suitable physical properties matching those of the replaced tissue by entailing minimal toxic response. Most of these materials, polymers included, were biologically inert. A second generation of materials was introduced in the eighties featuring capability to be resorbed and bond to human tissue (bioactivity). Numerous investigations have covered the use of biodegradable polymers in a pure form [53, 54] or in combination with synthetic ceramics, such as hydroxyapatite [55]. Some of these materials exhibited excellent bioactive properties and biodegradability which allowed for the continuous regeneration of new tissue at the interface to the implant. Today third generation biomaterials are being designed by introducing features which interact with cells and trigger the formation of bone accelerating the healing process [56]. Such properties might be obtained by appropriate surface morphologies in the nanometer range [57] or by the release of specific ions such as silicon, calcium, phosphates, sodium or magnesium [58].

## 1.7. References

- [1] Galloway P D and Wake W C 1946 The Direct Estimation of Polymer and Carbon Black in Vulcanised Butyl Rubber (Gr-I) *Analyst* **71** 505-10
- [2] Greenblatt J H and Fensom D 1947 Extrusion Properties of High Polymers with Included Crystalline Filler *Industrial and Engineering Chemistry* **39** 1037-42
- [3] Riseman J and Harper R C 1954 The Influence of High Polymer on the Rheological Properties of a Carbon Black Suspension *Journal of Colloid Science* **9** 438-50
- [4] Stearns R S and Johnson B L 1951 Interaction between Carbon Black and Polymer in Cured Elastomers *Industrial and Engineering Chemistry* **43** 146-54
- [5] Winslow F H, Baker W O, Pape N R and Matreyek W 1955 Formation and Properties of Polymer Carbon *Journal of Polymer Science* **16** 101-20
- [6] Gonzalez L, Rodriguez A, deBenito J L and Marcos A 1996 A new carbon black-rubber coupling agent to improve wet grip and rolling resistance of tires *Rubber Chem. Technol.* **69** 266-72
- [7] Medalia A I 1994 Effects of Carbon-Black on Abrasion and Tread Wear *Kautsch. Gummi Kunstst.* **47** 364-68
- [8] Grosch K A 1992 Abrasion of Rubber and Its Relation to Tire Wear *Rubber Chem. Technol.* **65** 78-106
- [9] Wagner M P and Sellers J W 1959 Kinetics of Filler-Polymer Interaction between Fine Particle Silica and Sbr or Butyl Rubber *Industrial and Engineering Chemistry* **51** 961-66

- 
- [10] Dogadkin B, Pechkovskaia K and Goldman E 1958 The Structure and the Reinforcing Effect of Colloidal Silica as a Loading Material for Synthetic Rubber *Doklady Akademii Nauk Sssr* **119** 1170-73
- [11] Stearns R S and Johnson B L 1956 Surface Treatment of Hydrated Silica Pigments for Reinforcement of Rubber Stocks *Industrial and Engineering Chemistry* **48** 961-63
- [12] Uhrlandt S and Blume A 2001 Silica in green tyres - Processes, products, properties *Kautsch. Gummi Kunstst.* **54** 520-28
- [13] Noordermeer J W M 1998 Recent developments in rubber processing, leading to new applications such as the "Green tyre" *Macromol. Symp.* **127** 131-39
- [14] Kim J K and Mai Y W 1991 High-Strength, High Fracture-Toughness Fiber Composites with Interface Control - a Review *Compos. Sci. Technol.* **41** 333-78
- [15] Dharan C K H 1975 Fatigue Failure in Graphite Fiber and Glass Fiber-Polymer Composites *J. Mater. Sci.* **10** 1665-70
- [16] Hardy G F and Wagner H L 1969 Tensile Behavior of Glass Fiber-Reinforced Acetal Polymer *J. Appl. Polym. Sci.* **13** 961-75
- [17] Jongsomjit B, Panpranot J and Praserttham P 2007 Effect of nanoscale SiO<sub>2</sub> and ZrO<sub>2</sub> as the fillers on the microstructure of LLDPE nanocomposites synthesized via in situ polymerization with zirconocene *Mater. Lett.* **61** 1376-79
- [18] Barna E, Rentsch D, Bommer B, Vital A, von Trzebiatowski O and Graule T 2007 Surface modification of nanoparticles for scratch resistant clear coatings *KGK-Kautsch. Gummi Kunstst.* **60** 49-51
- [19] Shi G, Zhang M Q, Rong M Z, Wetzel B and Friedrich K 2003 Friction and wear of low nanometer Si<sub>3</sub>N<sub>4</sub> filled epoxy composites *Wear* **254** 784-96
- [20] Wu C L, Zhang M Q, Rong M Z and Friedrich K 2002 Tensile performance improvement of low nanoparticles filled-polypropylene composites *Compos. Sci. Technol.* **62** 1327-40
- [21] Ajayan P M, Schadler L S, Giannaris C and Rubio A 2000 Single-walled carbon nanotube-polymer composites: Strength and weakness *Adv. Mater.* **12** 750-53
- [22] Giannelis E P 1996 Polymer layered silicate nanocomposites *Adv. Mater.* **8** 29-35
- [23] Balazs A C, Emrick T and Russell T P 2006 Nanoparticle polymer composites: Where two small worlds meet *Science* **314** 1107-10
- [24] Fiedler B, Gojny F H, Wichmann M H G, Nolte M C M and Schulte K 2006 Fundamental aspects of nano-reinforced composites *Compos. Sci. Technol.* **66** 3115-25
- [25] Vulic I, Stretanski J and Sanders B 2000 UV stabilization of polyolefin systems *Polym. Polym. Compos.* **8** 529-35
- [26] Bazgir S, Katbab A A and Nazockdast H 2004 Microstructure-properties correlation in silica-reinforced dynamically vulcanized EPDM/PP thermoplastic elastomers *Rubber Chem. Technol.* **77** 176-91
- [27] Wolff S, Wang M J and Tan E H 1994 Filler-Elastomer Interactions .10. the Effect of Filler-Elastomer and Filler-Filler Interaction on Rubber Reinforcement *Kautsch. Gummi Kunstst.* **47** 102-07
- [28] Yu K, Cong Y, Fu J, Xing R B, Zhao N and Han Y C 2004 Patterned self-adaptive polymer brushes by "grafting to" approach and microcontact printing *Surf. Sci.* **572** 490-96
- [29] Shirtcliffe N J, McHale G, Newton M I, Chabrol G and Perry C C 2004 Dual-scale roughness produces unusually water-repellent surfaces *Adv. Mater.* **16** 1929-32
- [30] Zhang J L, Huang W H and Han Y C 2006 A composite polymer film with both superhydrophobicity and superoleophilicity *Macromol. Rapid Commun.* **27** 804-08
- [31] Eldada L and Shacklette L W 2000 Advances in polymer integrated optics *IEEE J. Sel. Top. Quantum Electron.* **6** 54-68
- [32] McDonald J C, Duffy D C, Anderson J R, Chiu D T, Wu H K, Schueller O J A and Whitesides G M 2000 Fabrication of microfluidic systems in poly(dimethylsiloxane) *Electrophoresis* **21** 27-40

- [33] Overgaard S, Bromose U, Lind M, Bunger C and Soballe K 1999 The influence of crystallinity of the hydroxyapatite coating on the fixation of implants - Mechanical and histomorphometric results *J. Bone Joint Surg.-Br. Vol.* **81B** 725-31
- [34] Shan X C, Ikehara T, Murakoshi Y and Maeda R 2005 Applications of micro hot embossing for optical switch formation *Sens. Actuator A-Phys.* **119** 433-40
- [35] Hecke M and Schomburg W K 2004 Review on micro molding of thermoplastic polymers *J. Micromech. Microeng.* **14** R1-R14
- [36] Kragl H, Hohmann R, Marheine C, Pott W, Pompe G, Neyer A, Diepold T and Obermeier E 1998 Integrated optic polymeric components fabricated with microstructured strip-off covers *Electron. Lett.* **34** 1396-98
- [37] Kragl H, Hohmann R, Marheine C, Pott W and Pompe G 1997 Low cost monomode, integrated optics polymeric components with passive fibre-chip coupling *Electron. Lett.* **33** 2036-37
- [38] Owen T A, et al. 1990 Progressive Development of the Rat Osteoblast Phenotype Invitro - Reciprocal Relationships in Expression of Genes Associated with Osteoblast Proliferation and Differentiation During Formation of the Bone Extracellular-Matrix *J. Cell. Physiol.* **143** 420-30
- [39] Gordon G V, et al. 2000 Forcing the issue *Adhes. Age* **43** 41-44
- [40] Kobayashi H and Owen M J 1995 Surface-Properties of Fluorosilicones *Trends Polym. Sci.* **3** 330-35
- [41] Gordon G V, Moore P A, Popa P J, Tonge J S and Vincent G A 2002 Sticking lightly *Adhes. Age* **45** 24-31
- [42] Gordon G V, Perz S V, Tabler R L, Stasser J L, Owen M J and Tonge J S 1998 Silicone release coatings: An examination of the release mechanism *Adhes. Age* **41** 35-42
- [43] Ciebien J F, Cohen R E and Duran A 1999 Membrane catalysts for partial hydrogenation of 1,3-butadiene: catalytic properties of palladium nanoclusters synthesized within diblock copolymer films *Mater. Sci. Eng. C-Biomimetic Supramol. Syst.* **7** 45-50
- [44] Ciebien J F, Cohen R E and Duran A 1998 Catalytic properties of palladium nanoclusters synthesized within diblock copolymer films: hydrogenation of ethylene and propylene *Supramol. Sci.* **5** 31-39
- [45] Frusteri F, Parmaliana A, Ostrovskii N M, Iannibello A and Giordano N 1997 Selective oxidation of ethylene over carbon-supported pd and Pt catalytic membranes *Catal. Lett.* **46** 57-62
- [46] Gryaznov V M, Serebryannikova O S, Serov Y M, Ermilova M M, Karavanov A N, Mischenko A P and Orekhova N V 1993 Preparation and Catalysis over Palladium Composite Membranes *Appl. Catal. A-Gen.* **96** 15-23
- [47] Reyes P, Borda G, Rivas B L and Cardenas G 2002 Polymer-based catalysts for toluene hydrogenation *J. Appl. Polym. Sci.* **86** 381-85
- [48] Takano N, Kawakami Y and Takeno N 1996 Electrocatalytic hydrogenation of acetylenes on palladium incorporating poly[N-(5-hydroxypentyl)pyrrole] film-coated electrode *Chem. Lett.* 589-90
- [49] Takano N and Nakade A 1999 Incorporation of catalytic noble metals in conductive polymer film-coated electrode and electrocatalytic hydrogenation *Electrochemistry* **67** 463-65
- [50] Watkins J J and McCarthy T J 1995 Polymer/Metal Nanocomposite Synthesis in Supercritical CO<sub>2</sub> *Chem. Mat.* **7** 1991-94
- [51] Ulbricht M 2006 Advanced functional polymer membranes *Polymer* **47** 2217-62
- [52] Lu G Q and Wieckowski A 2000 Heterogeneous electrocatalysis: a core field of interfacial science *Curr. Opin. Colloid Interface Sci.* **5** 95-100
- [53] Gilding D K and Reed A M 1979 Biodegradable Polymers for Use in Surgery - Polyglycolic-Poly(Actic Acid) Homopolymers and Copolymers .1. *Polymer* **20** 1459-64
- [54] Ignatius A A and Claes L E 1996 In vitro biocompatibility of bioresorbable polymers: Poly(L,DL-lactide) and poly(L-lactide-co-glycolide) *Biomaterials* **17** 831-39

- [55] Kim S S, Park M S, Jeon O, Choi C Y and Kim B S 2006 Poly(lactide-co-glycolide)/hydroxyapatite composite scaffolds for bone tissue engineering *Biomaterials* **27** 1399-409
- [56] Hench L L and Polak J M 2002 Third-generation biomedical materials *Science* **295** 1014-17
- [57] Webster T J and Ahn E S 2007 Nanostructured biomaterials for tissue engineering bone *Tissue Engineering II: Basics of Tissue Engineering and Tissue Applications* ed (Berlin: Springer-Verlag Berlin) pp 275-308.
- [58] Jones J R, Ehrenfried L M and Hench L L 2006 Optimising bioactive glass scaffolds for bone tissue engineering *Biomaterials* **27** 964-73

## 2. Rapid production of micro-patterned surfaces using a fluid dynamical instability

### Abstract

The continuous, high speed patterning of polyethylene films with a micron-structured silicone coating was investigated in a roll coating process that did not depend on the use of pre-structured tools. Thermally curable poly(dimethylsiloxane) (PDMS) resin was rheologically modified by the addition of highly agglomerated, aerosol-derived silica and resulted in a Herschel-Bulkley fluid. Application of the modified siloxane in a roll coating process resulted in a fluid dynamical instability at high capillary numbers promoting the spontaneous formation of randomly branched surface structures. The shear-thinning properties of the nanoparticle doped PDMS resin were adjusted as to preserve the wet, structured coating during the following thermal curing step. The highly regular pattern was characterized in terms of averaged branch width and could be controlled from micro- to millimeter size by adjusting coating roll velocity and roll gap distance. The adhesive properties of the structured coating were compared to unstructured conventional silicone coatings by measuring the release force of pressure sensitive adhesives. For rubber-based tape the release force of patterned PDMS was reduced by a factor of up to eight if compared to smooth reference silicone. These ultra-low adhesive coatings may find applications in packaging, food processing, and for covering sanitary surfaces, offering a cost-effective alternative to conventional surface structuring methods.

Part of this chapter is published in **Polym. Eng. Sci.**, 46, 1541-1547 (2006) and has been applied for as a PCT patent application (PCT/CH2005/000540).

The films described in this chapter are today produced at a commercial level.

## 2.1. Introduction

Development and improvement of polymer surfaces with controlled or low adhesion properties have resulted in a vast number of commodity products in the last few decades. The application of low adhesion surfaces or release coatings in combination with pressure sensitive adhesives has become omnipresent in large scale manufacturing. Control on the peeling process and resulting forces are crucial for safe production [1]. Low adhesion to a substrate is further desired, where surfaces have to be prevented from fouling, dirt uptake or product cross-contamination. The reduction or careful control of adhesion towards biological agents such as proteins, tissue, microbes, algae or even invertebrates is of great interest for tissue engineering [2, 3] or the protection of ships against marine biofouling [4].

Adhesion may be altered using specific physico-chemical properties of the corresponding surface material: The most prominent polymers today are silicone or fluorocarbon based release coatings mainly due to their low surface free energy [5, 6]. For over fifty years, polydimethylsiloxane (PDMS) has been preferably used for release coatings because of its relatively low cost and easy processing. Release coatings for high-end applications preferably consist of materials with very low surface energies ( $< 20 \text{ mN m}^{-1}$ ) such as fluoropolymers. Unfortunately, latter are economically less favorable and often difficult to process. Fluorine-modified siloxanes (e.g. poly(methylnonafluorohexylsiloxane), PMNFHS) offer a solution to achieve very low surface energy [6, 7] while maintaining the easy processing properties of siloxane polymers. At present, their application is still restricted to the use of low swelling coatings for applications in contact to organic solvents and for PDMS based pressure sensitive adhesives [6]. Several detailed studies on siloxanes were carried out by Gordon and co-workers [1, 8, 9] focusing on pressure sensitive adhesives and controlled release. For relatively low peel rates ( $0.005\text{-}0.17 \text{ m s}^{-1}$ ) controlled release could alternatively be achieved by high release additives (HRA, e.g. methyl silicate) which increase substrate adhesion.

In contrast to this material-based approach, the adhesive properties of a surface may also be changed by the introduction of a specific surface pattern. Suitable structures reduce the amount of exposed surface area and limit the contact between adhesive and release liner. This reduced interaction facilitates the peel-off process. Micron-sized patterning can further

imply a self-cleaning effect [10, 11]. In part it is responsible for the so-called lotus effect [12-14] if the surface is inherently hydrophobic and exhibits surface features down to the nanometer scale. Another micron-structured surface observable in nature is the skin of a shark [15]. Latter has promoted numerous investigations on trying to mimic and understand the phenomena of reduced near wall drag forces [16-18]. For continuous 2-dimensional ribs a drag reduction of approximately 9% was attributed to a reduction of turbulent wall shear stress [17] for an optimal dimensionless lateral rib spacing  $s_{opt}^+$  in the range of

$$s_{opt}^+ = \frac{s_{opt} u_\tau}{\nu} \approx 10 - 30 \quad (2.1)$$

where,  $u_\tau$  is the shear velocity ( $\text{m s}^{-1}$ ) and  $\nu$  the kinematic viscosity ( $\text{m}^2 \text{s}^{-1}$ ). For technically important flows in water, an optimal rip spacing of several hundred micrometers can be calculated [17, 18]. The optimal rib height  $h_{opt}$  according to experimental investigations by Bechert [19] was observed around

$$h_{opt} \approx 0.5 \cdot s_{opt} \quad (2.2)$$

The tremendous demand for structured surfaces has brought up many different preparation methods for polymer processing. The structure dimensions accessible by these methods range from approximately  $1 \mu\text{m}$  to several  $100 \mu\text{m}$  [20]. Direct printing lithography excels by high accuracy and process latitude but is too expensive for large area manufacturing. Laser direct writing requires no pre-structured tools or masks but current scanning speeds are limited to around  $5 \text{ cm s}^{-1}$  [20]. Processes more suited for large scale, continuous series production are casting, molding, hot embossing, soft embossing, and microcontact printing [21-27]. Unfortunately, they all require complex processing tools carrying the negatively structured pattern.

It would therefore be most attractive to obtain structured pattern without the need of any pre-structured tools. The present study investigates the use of a generally undesired fluid-dynamical instability as the structure providing agent.

**Fluid stability during roll coating**

The tremendous industrial relevance of roll coating has motivated detailed investigations on the fluid dynamic behavior in the gap between two rolls [28-30]. Instabilities in the fluid film split result in an irregular meniscus and trigger the formation of generally undesired ribbed structures and irregularities [28, 31-35]. The instability in the meniscus was previously attributed to a small perturbation [31] which grows in time. Roll coating and rib-forming of Newtonian fluids has been well investigated [36-41]. Unfortunately, most fluids used in the coating industry exhibit highly non-Newtonian behavior (e.g. polymer precursors or solutions). The effect of elasticity on the ribbing instability has therefore attracted much interest [30, 42]. Previous studies on a two roll coating device with viscoelastic fluids have revealed a strongly enhanced susceptibility to fingering if compared to the use of Newtonian fluids [34, 39, 43].

For Newtonian fluids, a stability analysis in film splits was investigated by Saffman and Taylor [44] who related the onset of ribbing to a dimensionless capillary number  $Ca$ :

$$Ca = \frac{\mu U}{\sigma} \quad (2.3)$$

where  $\mu$  ( $\text{kg m}^{-1} \text{s}^{-1}$ ) is the fluid dynamic viscosity,  $U$  ( $\text{m s}^{-1}$ ) is the mean flow velocity, and  $\sigma$  ( $\text{N m}^{-1}$ ) surface tension of the applied fluid. For air-to-fluid displacement a critical condition in a Hele-Shaw cell with parallel walls was found as

$$Ca_{crit} = \frac{(\rho - \rho_{air})gb^2}{12\sigma}, \quad (2.4)$$

where  $\rho$  ( $\text{kg m}^{-3}$ ) is the fluid density,  $\rho_{air}$  ( $\text{kg m}^{-3}$ ) is the air density,  $g$  ( $\text{m s}^{-2}$ ) is the gravity constant, and  $b$  (m) is the gap thickness. Hence, the onset of ripping is favored for higher roll velocity or increasing viscosity of the fluid. For non-parallel walls the diverging or converging walls of the Hele-Shaw cell [34] have an influence on the stability of the flow.



Based on a one-dimensional stability analysis in the absence of gravitational effects and for constant mean flow velocity the critical condition can be expressed as

$$Ca_{crit} = \frac{1}{3} \tan\left(\frac{\alpha}{2}\right) \quad (2.5)$$

where  $\alpha$  is the divergence angle (Figure 2-1, 2-2). Including both gravitational stabilization and stabilization due to gap divergence leads to a modified Saffman-Taylor theory [34] for critical condition

$$Ca_{crit} = \frac{1}{3} \tan\left(\frac{\alpha}{2}\right) + \frac{(\rho - \rho_{air})gh^2 \cos(\beta)}{12\sigma} \quad (2.6)$$

where  $h$  is the local gap thickness at the meniscus (Figure 2-1), and  $\beta$  is the angular location of the meniscus (while  $\beta=0$  in horizontal position, Figure 2-2).

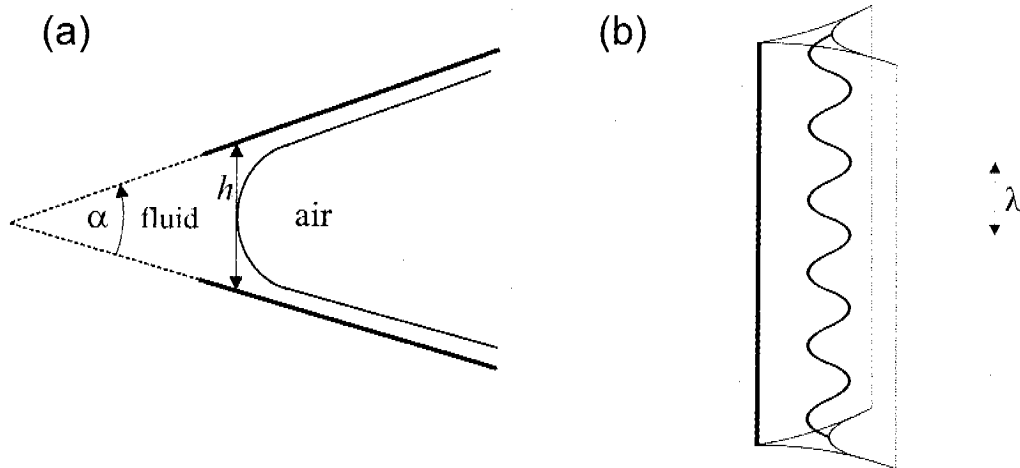


**Figure 2-1.** Schematic drawings of a formed split gap as observed during roll coating. (a) Side view. (b) Top view displaying the fluid instability with wavelength  $\lambda$ .

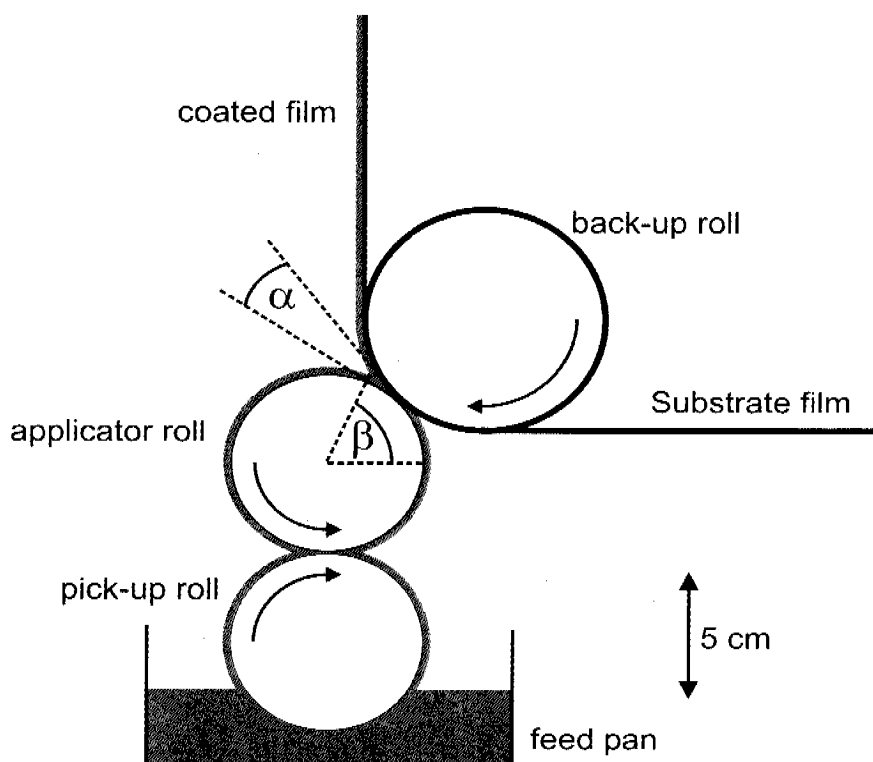


**Figure 2-2.** Schematic setup of a three roll coating device. Polymer precursor is taken up from the feed pan by the pick-up roll, transferred to the applicator roll and applied on the film.

Flow instability of yield-stress fluids can result in branched fingering of the fluid as observed by McCloud & Maher and Lindner & Coussot [45, 46] using Hele-Shaw cells where a high viscous fluid was pushed by a low viscous fluid (e.g. air). Very limited knowledge is available on the Saffman-Taylor instability of yield-stress fluids in roll coating flow. While previous studies aimed for elimination of rib forming in roll coating, we take advantage of the ribbing instability to apply a defined coating pattern. In order to illustrate one possible application for ultra low adhesion surfaces, continuous preparation of milli- to micrometer structured PDMS coatings was demonstrated by roll coating at  $3 \text{ m min}^{-1}$  thus allowing highly economic production [47].

## 2.2. Experimental

### 2.2.1. Materials and surface coating method

A solvent-free silicone coating system based on polydimethylsiloxane (PDMS) was used as a basic raw material consisting of the following weight proportions: 4700 parts vinyl-terminated polydimethylsiloxane (Dehesive® 610, Wacker Silicones, Germany), 270 parts hydrogen terminated polydimethylsiloxane (Crosslinking Agent V24, Wacker Silicones, Germany), 140 parts platinum-based catalyst (Catalyst OL, Wacker Silicones, Germany), and 10 parts 2-methyl-3-butyn-2-ol (purum,  $\geq 99.0\%$ , Fluka) as an inhibitor. Highly agglomerated silica nanoparticles (Aerosil® 200, Degussa, Germany) were added to the liquid polymer precursor to modify the rheology. In a typical run, 5 wt% silica was first added to the silicone basis and mixed with a conventional agitator (EUROSTAR digital, IKA Labortechnik) applying 500 rpm for 20 minutes. Increasing amounts (5, 10, 15, and 20wt% of the final resin mass) of 2-propanol (purum,  $\geq 99.0\%$ , Fluka) were then mixed with the modified silicone resin as to further adjust the rheological properties. Finally, the inhibitor, crosslinker, and catalyst were admixed and the resulting resin was applied on a high density polyethylene (HDPE) film (FOLIEtech, Kunststoffwerk AG, Germany, 150  $\mu\text{m}$  film thickness) by the aid of a laboratory scale three roll direct coating machine (Polytype AG, Switzerland) with co-rotating rolls (Figure 2-2). The line speed was kept constant at 3  $\text{m min}^{-1}$  while the coating roll speed and the gap distance between the coating roll and the substrate film was altered to achieve different coating properties. Curing of the as-applied topcoat was done by in-line thermal treatment at 120  $^{\circ}\text{C}$  until complete polymerization was reached. The experimental results obtained were compared to unmodified resin labeled as *Ref* (i.e. neither silica nor 2-propanol was added).

### 2.2.2. Characterization methods

The dynamic viscosity of the different coating resins was investigated on a controlled strain rate rheometer (ARES rheometer, Rheometric Scientific) with cone/plate (diameter 50 mm) geometry at a constant temperature of 25 $^{\circ}\text{C}$ . Steady rate sweep tests of the fluids were performed over a shear rate range of 0.1 to 100  $\text{rad sec}^{-1}$ .

The grammage (weight of cured silicone per square meter) of the roll coated silicone films was altered from 2 to 8  $\text{g m}^{-2}$  and measured by X-ray fluorescence (XRF) of silicon on a

ASOMA 200T (ASOMA Instruments Inc.) bench-top analyzer. The contribution of incorporated silica to the absorption caused by the silicone resin was considered negligible as its relative amount to the silicon of the PDMS is small. Images of the as-prepared films were taken on a light microscope (IX51, Olympus) equipped with a digital camera system (DP12, Olympus). Peel force testing was conducted on a tensile tester (Type BZ 2.5/TN1S, Zwick) according to the FINAT test method no. 10 (FTM 10, FINAT Technical Handbook 6<sup>th</sup> edition, 2001) at a constant peel rate of 0.3 m sec<sup>-1</sup>. Aging of the coatings was done for at least two weeks before testing the adhesion to industrially relevant, aggressive pressure sensitive adhesives. Two adhesives based on polyacrylic acid and butadiene-styrene rubber (tesa7476 and 7475, tesa, Germany) were chosen to cover a broad range of applications.

## 2.3 Results and Discussions

### 2.3.1. Rheology of the coating resin

Figure 2-3 compares the shear stress of the as-prepared silicone resins for increasing shear rate on a double logarithmic scale. The rheological behavior of polydimethyl siloxane resin before and after the addition of 5 wt% silica shows the strongly non-Newtonian effect of the highly agglomerated silica polymer filler. Different amounts of 2-propanol (0 to 20 wt%) were used to further control the final rheological behavior of the silicone polymer system allowing facile application. The shear stress can be expressed by the Herschel-Bulkley model:

$$\tau = \tau_0 + K \cdot \dot{\gamma}^n \quad 0 \leq \tau_0, \quad (2.7)$$

where  $\tau$  is the shear stress,  $\tau_0$  is the yield stress,  $K$  is the power law coefficient,  $\dot{\gamma}$  is the shear rate, and  $n$  is the power law exponent. Note that  $n=1$  corresponds to Bingham behavior and  $n<1$  is observed for shear-thinning fluids. The parameters  $\tau_0$ ,  $K$ , and  $n$  (Table 2-1) well described the properties of the here-used siloxane polymer and the experimentally measured (symbols) data could be fitted (lines) by nonlinear least-squares data fitting of the Herschel-Bulkley model.

**Table 2-1** Parameters of the fitted Herschel-Bulkley model for different resin compositions.

Solvent content / wt%	Herschel-Bulkley model		
	Yield stress <sup>a</sup> / N m <sup>-2</sup>	Power law coefficient <sup>b</sup> / N m <sup>-2</sup> s <sup>n</sup>	Power law exponent <sup>c</sup> / -
0, reference	0.02	0.24	1.01
5	63.6	2.54	0.80
10	30.5	7.12	0.57
15	16.5	5.10	0.60
20	9.09	3.78	0.59

<sup>a</sup> error ±10%<sup>b</sup> error ±10%<sup>c</sup> error ±0.02

The pure reference resin (*Ref*) exhibited a flow behavior close to Newtonian (i.e.  $\tau_0 = 0$ ,  $n=1$ , Table 2-1). For all modified silicone polymers a Herschel-Bulkley behavior with an increasing yield stress for lower solvent contents was observed. The power law coefficient was significantly higher for all silica-containing silicone resins and the shear-thinning effect was confirmed by the values of the power law exponent below unity. Changing the solvent content allowed adjustment of the rheological properties of the PDMS resin. The dynamic viscosity as a function of shear rate could then be calculated from the measured shear stress (Figure 2-3) and underlined the strong shear-thinning properties of the modified silicones (Figure 2-4).

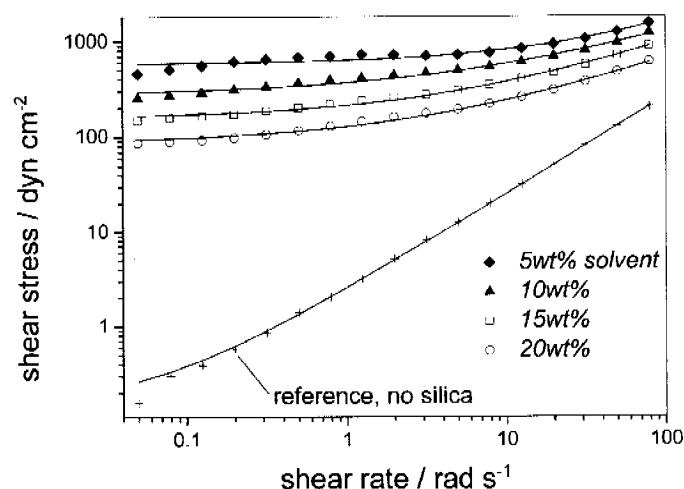


**Figure 2-3.** Shear stress versus shear rate of different silicone resins on a double logarithmic scale. The reference resin without silica or solvent exhibits a Newtonian behavior while the addition of silica to the resin results in a Herschel-Bulkley type fluid. Experimental data (symbols) are compared to the Herschel-Bulkley model (full line).

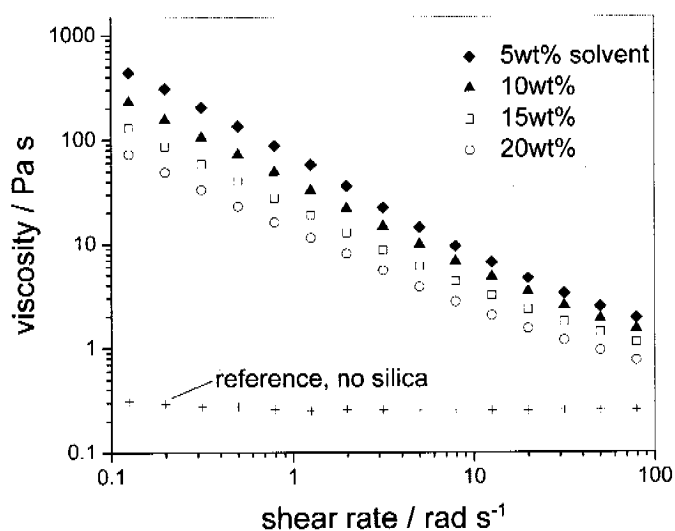


**Figure 2-4.** Viscosity as a function of shear rate reveals the shear-thinning behavior of the modified PDMS compared to the Newtonian behavior of the reference silicone.

### 2.3.2. Roll coating of a Herschel-Bulkley fluid

The as-prepared silicone resins were applied on HDPE-substrate films by direct three roll coating (Figure 2-2) and subsequent thermal curing at 120 °C. The application of pure silicone resin resulted in a smooth surface coating of silicone polymer on the polyethylene carrier film (Figure 2-5a). In contrast to this conventional coating, the application of a suitable silica-modified siloxane resulted in a clearly visible surface pattern (Figure 2-5b to f). In order to investigate the influence of the roll coating parameters, the relative coating roll speed and the coating gap distance were systematically changed.

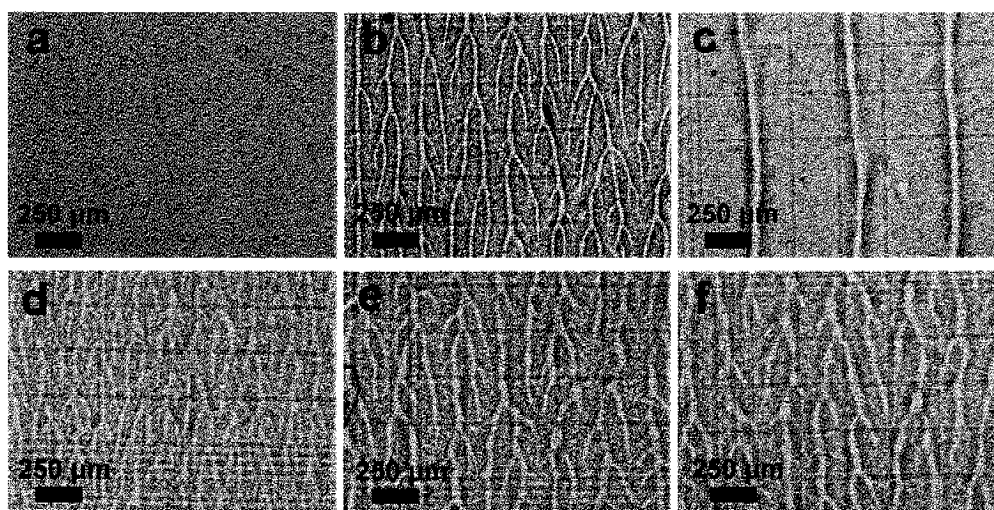


**Figure 2-5.** Light microscopy images of structured films for different solvent contents and silicone loadings (grammage) at a constant relative roll velocity of  $0.3 \text{ m min}^{-1}$ . Top images show the reference film with no silica, no solvent and grammage  $4 \text{ g m}^{-2}$  (a) and films with silica and 5wt% solvent  $3.3 \text{ g m}^{-2}$  (b), and  $5.5 \text{ g m}^{-2}$  (c) grammage. Bottom images refer to 20 wt% solvent content and  $2 \text{ g m}^{-2}$  grammage (d), 15 wt% and  $3.3 \text{ g m}^{-2}$  (e), and 15 wt% and  $4.3 \text{ g m}^{-2}$  (f). Thin black lines are caused by the pattern of a Neubauer cell used for scaling.

Figure 2-6 compares the rib distance (wavelength perpendicular to the machine direction) for different mass loadings (grammage) of silicone on the polyethylene film at a constant relative roll velocity of  $0.3 \text{ m min}^{-1}$ . A higher loading resulted in an increased rib distance irrespectively of the amount of solvent used for dilution.

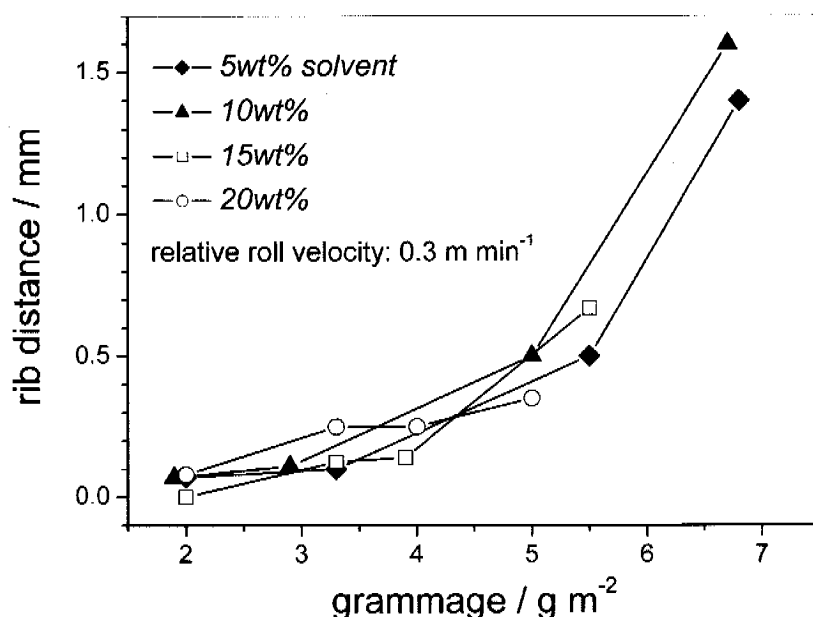


**Figure 2-6.** Rib distance versus the silicone loading of the films produced with the modified silicone resin.

Figure 2-7 depicts the influence of the relative roll speed on the rib distance for a series of siloxane polymers with increasing solvent content. The rib distance was not affected by the relative roll speed and accurate production was possible for varying roll speed. This effect corroborated the robustness of the here-proposed process. The solvent content could be easily adjusted prior to production and offers a readily usable control parameter for the rib distance. At low solvent content (5 wt% 2-propanol), the siloxane was very sticky and the process control was poor. At higher solvent content (10 to 20 wt%), the process was very stable and the rib distance decreased from around 1.2 mm to 400  $\mu\text{m}$ . The dimensions accessible with the here-used conditions range from 0.1 mm to 1.6 mm. The ribs showed more distinct patterning (rib height) for lower velocities while at very high relative speeds ( $> 60 \text{ m s}^{-1}$ ) the ribs leveled. Latter effect may again be attributed to the pronounced shear-thinning properties of the resin (Figure 2-3).



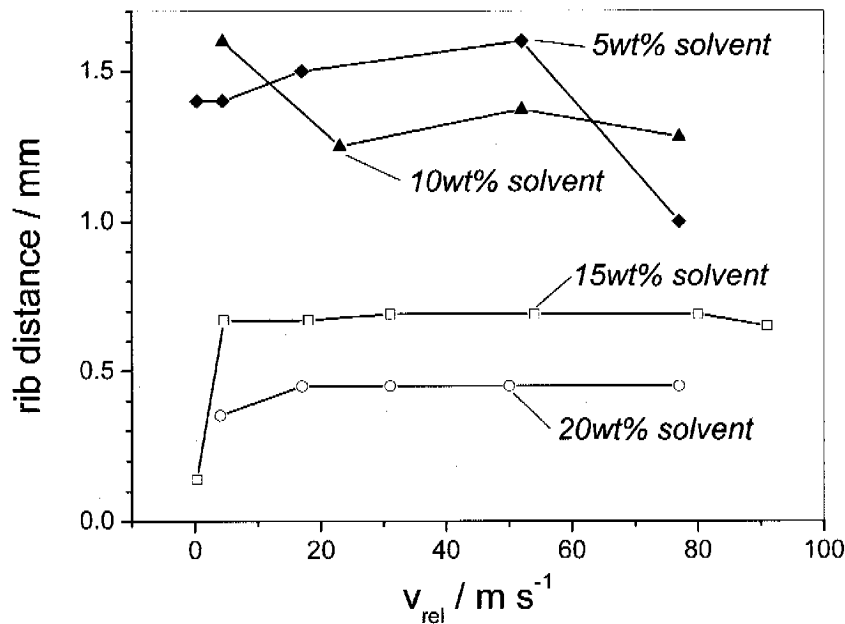


**Figure 2-7.** Rib distance versus the relative roll velocity  $v_{rel}$  at a constant gap width.

The present observations indicate that the critical capillary number has been exceeded in the investigated production runs. Using the measured Herschel-Bulkley parameters (Table 2-1) and the definition of the capillary number (Eq. 2.3), we find a capillary numbers of 5 to 25 which exceed the values attributed to stable film splitting laying below 0.1 for the conditions used (Eq. 2.6) [34]. The high capillary number can be primarily attributed to the relative high viscosity of the rheology-modified silicones (see Figure 2-4). The ribbing of the film was therefore a direct result of the instability at the film split. Once the structured polymer film leaves the roll gap, only the surface tension tries to smooth out the polymer film and thus exerts a shear stress onto the polymer. The high viscosity at low shear rate (Figure 2-4) results in high relaxation times. As a consequence, the structures formed at the film split were preserved throughout the fixation step by thermal curing. All structures (Figure 2-5) showed an alignment in machine direction as could be expected from the instability consideration. The most distinct pattern with high ribs was observed for low (5wt%) solvent content silicone i.e. for high viscosity of the fluid (Figure 2-5a, b, c). This behavior may rise from the fact that the higher the yield stress the higher the relaxation time and the lower the smoothing effect. The pattern of the structured surface ranged from branched ribs (Figure 2-

5a, b) for small gap distances (coating grammage  $\sim 3 \text{ g m}^{-2}$ ) to more parallel ribbing with less branching (Figure 2-5c) for larger gaps (coating grammage  $\sim 6 \text{ g m}^{-2}$ ). These results agree with earlier observations of saw tooth cusped patterns in forward coating roll flow for elastic fluids at high capillary numbers [34].

### 2.3.3. Adhesion properties

As an example of an industrially important application, the structured siloxane films were compared to conventionally prepared, smooth silicone coated polyethylene for their adhesion properties. The release forces of selected coatings were tested with commercially available pressure sensitive adhesives. Since all films were manufactured from the same silicone polymer, any influence caused by material properties could be excluded. The processing parameters and rib properties for all tested films are listed in Table 2-2.

**Table 2-2** Parameters of the fitted Herschel-Bulkley model for different resin compositions.

Sample	Solvent content, wt%	Grammage, $\text{g m}^{-2}$	Rel. velocity, $\text{m s}^{-1}$	Rib distance, mm
5sol	5	6.8	4.4	1.4
10sol	10	6.7	4.4	1.6
15sol	15	5.7	4.4	0.7
Ref	0	6	4.4	-

Release forces of a poly(acrylic acid) (tesa7475) and a rubber based (tesa7476) pressure sensitive adhesive were measured at a constant peel rate ( $0.3 \text{ m s}^{-1}$ ) and room temperature (Figure 2-8). For statistical relevance, at least ten measurements were conducted in parallel and the forces were averaged over the peel process. The errors were taken from the averaged minimal and maximal values. It can be clearly seen that the release force for the acrylic based adhesive (tesa7475) in general is rather low (around  $5 \text{ cN (25 mm)}^{-1}$ ) but a minimal value of  $2.7 \text{ cN (25 mm)}^{-1}$  was obtained for a structured sample prepared from 5wt% 2-propanol (5sol). Even the smooth reference silicone film showed relatively low adhesion values as silicone release films are generally more effective for acrylic based adhesives. As a consequence, the release properties are within a narrow range and predominantly depend on the material properties. A much larger effect on the release properties was observed for a rubber based adhesive which generally shows enhanced adhesion to silicone liners. The release forces could be drastically reduced by the ribbing as observed for samples 5sol, 10sol,

and 15sol (Figure 2-8). Again, a most effective reduction was found for sample 5sol with a long wavelength (1.4 mm) and distinct ribbing arising from the high yield stress of the low solvent content. Compared to a smooth surface (Ref) with similar coating thickness, the peel force of 5sol was reduced by a factor of eight. Moreover, the smaller standard deviation of the mean peel force values for structured films (approx.  $2 \text{ cN (25 mm)}^{-1}$ ) is much smaller than the one of an unstructured reference Ref (approx.  $6 \text{ cN (25 mm)}^{-1}$ ). This suggests that a higher control of the release properties could be achieved by using ribbed surface structures.

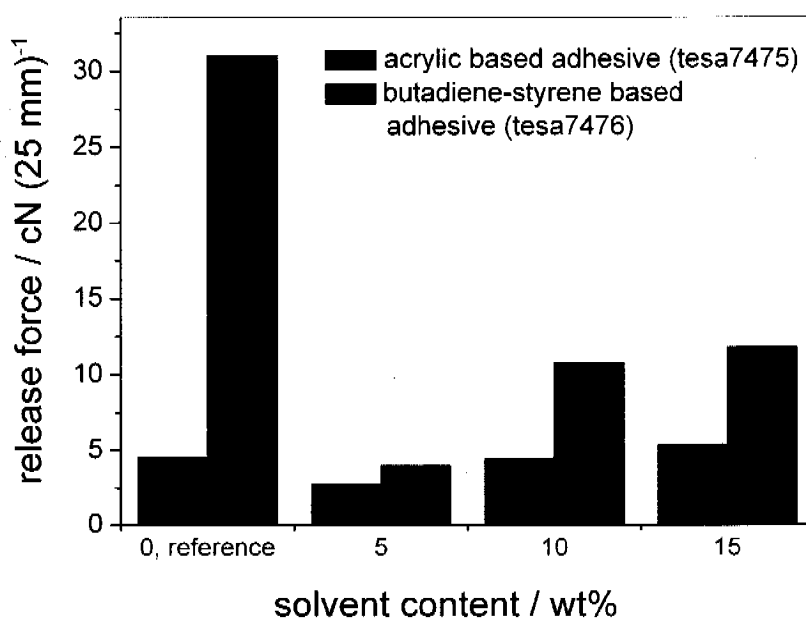


**Figure 2-8.** Release forces of two commercial pressure sensitive adhesives (tesa7475, tesa7476) for different coating properties.

## 2.4. Conclusions

A structured polymer coating was successfully applied on a flexible HDPE substrate by three roll direct coating in co-rotating mode which offers continuous, low cost production. The patterning arises due to the coating flow conditions chosen above the critical capillary number where instability in the film split occurs. The rheological behavior (Herschel-Bulkley fluid) of the silica-modified resin guarantees the preservation of the pattern throughout the fixation by thermal curing. Branched and single-tooth ribbing of high regularity were achieved with

dimensions of the pattern ranging from 0.1 mm to 1.6 mm. The ribbed PDMS coatings, having less adhesion-exposed surface area, exhibited up to eight times lower release forces if compared to the smooth reference coating. Effects were more significant for a rubber based adhesive (tesa7476) than for an acrylic based tape (tesa7475) attributed to inherent high adhesion of rubber tape to the PDMS. For this reason the proposed method is suitable for the production of very low adhesion surfaces and controlled release, especially for rubber based adhesives. The as-prepared PDMS patterns suggest the use for structure transfer to other substrates by means of stamping. Furthermore the highly economic production makes obtained structured coatings a promising candidate for application as friction reducing surface e.g. in aviation or seafaring.

## 2.5. Acknowledgements

Financial support by the Swiss Commission for Technology and Innovation, CTI project 7021.2 is kindly acknowledged.

## 2.6. References

- [1] Gordon G V, et al. 2000 Forcing the issue *Adhes. Age* **43** 41-44
- [2] Baier R E 1982 Conditioning Surfaces to Suit the Biomedical Environment - Recent Progress *J. Biomech. Eng.-Trans. ASME* **104** 257-71
- [3] Abbasi F and Mirzadeh H 2004 Adhesion between modified and unmodified poly(dimethylsiloxane) layers for a biomedical application *Int. J. Adhes. Adhes.* **24** 247-57
- [4] Yebra D M, Kiil S and Dam-Johansen K 2004 Antifouling technology - past, present and future steps towards efficient and environmentally friendly antifouling coatings *Prog. Org. Coat.* **50** 75-104
- [5] Owen M J 1996 Surface properties of silicone release coatings *JOCCA-Surf. Coat. Int.* **79** 400-03
- [6] Owen M J 2004 A review of significant directions in fluorosiloxane coatings *Surf. Coat. Int. Pt. B-Coat. Trans.* **87** 71-76
- [7] Kobayashi H and Owen M J 1995 Surface-Properties of Fluorosilicones *Trends Polym. Sci.* **3** 330-35
- [8] Gordon G V, Perz S V, Tabler R L, Stasser J L, Owen M J and Tonge J S 1998 Silicone release coatings: An examination of the release mechanism *Adhes. Age* **41** 35-42
- [9] Gordon G V, Moore P A, Popa P J, Tonge J S and Vincent G A 2002 Sticking lightly *Adhes. Age* **45** 24-31
- [10] Furstner R, Barthlott W, Neinhuis C and Walzel P 2005 Wetting and self-cleaning properties of artificial superhydrophobic surfaces *Langmuir* **21** 956-61
- [11] Otten A and Herminghaus S 2004 How plants keep dry: A physicist's point of view *Langmuir* **20** 2405-08
- [12] Barthlott W and Neinhuis C 1997 Purity of the sacred lotus, or escape from contamination in biological surfaces *Planta* **202** 1-8

- [13] Onda T, Shibuichi S, Satoh N and Tsujii K 1996 Super-water-repellent fractal surfaces *Langmuir* **12** 2125-27
- [14] Neinhuis C and Barthlott W 1997 Characterization and distribution of water-repellent, self-cleaning plant surfaces *Ann. Bot.* **79** 667-77
- [15] Ball P 1999 Engineering - Shark skin and other solutions *Nature* **400** 507-09
- [16] Bechert D W and Bartenwerfer M 1989 The Viscous-Flow on Surfaces with Longitudinal Ribs *Journal of Fluid Mechanics* **206** 105-29
- [17] Bechert D W, Bruse M and Hage W 2000 Experiments with three-dimensional riblets as an idealized model of shark skin *Exp. Fluids* **28** 403-12
- [18] Bechert D W, Bruse M, Hage W and Meyer R 2000 Fluid mechanics of biological surfaces and their technological application *Naturwissenschaften* **87** 157-71
- [19] Bechert D W, Bruse M, Hage W, VanderHoeven J G T and Hoppe G 1997 Experiments on drag-reducing surfaces and their optimization with an adjustable geometry *Journal of Fluid Mechanics* **338** 59-87
- [20] Eldada L and Shacklette L W 2000 Advances in polymer integrated optics *IEEE J. Sel. Top. Quantum Electron.* **6** 54-68
- [21] Yu K, Cong Y, Fu J, Xing R B, Zhao N and Han Y C 2004 Patterned self-adaptive polymer brushes by "grafting to" approach and microcontact printing *Surf. Sci.* **572** 490-96
- [22] Zhang Z X, Wang Z, Xing R B and Han Y C 2003 How to form regular polymer microstructures by surface-pattern-directed dewetting *Surf. Sci.* **539** 129-36
- [23] Tsukagoshi K, Mizutani W, Tokumoto H, Miyamae T and Nozoye H 2002 Selective vapor deposition polymerization on actively patterned surfaces *Surf. Sci.* **514** 48-53
- [24] McDonald J C, Duffy D C, Anderson J R, Chiu D T, Wu H K, Schueller O J A and Whitesides G M 2000 Fabrication of microfluidic systems in poly(dimethylsiloxane) *Electrophoresis* **21** 27-40
- [25] Xia Y N and Whitesides G M 1998 Soft lithography *Annu. Rev. Mater. Sci.* **28** 153-84
- [26] Kim E, Xia Y N and Whitesides G M 1995 Polymer Microstructures Formed by Molding in Capillaries *Nature* **376** 581-84
- [27] Becker H and Heim U 2000 Hot embossing as a method for the fabrication of polymer high aspect ratio structures *Sens. Actuator A-Phys.* **83** 130-35
- [28] Coyle D J, Macosko C W and Scriven L E 1986 Film-Splitting Flows in Forward Roll Coating *Journal of Fluid Mechanics* **171** 183-207
- [29] Benjamin D F, Anderson T J and Scriven L E 1995 Multiple Roll Systems - Steady-State Operation *Aiche Journal* **41** 1045-60
- [30] Greener Y and Middleman S 1975 Theory of Roll Coating of Viscous and Viscoelastic Fluids *Polym. Eng. Sci.* **15** 1-10
- [31] Carvalho M S and Scriven L E 1997 Deformable roll coating flows: Steady state and linear perturbation analysis *Journal of Fluid Mechanics* **339** 143-72
- [32] Carvalho M S and Scriven L E 1999 Three-dimensional stability analysis of free surface flows: Application to forward deformable roll coating *Journal of Computational Physics* **151** 534-62
- [33] Decre M, Gailly E and Buchlin J M 1996 Meniscus control by string in roll coating experiment *Aiche Journal* **42** 1583-89
- [34] Grillet A M, Lee A G and Shaqfeh E S G 1999 Observations of ribbing instabilities in elastic fluid flows with gravity stabilization *Journal of Fluid Mechanics* **399** 49-83
- [35] Hasegawa T and Sorimachi K 1993 Wavelength and Depth of Ribbing in Roll Coating and Its Elimination *Aiche Journal* **39** 935-45
- [36] Pearson J R A 1960 The Instability of Uniform Viscous Flow under Rollers and Spreaders *Journal of Fluid Mechanics* **7** 481-500
- [37] Pitts E and Greiller J 1961 The Flow of Thin Liquid Films between Rollers *Journal of Fluid Mechanics* **11** 33-50
- [38] Mill C C and South G R 1967 Formation of Ribs on Rotating Rollers *Journal of Fluid Mechanics* **28** 523-29

- [39] Greener J, Sullivan T, Turner B and Middleman S 1980 Ribbing Instability of a 2-Roll Coater - Newtonian Fluids *Chem. Eng. Commun.* **5** 73-83
- [40] Rabaud M, Michalland S and Couder Y 1990 Dynamical Regimes of Directional Viscous Fingering - Spatiotemporal Chaos and Wave-Propagation *Phys. Rev. Lett.* **64** 184-87
- [41] Coyle D J, Macosko C W and Scriven L E 1990 Stability of Symmetrical Film-Splitting between Counter-Rotating Cylinders *Journal of Fluid Mechanics* **216** 437-58
- [42] Shaqfeh E S G 1996 Purely elastic instabilities in viscometric flows *Annu. Rev. Fluid Mech.* **28** 129-85
- [43] Greener J and Middleman S 1981 Reverse Roll Coating of Viscous and Viscoelastic Liquids *Industrial & Engineering Chemistry Fundamentals* **20** 63-66
- [44] Saffman P G and Taylor G 1958 The Penetration of a Fluid into a Porous Medium or Hele-Shaw Cell Containing a More Viscous Liquid *Proceedings of the Royal Society of London Series a-Mathematical and Physical Sciences* **245** 312-29
- [45] McCloud K V and Maher J V 1995 Experimental Perturbations to Saffman-Taylor Flow *Phys. Rep.-Rev. Sec. Phys. Lett.* **260** 139-85
- [46] Lindner A, Coussot P and Bonn D 2000 Viscous fingering in a yield stress fluid *Phys. Rev. Lett.* **85** 314-17
- [47] Loher S and Stark W J 2005 *Method for the application of a structured coating upon a smooth surface* PCT patent application

### **3. Improved degradation and bioactivity of amorphous aerosol derived tricalcium phosphate nanoparticles in poly(lactide-co-glycolide)**

#### **Abstract**

The industrially used flame synthesis of silica polymer fillers was extended to amorphous tricalcium phosphate (ATCP) nanoparticles and resulted in a similar morphology as the traditionally used polymer fillers. Doping of poly(lactide-co-glycolide) (PLGA) with such highly agglomerated ATCP was investigated for mechanical properties, increased in vitro biodegradation and the formation of a hydroxyapatite layer on the surface of the nanocomposite. PLGA films with particle loadings ranging from 0 to 30 wt% were prepared by solvent casting. Degradation in simulated body fluid (SBF) at 37 °C under sterile conditions for up to 42 days was followed by Raman spectroscopy, scanning electron microscopy (SEM), thermal analysis and tensile tests. The presence of nanoparticles in the PLGA matrix slightly increased the Young's modulus up to 30% compared to pure polymer reference materials. The nanoparticles doped films showed a significantly increased loss of polymer mass during degradation. Scanning electron microscopy images of doped films showed that the SBF degraded the PLGA by corrosion as facilitated by the incorporation of nanoparticulate calcium phosphate. Raman spectroscopy and X-ray powder diffraction revealed that the deposition of about 10 nm sized hydroxyapatite crystallites on the surface of doped PLGA films was strongly increased by the addition of tricalcium phosphate fillers. The combination of increased hydroxyapatite formation and enhanced polymer degradation may suggest the use of such amorphous, aerosol derived ATCP fillers for applications in non-load-bearing implant sites.

### 3.1. Introduction

The use of biodegradable polymers in modern surgery has helped to strongly reduce postoperative stress and the need for secondary operations. Poly(lactide-co-glycolide) (PLGA) has been known for decades as a biocompatible and bioresorbable polymer [1-4] with applications ranging from drug delivery [5, 6] to soft tissue engineering [7], nerve regeneration [8] and bone surgery [9, 10]. Especially in orthopedics, many investigated characteristics such as an increased control on implant degradation rate and a tighter bond to existing bone are offering a continuing challenge to biomaterials development. PLGA itself is available from controlled copolymerization and allows in part control of the rate of degradation at the expense of mechanical properties [11, 12]. A reinforcement of PLGA may be achieved by addition of polymer fillers.

Calcium phosphates have been widely used as biomaterials because of their biocompatibility and osteoconductivity [13, 14]. Tricalcium phosphate ( $\text{Ca}_3(\text{PO}_4)_2$ ) excels in terms of degradability and bioactivity [13, 15, 16] which has resulted in frequent use in clinical applications. Amorphous calcium phosphate (ATCP) with enhanced solubility has attracted much interest as it has been postulated as a precursor of hydroxyapatite formation [17-20]. Earlier work on composite materials of polymethacrylate and precipitated, 0.1-80  $\mu\text{m}$  sized ATCP resulted in high-release of calcium and phosphate ions, enhanced bioactivity and the incorporation of undesired pyrophosphate impurities [21-23]. The use of micrometer sized, crystalline tricalcium phosphate with low surface area ( $< 1 \text{ m}^2 \text{ g}^{-1}$ ) in poly( $\alpha$ -hydroxy acids) led to hindered degradation [24] and additionally showed unfavorable mechanical properties upon degradation [25]. A comparison to industrially applied flame aerosol derived silica fillers shows that specific particle size and morphology are required for elastomer fillers.

It has been shown previously that the incorporation of nanometer-sized but persistent titania in PLGA resulted in higher osteoblast functions attributed to the obtained nanostructured surface mimicking the structure of natural bone [26, 27]. Additionally carbon nanotubes dispersed in a polymer matrix have been shown to promote osteoblast cell response [28] although the cytotoxicology of the non-degradable carbon nanotubes is fiercely debated. Therefore the application of nanoscale polymer fillers with desired morphology is not only expected to improve mechanical properties but may also result in more effective orthopedic implants.



Most recently, the industrial aerosol process has been extended to the preparation of complex materials such as phosphates, fluoro-apatites or doped salts [29, 30] in the form of agglomerated nanoparticles with similar morphology as the currently used silica polymer fillers. We therefore decided to investigate the use of such amorphous calcium phosphate aerosols as degradable polymer fillers. Composite materials with up to 30 wt% inorganic filler were compared to pure PLGA. Materials were investigated by a combination of thermo-analysis, X-ray diffraction, tensile tests, electron microscopy and Raman spectroscopy for up to 42 days of degradation in simulated body fluid. Our findings revealed an increased degradation of the polymer composite and strongly enhanced formation of hydroxyapatite crystallites on the composite surface.

## **3.2. Materials and methods**

In order to test PLGA/ATCP composite materials for their degradation properties, films of the corresponding materials were prepared by solvent casting. Since numerous clinical applications require degradable implant materials in the form of screws, plates, rods or other shapes, measurements on the tensile strength of the composites were included as to show how the addition of ATCP affected the mechanical properties of the PLGA polymer.

### **3.2.1. Preparation of PLGA/ATCP composites**

Clinically used poly(lactide-co-glycolide) (PLGA) with a copolymer ratio of 85:15 (Resomer® Sample MD Type RG) was purchased from Boehringer Ingelheim with a weight and number average molecular weight of 453'100 g/mol and 203'300 g/mol, respectively. Amorphous tricalcium phosphate nanoparticles (ATCP, chemical formula:  $\text{Ca}_3(\text{PO}_4)_2$ ) were prepared by flame spray pyrolysis [29]. PLGA/ATCP films were synthesized using solvent casting for PLGA/ATCP weight ratios of 100/0, 90/10, 80/20, and 70/30. As-prepared ATCP nanoparticles were sieved (315  $\mu\text{m}$  mesh) and dispersed in chloroform ( $\geq 99\%$ , MERCK) at a concentration of 0.01-0.02 g  $\text{ml}^{-1}$  using an ultrasonic processor (UP400S, 24 kHz, Hielscher GmbH) at 200W for 4 min using pulsed intervals (50%) to allow for relaxation of the particles in the solvent. Corresponding amounts of polymer were subsequently dissolved in the dispersion up to a final polymer concentration of 5 wt%. For references, the neat solvent was used for polymer dissolution. As-obtained solutions were poured in Teflon molds, fixed on pre-cooled (30min at 4 °C) glass plates and dried at room temperature (12 hours). The

films were put in a vacuum oven at 75°C for 48 hours to guarantee removal of residual solvent as confirmed by thermo-gravimetric analysis (TGA). For all degradation studies, all required films were prepared simultaneously from the same batch of material. Films with a thickness of 120-150  $\mu\text{m}$  were then cut into dogbones (stressed length 12.6 mm, width 2 mm) and randomly assigned to be used for different degradation times. Experiments with different PLGA/ATCP composition were made using at least 5 identically treated samples in parallel.

### **3.2.2. Characterization of ATCP nanoparticles and PLGA/ATCP composites**

The specific surface area of the ATCP was analyzed by nitrogen adsorption at 77K using the Brunauer-Emmett Teller (BET) method on a Tristar instrument (Micromeritics Instruments) after outgassing at 150 °C for 1 h. For Fourier transform infrared spectroscopy (FTIR), 1wt% of powder was mixed with KBr (Fluka, puriss) and examined on a Tensor 27 spectrometer (Bruker Optics, 4000  $\text{cm}^{-1}$  <  $\lambda$  < 400  $\text{cm}^{-1}$ , 16 scans, 4 $\text{cm}^{-1}$  resolution) equipped with a diffuse reflectance accessory (DiffusIR™, Pike Technologies). Mechanical properties were obtained by tensile tests of at least five specimens on a Instron 4411 (Instron Co.) at ambient conditions with a crosshead speed of 12.6 mm min<sup>-1</sup>. The morphology of the polymer films was followed by scanning electron microscopy (SEM, Hitachi S-900 operated at 1 kV) after platinum-sputtering. Differential scanning calorimetry (DSC) was performed on a Mettler Toledo DSC-822e in a temperature range of -20 to 200 °C using a heating rate of 10 °C min<sup>-1</sup>. Surface properties and composition of polymer films were further studied by Raman spectroscopy on an EQUINOX 55 spectrometer equipped with a FT-Raman accessory FRA 160/S (Bruker Optics) in backscattering mode (laser power 450 mW, 4000 scans, 4  $\text{cm}^{-1}$  resolution). For thermo-gravimetric analysis (TGA) approximately 20 mg of sample were heated from room temperature up to 700 °C at 5 °C min<sup>-1</sup> under air (TGA/SDTA851e, Mettler Toledo).

The influence of immersion in simulated body fluid on the crystal phase of the tricalcium phosphate filler was investigated by X-ray powder diffraction (XRD). Selected sample films were dissolved in chloroform to remove the polymer and the insoluble, calcium phosphate residual was extracted and washed repeatedly with pure chloroform. XRD patterns were collected from the as-extracted or additionally sintered (1 h at 900 °C) residuals using a Siemens powder X-ray diffractometer (Ni-filtered  $\text{CuK}_\alpha$  radiation, step mode, step size of

0.3°, ambient conditions). Crystallite size was calculated using the Scherrer equation following the procedure outlined by Langford and Wilson [31].

### **3.2.3. Degradation protocol**

Simulated body fluid (SBF) was prepared according to Kokubo et al. [32] and sterile-filtered through a Nalgene® pre-sterilized filter unit. Sample weights before ( $W_0$ ) and after degradation ( $W_d$ ,  $W_w$ , see below) were recorded individually. After UV-sterilization (50 W/m<sup>2</sup>, 2 hours), samples were immersed in 500 ml SBF for 1, 3, 7, 21, and 42 days at 37 °C (climatized room). The SBF was changed after 1 and 4 weeks to guarantee a constant liquid composition. Furthermore, the amount of Ca<sup>2+</sup> ions that could be released from the samples was small in comparison to the Ca<sup>2+</sup> content of the 500 ml SBF. After removal, samples were rinsed with Millipore water, carefully wiped, and weighted before (wet weight,  $W_w$ ) and after air drying for 12 h at room temperature (dry weight,  $W_d$ ). The weight loss ( $L$ ) was determined by  $L = (W_0 - W_d)/W_0$  and the water uptake ( $U$ ) calculated according to  $U = (W_w - W_d)/W_d$ . The mechanical properties were tested after the 12 h drying (see above) and measured at room temperature (298 K).

### **3.2.4. Statistical methods**

Experiments were carried out using five samples of identically treated and processed materials from the same batch of polymer or ATCP nanoparticles in parallel. For all figures data were represented as values  $\pm$  standard error for absolute values and as (values  $\pm$  standard error) over (mean experimental values) for relative changes of a measurable quantity, e.g. polymer mass loss, inorganics content with respect to pure PLGA or the corresponding property before degradation. Effects of the various ATCP content on the composite were statistically analyzed with a  $p < 0.05$  significance level using a two-factorial Bonferroni/Dunn analysis of variance test taking experiment number and ATCP content as factors.

### 3.3. Results and Discussions

#### 3.3.1. Tricalcium phosphate nanoparticle filler properties

Flame spray synthesis resulted spherical, amorphous and highly agglomerated tricalcium phosphate nanoparticles (Figure 3-1) [29]. This powder morphology is similar to the one of industrially used silica polymer fillers. As-prepared nanoparticles exhibited a specific surface area of  $80 \pm 2 \text{ m}^2 \text{ g}^{-1}$  which is consistent with earlier studies [29].

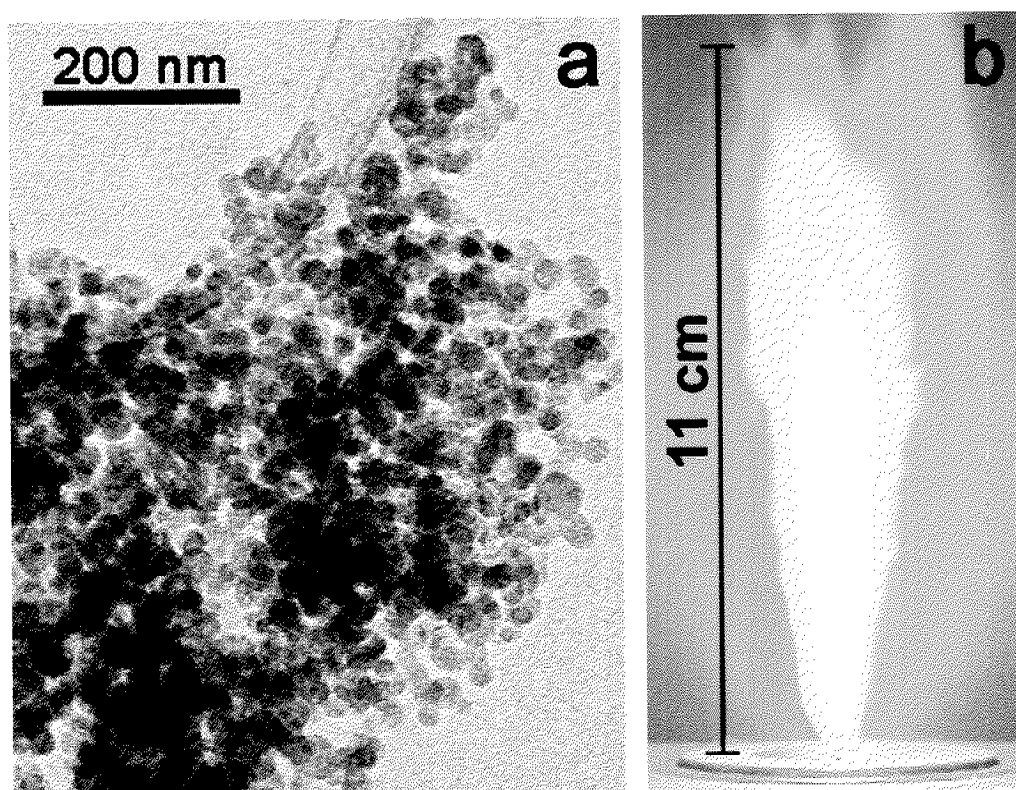


**Figure 3-1.** Transmission electron microscopy image of as-prepared tricalcium phosphate nanoparticles (a). Spherical, highly agglomerated particles result from the flame spray process resembling the morphology of silica produced by flame aerosol synthesis. The burning spray of a flame synthesis reactor during production of tricalcium phosphate (b) showing orange light emission of calcium.

X-ray diffraction (XRD) showed no distinct pattern and Fourier transform Infrared spectroscopy (FTIR) spectroscopy (Figure 3-2a) resulted in broad absorption bands. Both measurements corroborated the amorphous structure of the as-prepared powder. FTIR-

absorptions between  $1550\text{ cm}^{-1}$  and  $1400\text{ cm}^{-1}$  indicated the presence of minute amounts of carbonate in the as-prepared material while the bands at  $3800\text{ cm}^{-1}$  to  $3200\text{ cm}^{-1}$  and around  $1600\text{ cm}^{-1}$  corresponded to physisorbed water. After sintering at  $900\text{ }^{\circ}\text{C}$  for 1 hour in air, distinct, characteristic peaks for  $\beta$ -TCP [33] were observed.

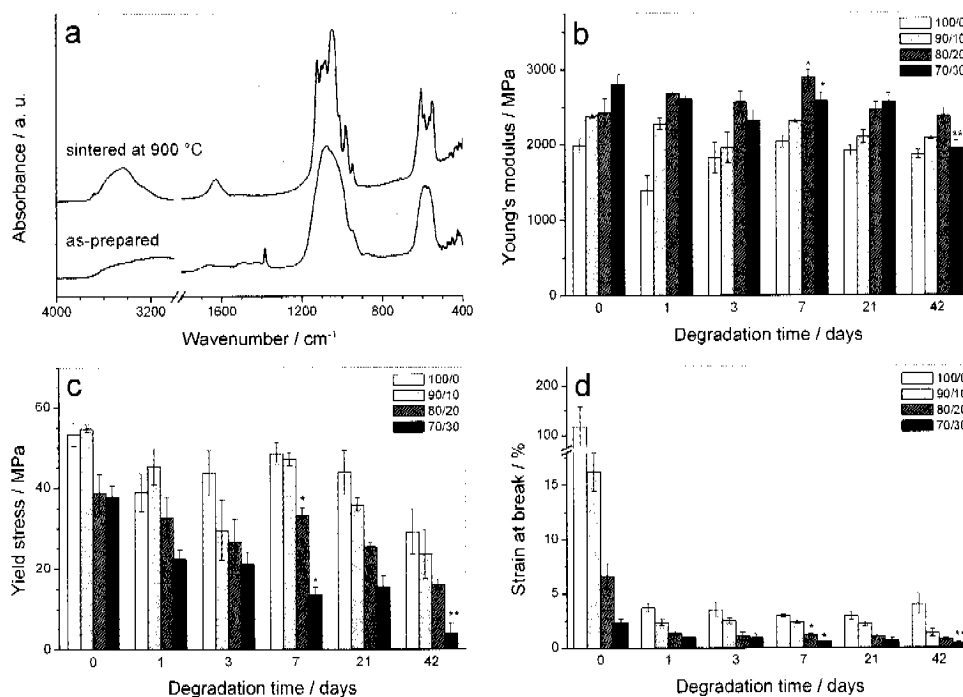


**Figure 3-2.** Fourier transform infrared spectra of as-prepared and sintered tricalcium phosphate nanoparticles produced by flame spray synthesis (a). Broad absorption bands for as-prepared powder transform into distinct peaks characteristic for  $\beta$ -TCP after crystallization by calcination. Young's modulus (b), yield stress (c), and strain at break (d) of undoped and ATCP-doped PLGA as a function of degradation time. \* two specimens tested, \*\* one specimen tested.

### 3.3.2. Mechanical properties of PLGA/ATCP nanocomposites

In order to study the influence of aerosol derived tricalcium phosphate fillers on the mechanical properties of PLGA, a series of doped polymer samples was tested before and after degradation in SBF at  $37\text{ }^{\circ}\text{C}$ . Sterile conditions ensured that no bacterial or fungal degradation contributed to polymer dissolution. The incorporation of calcium phosphate nanoparticles had a positive effect on the Young's modulus (Figure 3-2b): For as-prepared samples the elastic modulus was increased by 20 – 40 % relative to PLGA references and

remained consistent during degradation. In contrast, the yield stress (Figure 3-2c) was negatively affected by the addition of the inorganic filler and reduced by 30 to 50 % depending on the loading and the degradation time. Strong changes were observed for the strain at break (Figure 3-2d). Pure PLGA showed a 120% elongation at break before degradation. Latter value was strongly reduced to 15 or 2.4% elongation for materials containing 10 or 30 wt% ATCP. However, after one day of immersion in SBF, the pure PLGA (100/0) also lost most of its ductility (strain at break of 3.7%) and became comparable to doped samples (2.4% for sample 90/10, see Figure 3-2d). After this initial strong decrease of elongation at break for pure PLGA, the brittleness of all materials remained relatively constant during up to 6 weeks degradation.

### **3.3.3. Mass loss and water uptake**

Increasing or controlling the rate of polymer degradation is a major target in polymer based biomaterials development. During in vitro treatment with simulated body fluid, two processes are altering the structure and composition of a bioactive polymer composite: Polymer degradation removes PLGA mass. Hydroxyl-apatite deposition simultaneously occurs and enables the surrounding bone tissue to better bind the implant material. Ideally, the degradation process offers a smooth transition between a mainly polymer based stability to a regenerated bone material.

In order to accurately follow these two competing processes, we measured the composite or polymer mass loss after degradation, the reversible water uptake as a measure for porosity and swelling (Figure 3-3) and the inorganic content of the composite (Figure 3-6a). Since the mass of the composite after degradation consists of inorganics (measured thermo-gravimetrically after removal of the polymer by combustion), water (measured as the weight difference before and after drying) and remaining PLGA, the polymer degradation could be calculated from the sample mass and the content of water and inorganics. While for the pure PLGA (100/0) hardly any change in mass was detectable even after six weeks (0.5% mass loss at 42 days) the tricalcium phosphate doped PLGA composites degraded significantly faster (Figure 3-3a) and the weight of samples 80/20 and 90/10 was reduced by about 4% after 42 days. Doping of 30 % inorganic tricalcium phosphate filler (sample 70/30) even resulted in the degradation of ~7% of the composite mass. Pure PLGA was not prone to pronounced swelling (water uptake around 2 % after 42 days) while the water uptake of doped

PLGA increased gradually to 14 wt% for a composite with 30 wt% tricalcium phosphate (Figure 3-3b). Obviously, the pure PLGA degraded very slowly while the incorporation of amorphous tricalcium phosphate filler accelerated the degradation process. The higher water uptake indicated the formation and later filling of pores generated during the degradation process. One possible mechanism would involve such pores remaining from the degradation of amorphous tricalcium phosphate to result in a larger polymer surface being exposed to the surrounding liquid. The strongly increased exchange surface would favor the relatively slow polymer degradation. Obviously, the deposition of hydroxyl-apatite was significantly slower than the degradation of ATCP since the formation of deposits would contribute to the sample mass. In order to test this hypothesis, we investigated the surface of degraded samples by scanning electron microscopy (SEM) after sputtering with platinum for increased contrast.

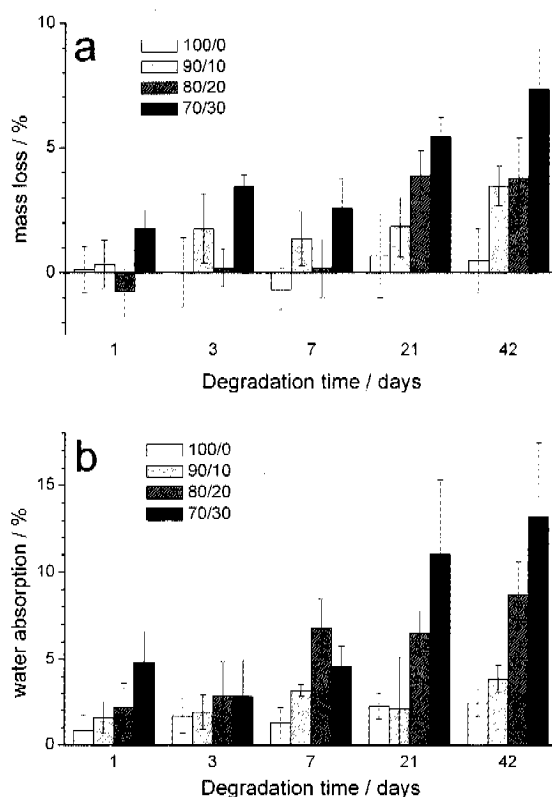


**Figure 3-3.** Mass loss (a) and water absorption (b) of different PLGA/ATCP nanocomposites in percent as a function of degradation time.

### 3.3.4. Surface properties

Non-degraded, pure PLGA (Figure 3-4a) exhibited a very smooth surface with virtually no visual changes even after immersion in SBF for 42 days (Figure 3-4b). Doping of tricalcium phosphate into the PLGA resulted in a minor surface roughness for sample 90/10 (Figure 3-4c) before immersion. The surface topography was substantially altered for samples containing 30wt% of ATCP (Figure 3-4e): After degradation for 6 weeks, samples exhibited clearly observable surface features (Figure 3-4d and f). This superficial roughening could now be attributed to either formation of hydroxyapatite crystals or the exposure of agglomerated ATCP nanoparticles as a result of degradation of polymer.

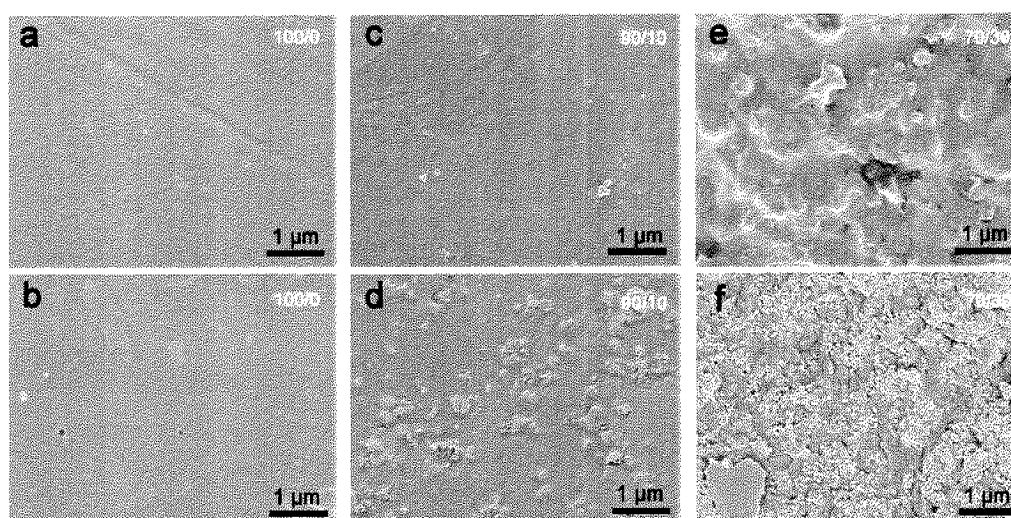


**Figure 3-4.** Surface morphology of PLGA/ATCP nanocomposites before (top) and after degradation for 42 days (bottom) in SBF. Undoped PLGA (a, b) showed a smooth surface with no visual detectable changes after degradation. Low-doped sample 90/10 (c, d) and especially high-doped sample 70/30 (e, f) inherently exhibited a roughened surface. After degradation those samples showed a clearly distinct patterned surface which can be attributed either to degradation of the polymer and/or to hydroxyapatite deposition.

### 3.3.5. Thermal analysis

Differential scanning calorimetry (DSC) of samples before degradation (Figure 3-5) revealed the amorphous state of the polymer through a pronounced exothermic peak at the glass transition temperature  $T_g$  of the PLGA. Incorporation of particles had no influence on the thermal properties of the composites in the investigated temperature range. After degradation,



samples still exhibited an amorphous structure since no melting could be detected. Since the endothermic DSC signal is proportional to the polymer mass in the sample, the much lower DSC signal of sample 70/30 after 6 weeks of degradation corroborated a larger polymer loss for doped PLGA. A corresponding blind experiment ruled out the influence of the solvent casting.

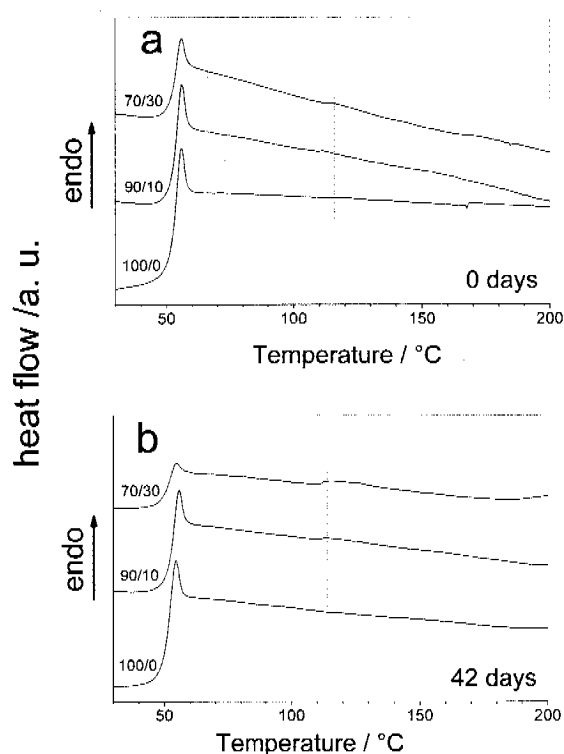


**Figure 3-5.** Differential scanning calorimetry of PLGA/ATCP nanocomposites before (a) and after (b) degradation for 42 days revealed the amorphous state of the polymer. The endothermic event at around 110 °C may be attributed to desorbing water.

Thermo-gravimetric analysis further allowed the determination of content of inorganic filler and deposits in the sample during degradation by selectively burning off the organic polymer at around 600 °C (Figure 3-6a). An increase of the inorganic content could either be attributed to the resorption/loss of polymeric matrix or to the formation of hydroxyapatite on the surface of the sample. Starting from 29.1% inorganics in sample 70/30 before degradation, the inorganics content linearly increased over degradation time to 45.6 wt% after six weeks of

immersion in SBF. In contrast, the pure PLGA polymer contained less than 3 wt% inorganics before or after degradation and did not show a statistically significant change in inorganics content. These results strongly suggest that the incorporation of ATCP at up to 30 wt% clearly enhanced the resorption of PLGA *in vitro* and promoted the deposition of minerals on the composite surface.

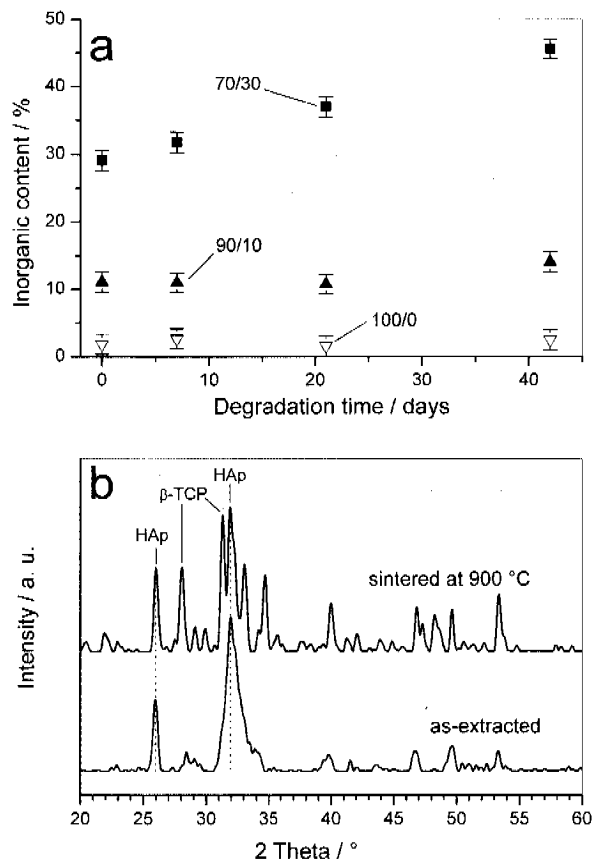


**Figure 3-6.** Inorganic content (a) of PLGA (open triangles) and PLGA/ATCP composites (closed symbols) over degradation time as detected by thermo-gravimetric analysis. X-ray powder diffraction patterns (b) of as-extracted and sintered residual of sample 80/20 after 42 days of immersion in SBF.

### 3.3.6. Surface composition of PLGA/ATCP composites

In order to further investigate the properties of the inorganic deposits, the surface composition of samples before and after degradation was followed by Raman spectroscopy (Figure 3-7) as suggested by Notingher et al. [34]. Spectra of as-prepared PLGA/ATCP samples before

degradation (Figure 3-8) revealed increasing absorption bands of ATCP for increasing calcium phosphate content and corroborated the presence of TCP in the material. The broad, intense absorption of  $\text{PO}_4^{3-}$  bands from ATCP disappeared after one day of immersion indicating the fast dissolution of calcium phosphate from regions at the vicinity of the film surface. These findings ruled out the previous stated hypothesis of ATCP exposure by degradation of PLGA. Strong absorption bands at  $3000\text{ cm}^{-1}$  ( $\nu_{\text{asymmetric}}\text{CH}_3$ ),  $2944\text{ cm}^{-1}$  ( $\nu_{\text{symmetric}}\text{CH}_3$  and  $\nu_{\text{asymmetric}}\text{CH}_2$ ),  $2881\text{ cm}^{-1}$  ( $\nu\text{CH}$ ) and  $870\text{ cm}^{-1}$  ( $\nu\text{CC}$ ) could be attributed to amorphous PLGA [35-37] and were detected throughout the whole *in vitro* study (Figure 3-8).

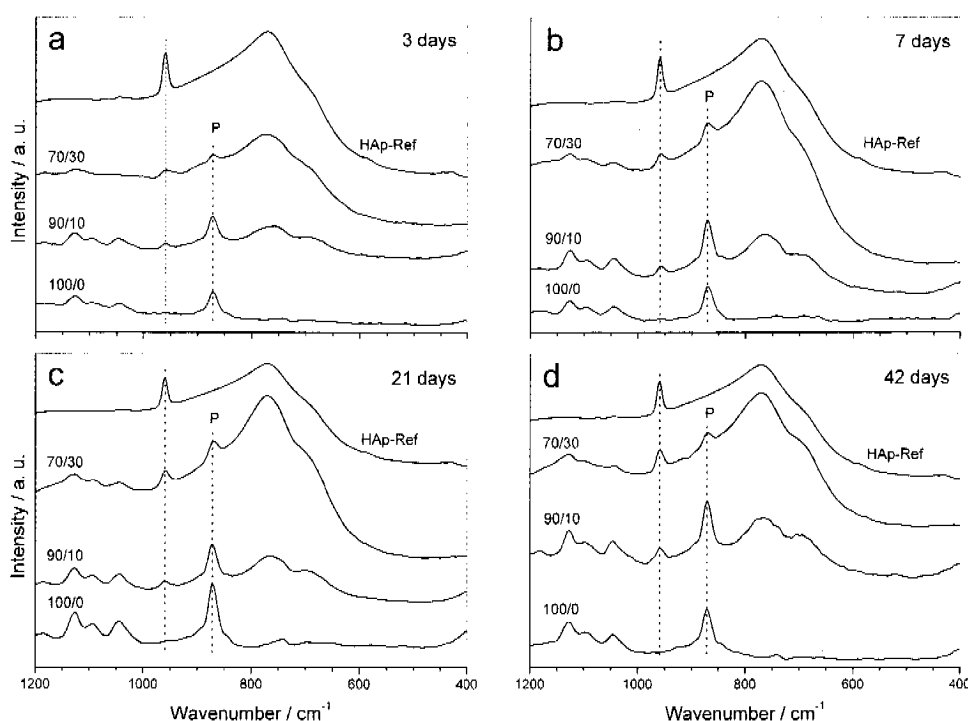


**Figure 3-7.** Raman spectra of pure PLGA and PLGA/ATCP nanocomposites after degradation for 3 days (a), 7 days (b), 21 days (c), and 42 days (d). Distinct peaks at  $960\text{ cm}^{-1}$  characteristic for hydroxyapatite (HAp) were observed for ATCP containing samples. The ratio of the polymer-specific signal (P,  $870\text{ cm}^{-1}$ ) to the HAp signal ( $960\text{ cm}^{-1}$ ) strongly increased with filler content and degradation time.

The ability of a biomaterial to induce or assist the formation of novel bone material on an implant surface, i.e. its osteoconductive properties, can be estimated by the *in vitro* formation of hydroxyapatite on the implant surface [38-40]. Raman spectra of hydroxyapatite

(HAp) are characterized by a pronounced absorption peak at  $960\text{ cm}^{-1}$  corresponding to the P-O symmetric vibration of the  $\text{PO}_4^{3-}$  groups [41, 42]. After immersion in SBF for 3 days (Figure 3-7a), small absorption bands at  $960\text{ cm}^{-1}$  were present in ATCP containing samples (samples 90/10 and 70/30), indicating the presence of hydroxyapatite. These peaks continuously grew with degradation time while for the pure PLGA (100/0), no absorption was observed over the investigated period of time (Figure 3-7b, c, d).

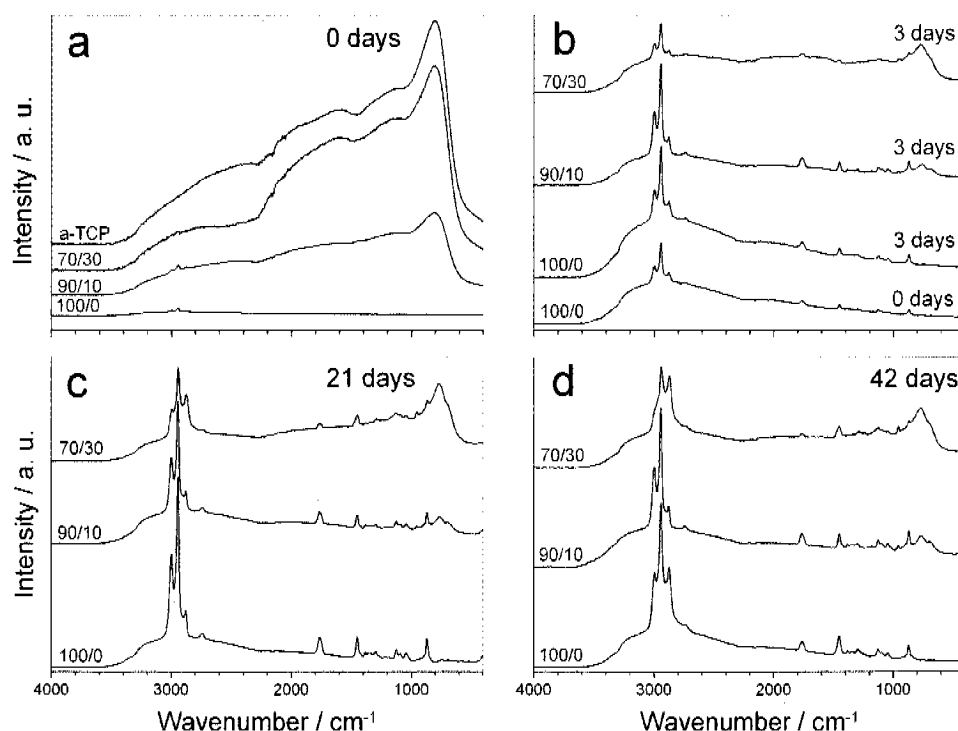


**Figure 3-8.** Raman spectra of pure PLGA and PLGA/ATCP nanocomposites after degradation for 3 days (a), 7 days (b), 21 days (c), and 42 days (d). Distinct peaks at  $960\text{ cm}^{-1}$  characteristic for hydroxyapatite (HAp) were observed for ATCP containing samples. The ratio of the polymer-specific signal (P,  $870\text{ cm}^{-1}$ ) to the HAp signal ( $960\text{ cm}^{-1}$ ) strongly increased with filler content and degradation time.

The composition of the inorganic material was further investigated by X-ray powder diffraction (XRD). XRD pattern (Figure 3-6b) of the as-extracted residual of degraded sample 80/20 showed distinct peaks characteristic for hydroxyapatite with most pronounced intensity at  $2\theta$  equal  $31.8^\circ$  [43]. Using the Scherrer equation, a crystallite size of approximately 10

nm could be determined. Similar values are found for natural bone material [44]. After sintering at 900 °C a second set of peaks could be assigned to  $\beta$ -TCP (2 $\theta$  equal 31°) [45]. The formation of  $\beta$ -TCP was attributed to the crystallization of remaining ATCP in the nanocomposite at temperatures around 900 °C and stays in agreement with earlier studies [29].

### 3.4. Conclusions

The use of a similar manufacturing method as for industrially used silica polymer fillers allowed the production of highly agglomerated amorphous tricalcium phosphate nanoparticles. The aerosol derived degradable filler could readily be incorporated into PLGA polymer films by solvent casting. Doping with up to 30wt% of filler increased the elastic modulus by about 30% while the ductility decreased. The composite material showed a strongly enhanced polymer degradation rate if compared to the pure, undoped PLGA polymer. While for pure PLGA no hydroxyapatite formation was observed during degradation, tricalcium phosphate filled polymers showed deposition of small, 10 nm sized hydroxyapatite crystals on the surface of the composite. This indicates improved osteoconductive properties of PLGA doped with aerosol derived ATCP. The fast degradation and the superior bioactivity make these nanocomposites a promising material for application in orthopedic medicine.

### 3.5. Acknowledgements

Financial support by the Swiss Commission for Technology and Innovation, CTI project 7021.2 and the Gebert-Rüf Foundation Project No. 048/04 is kindly acknowledged. Further we thank Kirill Feldman and Matthias Goessi (ETH Zurich) for help and support on mechanical testing.

### 3.6. References

- [1] Gilding D K and Reed A M 1979 Biodegradable Polymers for Use in Surgery - Polyglycolic-Poly(Actic Acid) Homopolymers and Copolymers .1. *Polymer* **20** 1459-64
- [2] Reed A M and Gilding D K 1981 Biodegradable Polymers for Use in Surgery - Poly(Glycolic)-Poly(Lactic Acid) Homo and Co-Polymers .2. Invitro Degradation *Polymer* **22** 494-98

- 
- [3] Ignatius A A and Claes L E 1996 In vitro biocompatibility of bioresorbable polymers: Poly(L,DL-lactide) and poly(L-lactide-co-glycolide) *Biomaterials* **17** 831-39
  - [4] Bostman O and Pihlajamaki H 2000 Clinical biocompatibility of biodegradable orthopaedic implants for internal fixation: a review *Biomaterials* **21** 2615-21
  - [5] Song C X, Labhasetwar V, Murphy H, Qu X, Humphrey W R, Shebuski R J and Levy R J 1997 Formulation and characterization of biodegradable nanoparticles for intravascular local drug delivery *J. Control. Release* **43** 197-212
  - [6] Huang Y C, Connell M, Park Y, Mooney D J and Rice K G 2003 Fabrication and in vitro testing of polymeric delivery system for condensed DNA *J. Biomed. Mater. Res. Part A* **67A** 1384-92
  - [7] Pattison M A, Wurster S, Webster T J and Haberstroh K M 2005 Three-dimensional, nano-structured PLGA scaffolds for bladder tissue replacement applications *Biomaterials* **26** 2491-500
  - [8] Bini T B, Gao S J, Tan T C, Wang S, Lim A, Hai L B and Ramakrishna S 2004 Electrospun poly(L-lactide-co-glycolide) biodegradable polymer nanofibre tubes for peripheral nerve regeneration *Nanotechnology* **15** 1459-64
  - [9] Middleton J C and Tipton A J 2000 Synthetic biodegradable polymers as orthopedic devices *Biomaterials* **21** 2335-46
  - [10] An Y H, Woolf S K and Friedman R J 2000 Pre-clinical in vivo evaluation of orthopaedic bioabsorbable devices *Biomaterials* **21** 2635-52
  - [11] Agrawal C M, Athanasiou K A and Heckman J D 1997 Biodegradable PLA-PGA polymers for tissue engineering in orthopaedics *Porous Materials for Tissue Engineering* ed Liu D M, Dixit V (Zurich-Uetikon: Trans Tec Publications Ltd) pp 115-28.
  - [12] Athanasiou K A, Niederauer G G and Agrawal C M 1996 Sterilization, toxicity, biocompatibility and clinical applications of polylactic acid polyglycolic acid copolymers *Biomaterials* **17** 93-102
  - [13] Jarcho M 1981 Calcium-Phosphate Ceramics as Hard Tissue Prosthetics *Clin. Orthop. Rel. Res.* 259-78
  - [14] de Groot K 1983 *Bioceramics of Calcium Phosphate*. (Boca Raton: CRC Press)
  - [15] Klein C, Deblieckhogervorst J M A, Wolke J G C and Degroot K 1990 Studies of the Solubility of Different Calcium-Phosphate Ceramic Particles Invitro *Biomaterials* **11** 509-12
  - [16] Klein C, Driessen A A and Degroot K 1984 Relationship between the Degradation Behavior of Calcium-Phosphate Ceramics and Their Physical-Chemical Characteristics and Ultrastructural Geometry *Biomaterials* **5** 157-60
  - [17] Eanes E D 1998 Amorphous Calcium Phosphate: Thermodynamic and Kinetic Considerations *Calcium Phosphates in Biological and Industrial Systems* ed Amjad Z (Boston, MA: Kluwer Academic Publ.) pp 21-40.
  - [18] Tung M S 1998 Calcium Phosphates: Structures, Composition, Solubility and Stability *Calcium Phosphates in Biological and Industrial Systems* ed Amjad Z (Boston, MA: Kluwer Academic Publ.) pp 1-20.
  - [19] Meyer J L and Eanes E D 1978 A thermodynamic analysis of the amorphous to crystalline calcium phosphate transformation *Calcified Tissue International* **25** 59-68
  - [20] Meyer J L and Eanes E D 1978 A thermodynamic analysis of the secondary transition in the spontaneous precipitation of calcium phosphate *Calcified Tissue International* **25** 209-16
  - [21] Antonucci J M, Skrtic D and Eanes E D 1995 Remineralizing Dental Composites Based on Amorphous Calcium-Phosphate *Abstracts of Papers of the American Chemical Society* 209 6-MACR Part 2
  - [22] Antonucci J M, Skrtic D and Eanes E D 1996 Bioactive polymeric dental materials based on amorphous calcium phosphate *Hydrogels and Biodegradable Polymers for Bioapplications* ed M. O R, Huang S J, Park K (Washington, DC: American Chemical Society) pp 243-54.
  - [23] Skrtic D, Antonucci J M, Eanes E D and Eldelman N 2004 Dental composites based on hybrid and surface-modified amorphous calcium phosphates *Biomaterials* **25** 1141-50

- [24] Lin F H, Chen T M, Lin C P and Lee C J 1999 The merit of sintered PDLA/TCP composites in management of bone fracture internal fixation *Artificial Organs* **23** 186-94
- [25] Heidemann W, Jeschkeit S, Ruffieux K, Fischer J H, Wagner M, Kruger G, Wintermantel E and Gerlach K L 2001 Degradation of poly(D,L)lactide implants of calcium phosphates with or without addition in vivo *Biomaterials* **22** 2371-81
- [26] Palin E, Liu H N and Webster T J 2005 Mimicking the nanofeatures of bone increases bone-forming cell adhesion and proliferation *Nanotechnology* **16** 1828-35
- [27] Liu H N, Slamovich E B and Webster T J 2005 Increased osteoblast functions on nanophase titania dispersed in poly-lactic-co-glycolic acid composites *Nanotechnology* **16** S601-S08
- [28] Webster T J, Waid M C, McKenzie J L, Price R L and Ejiofor J U 2004 Nano-biotechnology: carbon nanofibres as improved neural and orthopaedic implants *Nanotechnology* **15** 48-54
- [29] Loher S, Stark W J, Maciejewski M, Baiker A, Pratsinis S E, Reichardt D, Maspero F, Krumeich F and Gunther D 2005 Fluoro-apatite and calcium phosphate nanoparticles by flame synthesis *Chemistry of Materials* **17** 36-42
- [30] Stark W J, Pratsinis S E, Maciejewski M, Loher S and Baiker A 2005 *Flame Synthesis of Metal Salt Nanoparticles, in particular Calcium and Phosphate comprising Nanoparticles* patent WO2005087660
- [31] Langford J I and Wilson A J C 1978 Scherrer after 60 Years - Survey and Some New Results in Determination of Crystallite Size *J. Appl. Crystallogr.* **11** 102-13
- [32] Kokubo T, Kushitani H, Sakka S, Kitsugi T and Yamamuro T 1990 Solutions Able to Reproduce In vivo Surface-Structure Changes in Bioactive Glass-Ceramic a-W3 *Journal of Biomedical Materials Research* **24** 721-34
- [33] Jilavenkatesa A and Condrate R A 1998 The infrared and Raman spectra of beta- and alpha-tricalcium phosphate (Ca-3(PO<sub>4</sub>)(2)) *Spectroscopy Letters* **31** 1619-34
- [34] Notingher I, Boccaccini A R, Jones J, Maquet V and Hench L L 2002 Application of Raman microspectroscopy to the characterisation of bioactive materials *Materials Characterization* **49** 255-60
- [35] Cassanas G, Morssli M, Fabregue E and Bardet L 1991 Vibrational-Spectra of Lactic-Acid and Lactates *Journal of Raman Spectroscopy* **22** 409-13
- [36] Kister G, Cassanas G, Fabregue E and Bardet L 1992 Vibrational Analysis of Ring-Opening Polymerizations of Glycolide, L-Lactide and D,L-Lactide *European Polymer Journal* **28** 1273-77
- [37] Kister G, Cassanas G and Vert M 1998 Structure and morphology of solid lactide-glycolide copolymers from C-13 nmr, infra-red and Raman spectroscopy *Polymer* **39** 3335-40
- [38] LeGeros R Z 2002 Properties of osteoconductive biomaterials: Calcium phosphates *Clin. Orthop. Rel. Res.* **81**-98
- [39] Maquet V, Boccaccini A R, Pravata L, Notingher I and Jerome R 2004 Porous poly(alpha-hydroxyacid)/Bioglass (R) composite scaffolds for bone tissue engineering. I: preparation and in vitro characterisation *Biomaterials* **25** 4185-94
- [40] Bloemers F W, Blokhuis T J, Patka P, Bakker F C, Wippermann B W and Haarman H 2003 Autologous bone versus calcium-phosphate ceramics in treatment of experimental bone defects *J. Biomed. Mater. Res. Part B* **66B** 526-31
- [41] Walters M A, Leung Y C, Blumenthal N C, Legeros R Z and Konsker K A 1990 A Raman and Infrared Spectroscopic Investigation of Biological Hydroxyapatite *Journal of Inorganic Biochemistry* **39** 193-200
- [42] Rehman I, Hench L L, Bonfield W and Smith R 1994 Analysis of Surface-Layers on Bioactive Glasses *Biomaterials* **15** 865-70
- [43] Sudarsan.K and Young R A 1969 Significant Precision in Crystal Structural Details - Holly Springs Hydroxyapatite *Acta Crystallographica Section B-Structural Crystallography and Crystal Chemistry B* **25** 1534-43
- [44] Weiner S and Wagner H D 1998 The material bone: Structure mechanical function relations *Annual Review of Materials Science* **28** 271-98

- [45] Yashima M, Sakai A, Kamiyama T and Hoshikawa A 2003 Crystal structure analysis of beta-tricalcium phosphate  $\text{Ca}_3(\text{PO}_4)_2$  by neutron powder diffraction *Journal of Solid State Chemistry* **175** 272-77



## 4. Cotton wool-like nanocomposite biomaterials: *In vitro* biocompatibility and osteogenic differentiation of human mesenchymal stem cells

### Abstract

The present study evaluates the *in vitro* biocompatibility of an electrospun, flexible, and cotton wool-like poly(lactide-co-glycolide) (PLGA)/amorphous tricalcium phosphate (ATCP) nanocomposite. A cell culture study with human mesenchymal stem cells (hMSC) allowed assessing the application of the material for potential use as a bone graft. ATCP powder was prepared by flame spray synthesis and exhibited a particles size between 20-80 nm. Scaffolds with nanoparticle loadings ranging from 0 to 40% (w/w) were prepared by electrospinning of a PLGA-based composite. Three different scaffolds containing no ATCP (reference) and two samples with 40% (w/w) ATCP in PLGA (as-prepared and pre-immersed in SBF for 15 hours) were seeded with hMSC. Proliferation and osteogenic differentiation was assessed by incubating cells in osteogenic medium for 4 weeks. Proper adhesion and an unaffected morphology of the cells were observed by confocal laser scanning microscopy (CLSM) for all samples. Fluorometric quantification of dsDNA and analysis of alkaline phosphatase (ALP) activity revealed no significant difference between the three scaffolds tested and excluded any acute cytotoxic effects of the nanoparticles. The osteocalcin content for all scaffolds was 0.12 to 0.19 ng per ng DNA confirming osteogenic differentiation of human mesenchymal stem cells on these flexible bone implants.

Part of this chapter is submitted to the **J. Biomed. Res. Part B** and has been applied for as a PCT patent application (PCT/CH2006/000589).

## 4.1. Introduction

The world-wide demographic shift to an increasingly older population has been estimated to result in over 500'000 bone graft substitutions annually performed in the United States [1] alone. Most fractures and bone defects are currently repaired using auto- and allografts but often suffer from donor-site morbidity, insufficient availability, risk of disease-transfer, and a potential negative immune response. Alternatively, synthetic products [2-4] can be used as bone substitute materials and are predominately derived from ceramic materials such as hydroxyapatite (HAp) [5] or tricalcium phosphate (TCP) [6], since natural bone mineral consists of about 70wt% carbonated hydroxyapatite [7]. Considerable osteoconductivity [8, 9] and the ability to serve as a precursor to bone apatite formation [10, 11] have resulted in a broad clinical use of such ceramics in spite of brittleness, incompressibility and difficulty in shaping [12, 13] during surgery. For applications requiring soft and shapeable implants, bone cements are currently used for their easy application by injection [14-16]. The resorption capacity, however, is often limited by their chemical composition or hindered accessibility in the resulting dense, hardened material. A possible way to overcome the brittleness of pure ceramic biomaterials is the use of polymers as a continuous phase in composites or in a pure form. Among biocompatible and bioresorbable polymers, poly(lactide-co-glycolide) (PLGA) has attracted significant attention for its application in drug delivery [17, 18], soft tissue engineering [19], nerve regeneration [20] and orthopaedics [21].

The concept of combining the ductility of a polymer and the bioactivity of calcium phosphates, most preferably in a nanoparticulate form, has already resulted in numerous investigations on such composite materials: Ambrosio et al. [22] and Khan et al. [23] have developed a method to in-situ form amorphous calcium phosphate in PLGA microspheres by a modified emulsion/solvent evaporation technique. The composite microspheres could be subsequently sintered to a porous 3D-scaffold. Most recently, a study on PLGA/nano-HAp composite scaffolds produced by a simultaneous gas forming and particulate leaching method claimed an enhancement of bone regeneration *in vivo* [24]. The *in vitro* biodegradation of PLGA films doped with amorphous tricalcium phosphate nanoparticles most recently revealed a strongly enhanced hydroxyapatite deposition and an up to eight fold accelerated polymer degradation [25]. Mechanical properties may also be strongly increased by the incorporation of nanomaterials as shown in a recent study on biphasic calcium phosphate

nanocomposite, porous scaffolds [26]. The use of titania/PLGA nanocomposite films has recently shown enhanced osteoblast functions corroborating the importance of nanometre surface features that mimic natural bone [27, 28].

Electrospinning is a most suitable tool for the preparation of open structured, highly accessible networks of polymer fibres [18, 29-31] for application in reinforcement, filtration, medical prostheses engineering, wound dressings and tissue engineering [18]. In order to combine the most advantageous properties of nanostructured composites and the morphology of electrospun biomaterials, the present study investigates the use of aerosol derived amorphous tricalcium phosphate (ATCP) nanoparticles [32-34] and PLGA for the preparation of non-woven composite fibres by electrospinning [35]. Amorphous calcium phosphate has been postulated as a precursor of hydroxyapatite formation [36, 37] and exhibits an increased solubility attributed to its high enthalpy of formation. *In vitro* biodegradation experiments of the nanocomposites and cell culture tests with human mesenchymal stem cells (hMSC) allowed to access bioactivity and performance in osteogenic differentiation.

## 4.2. Materials and Methods

### 4.2.1. Preparation of ATCP particles

Amorphous tricalcium phosphate nanoparticles (ATCP, chemical formula:  $\text{Ca}_3(\text{PO}_4)_2$ ) were prepared by flame spray pyrolysis [38] using calcium hydroxide (Riedel de Haen, Ph. Eur.) dissolved in 2-ethylhexanoic acid (Soctech, Rumania) and tributyl phosphate (97%, Aldrich) as precursors [32, 33]. The liquid mixture was diluted with xylene (2:1 vol/vol) and fed through a capillary (diameter 0.4 mm) into a methane/oxygen flame at a rate of 5 ml min<sup>-1</sup>. Oxygen (5 L min<sup>-1</sup>, 99.8%, Pan Gas) was used to disperse the liquid leaving the capillary and resulted in a burning spray of about 10 cm height [33]. A more detailed view on the nanoparticle formation may be found in [39]. The as-formed particles (production rate: 8 g h<sup>-1</sup>) were collected on a glass fibre filter (Whatmann GF/A, 25.7 cm diameter), placed on a cylinder mounted above the flame, by the aid of a vacuum pump (Busch Seco SV 1040 C).

### 4.2.2. Particle characterization

The specific surface area (SSA) of the ATCP powder was measured by nitrogen adsorption at 77 K (Tristar, Micromeritics) according to the Brunauer-Emmett-Teller (BET) method after outgassing at 150 °C for 1h. The primary particle diameter was calculated according to  $d_{\text{BET}} = 6/(\rho_{\text{ATCP}} \cdot \text{SSA})$  assuming spherical particles. Hydrodynamic particle size distributions were measured on an X-ray disc centrifuge (BI-XDC, Brookhaven Instruments) [40, 41] using 1.5 % (wt/vol) of powder in absolute ethanol (Fluka) and the mean particle diameter was denoted as  $d_{\text{XRD}}$ . Prior to analysis the powder was dispersed by ultrasonication (UP400S, 24 kHz, Hielscher GmbH) at 200 W for 5 min. The average number of primary particles per aggregate ( $n_p$ ) was roughly estimated [41] using the fractal scaling relationship ( $n_p = [d_c/d_p]^D$ ) applying  $d_{\text{BET}}$  as primary particle diameter ( $d_p$ ),  $d_{\text{XDC}}$  as collision diameter ( $d_c$ ) and a constant fractal dimension ( $D$ ) of 1.8 consistent with theory for nanoparticle formation in flames [42]. For Fourier transform infrared (FTIR) spectroscopy, 1% (w/w) of powder was mixed with KBr (Fluka, puriss) and examined on a Tensor 27 spectrometer (Bruker Optics,  $4000 \text{ cm}^{-1} < \lambda < 400 \text{ cm}^{-1}$ , 16 scans,  $4 \text{ cm}^{-1}$  resolution) equipped with a diffusive reflectance accessory (DiffusIR™, Pike Technologies). Transmission electron microscopy (TEM) images were recorded on a CM30 ST (Philips, LaB6 cathode, operated at 300 kV, point resolution  $\sim 4 \text{ \AA}$ ). Particles were deposited onto a carbon foil supported on a copper grid.

### 4.2.3. Scaffold preparation

Clinically approved poly(lactide-co-glycolide) (PLGA) with a copolymer ratio of 85:15 (Resomer® Sample MD Type RG) was purchased from Boehringer Ingelheim with a weight and number average molecular weight of  $380'300 \text{ g mol}^{-1}$  and  $181'900 \text{ g mol}^{-1}$ , respectively. Randomly oriented PLGA/ATCP fibres were fabricated in different weight ratios (100/0, 90/10, 80/20 and 60/40) by an electrospinning process [30, 43]. Each electrospinning solution was prepared with a concentration of 8% (w/w) PLGA in chloroform (Riedel de Haen, Ph. Eur.) containing 5% (w/w) Tween20 (Fluka, Ph. Eur.) referred to the polymer. For the preparation of the electrospinning solution, corresponding amounts of ATCP nanoparticles were first dispersed in a chloroform/Tween20 parent solution using an ultrasonic processor (UP400S, 24 kHz, Hielscher GmbH) at 320 W for 5 min applying pulsed intervals to allow for relaxation of the particles. PLGA was subsequently added and dissolved for 15 h by magnetic stirring. The viscosity of the resulting mixture was measured with a rheometer

(Rheometric Scientific, cone plate 50 mm, shear rate 10-100 s<sup>-1</sup>). Electrospinning was done feeding the solutions through a capillary (inner diameter 1.0 mm) using a syringe pump (Seringue, Bioblock Scientific). The feeding rate was set to 2 ml h<sup>-1</sup> for PLGA/ATCP 60/40 and 4 ml h<sup>-1</sup> for all other solutions. A high voltage supply (Glassman High Voltage) was used to apply voltages of 20 kV to the needle tip which was kept in a chloroform/air stream (1 l min<sup>-1</sup>) by a concentrically mounted sheath tube [44]. A positively charged jet was formed from the Taylor cone and was sprayed onto a rotating (130 rpm) collection tube covered by aluminium foil. The distance between the needle tip and the collection tube (diameter 8 cm) was kept at 10 cm for PLGA/TCP 60/40 and 20 cm for all other samples. The as-spun scaffolds were dried and stored under vacuum at room temperature.

#### **4.2.4. Scaffold characterization**

The morphology of the electrospun fibres was characterized using scanning electron microscopy (SEM; Hitachi S-900) at a voltage of 3 kV after sputtering the samples with platinum (4 nm, Bal-Tec SCD 050). The porosities of the scaffolds were calculated according to  $\epsilon = (V_{\text{tot}} - V_{\text{solid}})/V_{\text{tot}}$ , whereas the total volume ( $V_{\text{tot}}$ ) was determined from the base area of the sample and its thickness as measured by SEM. The solid volume ( $V_{\text{solid}}$ ) is given by the sample mass and its density. X-ray diffraction (XRD) patterns were collected on a Stoe STADI-P2 (Ge monochromator, CuK $\alpha$ 1, PSD detector). Mechanical properties were obtained by tensile tests on an Instron 4411 (Instron Co.). In order to study the wettability of pure PLGA and PLGA/ATCP composite materials, films with a thickness of 100  $\mu$ m were prepared by solvent casting from the electrospinning solution and the contact angle was measured (Goniometer, ramé-hart inc).

#### **4.2.5. Cell culture**

Total human bone marrow (25 cm<sup>3</sup>, Clonetics, Santa Rosa, CA) from one donor was processed and diluted in 100 ml of isolation medium (5% FBS in RPMI 1640 medium). Cells were separated by density gradient centrifugation. Briefly, 20 ml aliquots of bone marrow suspension were overlaid onto 15 ml of a polysucrose gradient ( $\rho = 1077$  g cm<sup>-3</sup>, Histopaque, Sigma, St. Louis, MO) and centrifuged at 800g for 30 min at room temperature. The cell layer was carefully removed, washed in 10 ml isolation medium, pelleted and contaminating red blood cells were lysed in 5ml of RBC lysis buffer (Gentra Systems, Minneapolis, MN)

solution. Cells were pelleted and suspended in expansion medium (DMEM, 10% FBS, 1 ng ml<sup>-1</sup> bFGF) and seeded in 75 cm<sup>2</sup> flasks at a density of  $5 \times 10^4$  cells cm<sup>-2</sup>. The adherent cells were allowed to reach approximately 80% confluence (12–17 days for the first passage). Cells were trypsinized, replated and passage 2 (P2) cells (80% confluence after 6–8 days), were used for the experiments.

Scaffolds (n=4) were placed in 12 well culture plastic polystyrene (TPP AG, Trasadingen, Switzerland) and fixed with sterile polycarbonate rings. Osteogenic medium (DMEM 10% FBS, Pen-Strep, Fungizone, 50 µg ml<sup>-1</sup> ascorbic acid-2-phosphate, 100 nM dexamethasone and 7 mM β-glycerolphosphate) was used for all scaffold samples. As a control non-osteogenic medium (without ascorbic acid-2-phosphate, dexamethasone and β-glycerolphosphate) was used in tissue culture plastic wells and polycarbonate rings were placed for consistency. Cells were suspended in corresponding medium (osteogenic or non-osteogenic) at a concentration of  $3 \times 10^5$  cells ml<sup>-1</sup> and 2 ml aliquots of the corresponding suspension ( $6 \times 10^5$  cells) were seeded into each well (corresponding to a initial seeding density of  $2 \times 10^5$  cells cm<sup>-2</sup>). Seeded scaffolds were incubated at 37 °C and 5% CO<sub>2</sub>. Osteogenic or non-osteogenic medium was changed three times a week for a period of 4 weeks.

#### **4.2.6. Confocal laser scanning microscopy**

Prior to confocal microscopy, scaffolds were rinsed twice with PBS and fixed in 4% paraformaldehyde solution for 15 min at 37°C. Subsequently, samples were extracted in 0.5% Triton-X 100 for 3 min followed by blocking non-specific binding with 3% bovine serum albumin for 30 min at RT. Cells were incubated with phalloidine 488 in 0.1 % bovine serum albumin/PBS for 30 min followed by incubation with 4',6-diamidino-2-phenylindole (DAPI) for 15 min at RT. After a washing step cells were fixed again (4% paraformaldehyde) and confocal micrographs were recorded on a Axiovert 35 fluorescence microscope (Karl Zeiss AG, Germany) equipped with a AxioCam MRc 5 camera (Karl Zeiss AG, Germany) using Openlab imaging.

#### **4.2.7. Alkaline phosphatase activity, osteocalcin and DNA content**

For all analyses, scaffolds were collected after 4 weeks and disintegrated in 0.2% Triton X-100, 5mM MgCl<sub>2</sub> solution using steel balls and a MinibeadBeater™ (Biospec, Bartlesville, OK) performing 3 cycles at 25 kHz for 10 s per cycle. Cells incubated on tissue culture plastic in non-osteogenic medium were lysed in the wells (n=4). Alkaline phosphatase (ALP) activity was investigated directly after sample collection using a biochemical assay from Sigma (St. Louis, MO), based on conversion of *p*-nitrophenyl phosphate (*p*NPP) to *p*-nitrophenol. The reaction was stopped after 5 minutes using 0.2 M NaOH. For both DNA and osteocalcin analyses all samples were additionally pre-treated with 10% (w/w) EDTA solution (pH=8) for 2h on a bench shaker at RT. The DNA content was measured using the PicoGreen assay (Molecular Probes, Eugene, OR), according to the protocol of the manufacturer. Samples were measured fluorometrically at an excitation wavelength of 480 nm and an emission wavelength of 520 nm. Osteocalcin was determined by an immunoenzymetric ELISA assay (Demeditec Diagnostics GmbH, Germany) following the manufacturer's protocol. Samples were examined spectrophotometrically at 405 nm.

#### **4.2.8. Statistical analysis**

For biochemical analyses, a total of four samples (n=4) were examined and expressed as average ± standard deviation of the mean. Statistical significance was evaluated by Student's t-test.

### **4.3. Results**

#### **4.3.1. Amorphous tricalcium phosphate nanoparticles**

Production of ATCP particles by flame spray synthesis yielded spherical, amorphous and highly agglomerated tricalcium phosphate nanoparticles of 20-50 nm diameter as observed by transmission electron microscopy (TEM, Figure 4-1a). The as-prepared ATCP exhibited a specific surface area of 78 (±3%) m<sup>2</sup> g<sup>-1</sup> resulting in a calculated primary particle diameter (*d*<sub>BET</sub>) of 25 nm assuming spherical particles. X-ray disc centrifugation revealed a unimodal size distribution with a mean particle diameter (*d*<sub>XDC</sub>) of 40 nm (Figure 4-1b). The average number of primary particles per aggregate (*n*<sub>p</sub>) was therefore calculated to 2.4. X-ray powder

diffraction (XRD) showed no distinct pattern for the as-prepared powder indicating its amorphous structure. The broad unspecific peaks in the FTIR spectrum (Figure 4-2) corroborated the amorphous state of the material. After sintering (900 °C, 30 min) distinct absorption bands characteristic for  $\beta$ -TCP [45] were observed in agreement with earlier studies [25]. FTIR absorption around 1400-1500  $\text{cm}^{-1}$  indicate the presence of minute amounts of carbonate in the as-prepared material. Since the absorption peaks at 1215  $\text{cm}^{-1}$  to 1140  $\text{cm}^{-1}$ , at 727 and 496  $\text{cm}^{-1}$  are absent, we can exclude the presence of calcium pyrophosphate, a major impurity in commercial TCP.

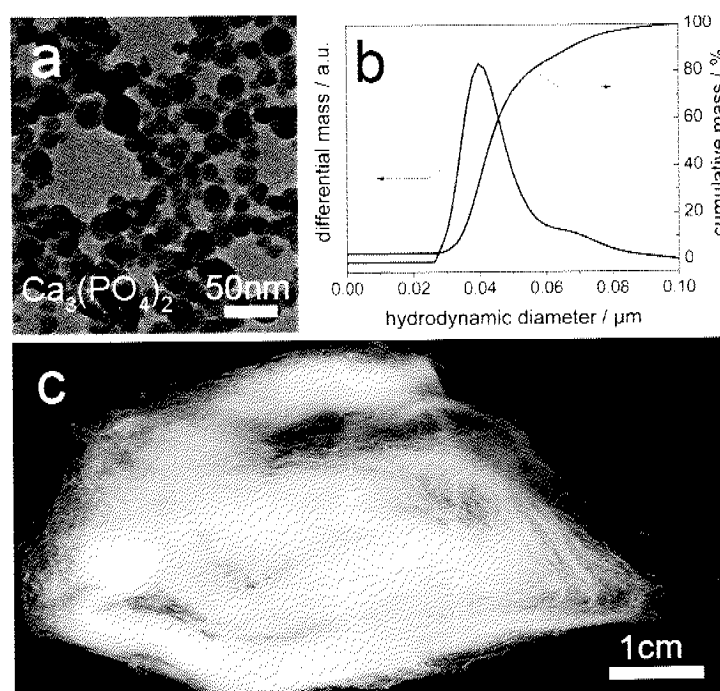


**Figure 4-1.** Particle characteristics and cotton wool-like appearance: (a) Transmission electron micrograph of as-prepared ATCP. (b) Corresponding hydrodynamic particle size distribution of ATCP measured by X-ray disc centrifugation. (c) Photograph of as-electrospun PLGA/ATCP scaffold processed into a cotton wool-like biomaterial.

#### 4.3.2. PLGA/ATCP nanocomposite scaffolds

Scaffolds consisting of pure PLGA and up to 40% (w/w) ATCP were prepared by electrospinning. The as-electrospun scaffold was manually uncompressed into a cotton wool-like biomaterial (Figure 4-1c). Tests with post-processed scaffolds to fill simulated sockets or defects with hindered accessibility will be discussed at a later stage of this work. SEM micrographs (Figure 4-3a, c) of the as-spun materials



showed homogeneous three-dimensional fibrous meshes for both pure PLGA and PLGA/ATCP scaffolds with an overall thickness of about 250  $\mu\text{m}$ . The scaffold predominately consisted of fibres within a diameter range of 5-10  $\mu\text{m}$  and porosities of  $90\pm 3\%$ . The surface of the pure, non-degraded polymer fibres was smooth (Figure 4-3b) compared to ATCP nanoparticle containing fibres which clearly revealed an increased roughness (Figure 4-3d). The small features in the submicron range arose from incorporated agglomerates of nanoparticles exposed to the surface resulting in a strongly increased exchange area.

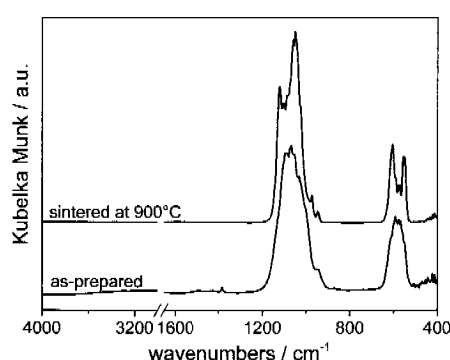


**Figure 4-2.** Fourier transform infrared spectra of as-prepared amorphous tricalcium phosphate nanoparticles produced by flame synthesis and the distinct peaks characteristic for  $\beta$ -TCP after crystallization by calcination.

Incorporation of particles had a major influence on the scaffold precursor and therefore the synthesis parameters. The viscosity of the PLGA/ATCP 60/40 electrospinning solution measured at shear rates between  $10\text{ s}^{-1}$  and  $100\text{ s}^{-1}$  was 2-3 times higher compared to the other electrospinning solutions (Figure 4-4). To avoid drop formation at the capillary tip the feeding rate for PLGA/ATCP 60/40 was adjusted to lower values ( $2\text{ ml h}^{-1}$  instead of  $4\text{ ml h}^{-1}$  for all other samples) which would theoretically result in thinner fibres. The lower feed rate was compensated by decreasing the distance between the needle and the collection tube (from 20 cm to 10 cm) in order to obtain consistent scaffold properties without undesired morphology changes [30]. Contact angle measurements on the films prepared from the electrospinning solutions showed that the wettability of the pure PLGA (contact angle:  $76\pm 1^\circ$ ) was significantly lower compared to the PLGA/ATCP 60/40 nanocomposite (contact angle:  $52\pm 7^\circ$ ). This fact was reflected by the facilitated soaking of the particle-containing scaffolds in SBF if compared to the reference (PLGA/ATCP 100/0).

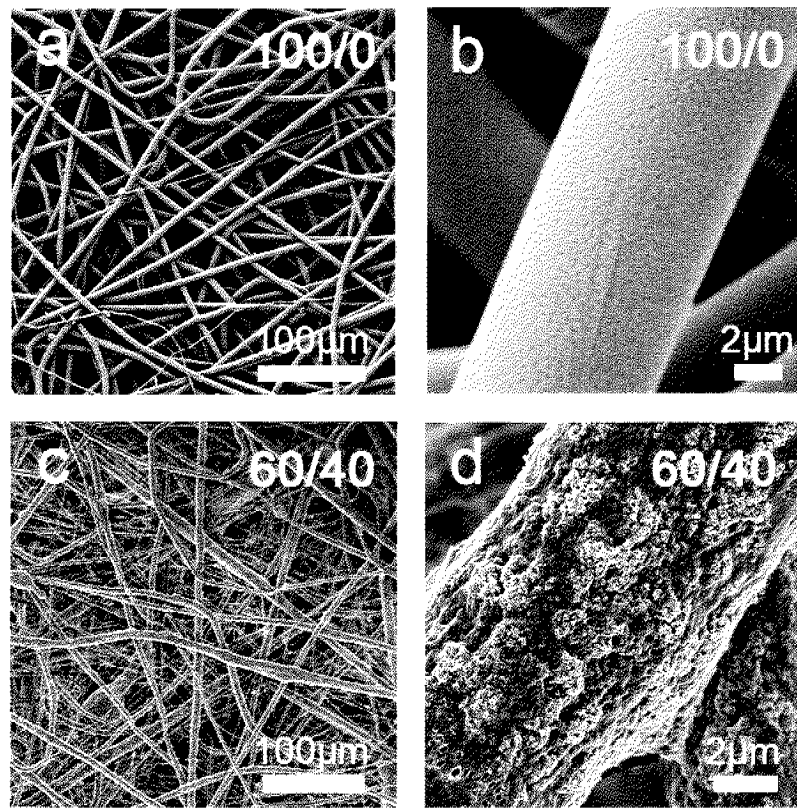


**Figure 4-3.** Scanning electron microscopy images of as-electrospun scaffolds: PLGA/ATCP 100/0 (a) overview and (b) close-up; PLGA/ATCP 60/40 (c) fibres and (d) fibre surface structure.

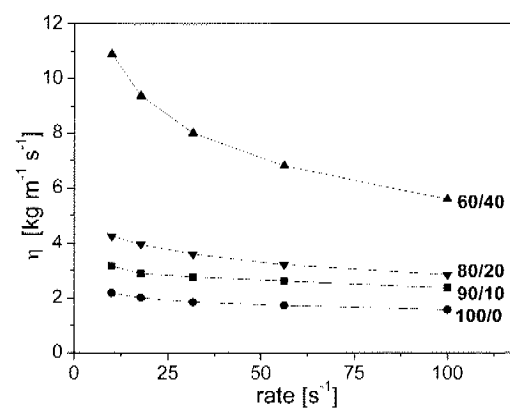


**Figure 4-4.** Viscosities of the different PLGA/ATCP electrospinning solutions as a function of the shear rate.

### 4.3.3. Simulation of bone defect repair

The application of the present cotton-wool like composite was evaluated using simulated bone defect sites with hindered accessibility as it might exist in practical surgical situations (Figure 4-5). Defects with different opening diameters  $\phi_B$  (3-8 mm) and depths  $l_B$  (5-40 mm) could be completely filled with the prepared cotton wool-like material within less than one minute. No pre-shaping of the defect or implant material preparation were required. Additionally, the implant material may be removed in one piece in case of misplacement or unpredicted complications. The packing density can be estimated in advance by the weight of the applied material and the void volume to fill.

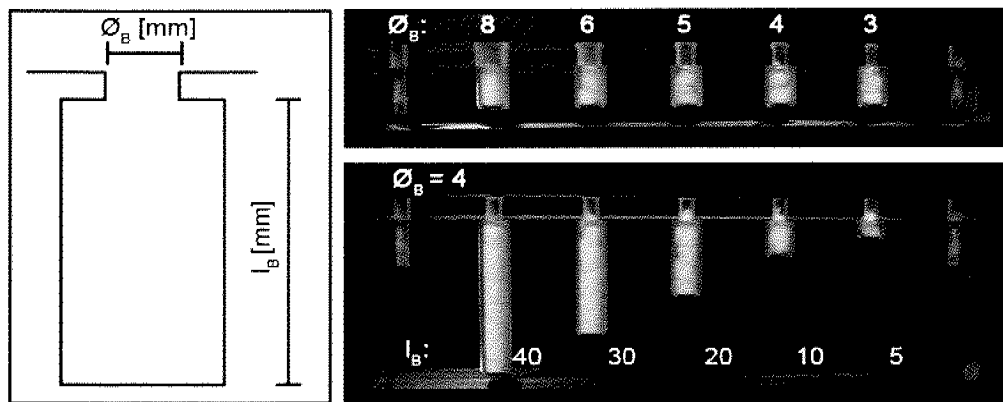


**Figure 4-5.** Simulation of a bone defect site with hindered accessibility: Defects with different opening diameters  $\phi_B$  and depths  $l_B$  could rapidly be filled completely with the prepared cotton wool-like material.

### 4.3.4. Proliferation and osteogenic differentiation of hMSC

For an evaluation of biocompatibility, proliferation and osteogenic differentiation, three different scaffolds were seeded with mesenchymal stem cells and incubated in osteogenic medium (ascorbic acid-2-phosphate,  $\beta$ -glycerolphosphate, dexamethasone). Pure PLGA 100/0 and 40% (w/w) ATCP in PLGA (sample 60/40) as prepared or pre-incubated in SBF for 15 h (sample 60/40 SBF) were investigated. A SBF-pretreated sample was chosen to avoid a possible calcium ion burst when the cell suspension is put in contact with the relatively soluble ATCP at the surface of the scaffold. Control experiments were conducted on tissue culture plastic in non-osteogenic medium. Confocal fluorescence microscopy of the scaffolds after 4 weeks did not reveal any significant difference in cell adhesion or cell morphology

(Figure 4-6a) for the three different scaffolds. On all three samples, cells reached confluence by the time tested and adhered normally to the fibres, building a 10  $\mu\text{m}$  thick cellular layer. Statistically significantly ( $p < 0.0001$ ) higher amounts of double-stranded DNA (dsDNA) were present in all scaffold samples incubated in osteogenic medium as compared to non-osteogenic tissue culture plastic samples (Figure 4-6b). All three scaffolds showed a remarkable similarity in proliferation after 4 weeks of incubation.

Osteogenic differentiation was assessed by two biochemical assays to analyze the alkaline phosphatase activity and osteocalcin content. Both parameters were normalized by the DNA content measured by the PicoGreen assay (Figure 4-6b) to account for the different number of cells.

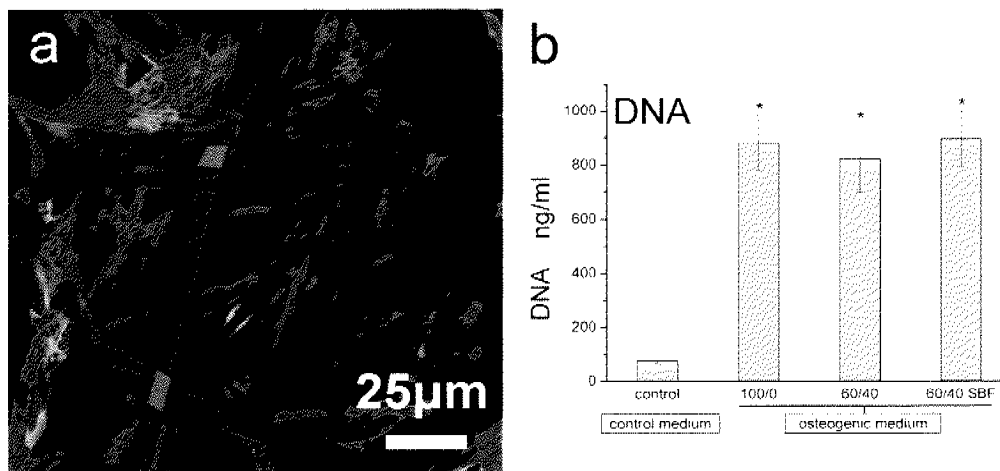


**Figure 4-6.** Cell morphology and proliferation after 4 weeks scaffold immersion: (a) CLSM of sample PLGA/ATCP 60/40. Stained cell nucleus (blue) and the actin skeleton (green) of cells which adhere to the scaffold (indicated in red). (b) The dsDNA content of scaffolds in osteogenic medium showed a large significantly significant difference to the control in non-osteogenic medium (\*  $p < 0.0001$ ).

No statistically significant difference among the samples was observed for ALP activity (Figure 4-7) although pure PLGA 100/0 showed the highest average value followed by the SBF-treated nanocomposite. Both, the control and the as-prepared PLGA/ATCP 60/40 exhibited a very similar ALP activity. The difference of osteocalcin content (Figure 4-7) for all scaffolds was statistically highly significant ( $p < 0.0001$ ) if compared to the control. Osteocalcin contents of the control were all within the error of measurement. Pure PLGA and

Figure 1 consists of two bar graphs. The left graph shows ALP activity (μg p-nitrophenol / ng DNA) for control and osteogenic medium conditions. The right graph shows osteocalcin levels (ng osteocalcin / ng DNA) for the same conditions. The osteogenic medium conditions are further divided into 100/0, 60/40, and 60/40 SBF.

**ALP Activity (μg p-nitrophenol / ng DNA)**

Condition	ALP Activity (μg p-nitrophenol / ng DNA)
control	~0.055
100/0	~0.088
60/40	~0.055
60/40 SBF	~0.072

**Osteocalcin Levels (ng osteocalcin / ng DNA)**

Condition	Osteocalcin Levels (ng osteocalcin / ng DNA)
control	~0.005
100/0	~0.190
60/40	~0.130
60/40 SBF	~0.165

Significance markers: \* indicates p < 0.05, \*\* indicates p < 0.01. A bracket with \*\* indicates a significant difference between 100/0 and 60/40.

#### 4.4. Discussion

Several most recent studies have corroborated the trend of using polymer/calcium phosphate composites for regeneration of bone defects [22-24, 46-48]. These materials combine beneficial properties such as elasticity of the polymer with the stability and bioactivity of the calcium phosphate ceramic. Today, they are applied in granular form or as solid blocks. In this study a new, flexible, compressible nanocomposite was evaluated in terms of bioactivity and biocompatibility. Its typical cotton wool-like appearance (Figure 4-1c) may facilitate

rapid application by the surgeon and allow for complete defect filling as well as proper removal or adjustment of misfit implant material (Figure 4-5).

The use of amorphous tricalcium phosphate (ATCP) nanoparticles has arisen from its postulated important role in the formation of hydroxyapatite and from its enhanced solubility compared to crystalline phases of TCP such as  $\beta$ -TCP. The thermodynamically most active, amorphous, nanoparticulate form of TCP has most recently become readily available by flame spray synthesis (Figure 4-1a, b). Non-woven scaffolds prepared by electrospinning resulted in homogeneous distribution of up to 40% (w/w) ATCP nanoparticles in a PLGA matrix (Figure 4-3).

*Biocompatibility and osteogenic differentiation.* Two different nanocomposites, as-prepared 40% (w/w) ATCP in PLGA (60/40) and SBF pre-immersed (15 hours) PLGA/ATCP (60/40 SBF), were compared to reference PLGA in terms of *in vitro* biocompatibility and osteogenic differentiation. Scaffolds were seeded with human MSC and cultured in osteogenic medium without any supplementation of BMP-2 using standard composition [49]. The detection of normal cell morphology and nearly identical proliferation after 4 weeks on all three scaffolds (Figure 4-6) indicated an *in vitro* biocompatibility comparable to pure PLGA. A previous study with MSTO and 3T3 cells at ATCP nanoparticle concentrations up to 15 ppm (mass based parts per million) resulted in similar cell viability than nano-sized titania [50] and corroborated its *in vitro* biocompatibility. The significantly ( $p < 0.0001$ ) lower DNA content of the control may be attributed to the surface texture or the decreased space available if compared to the scaffolds. ALP activity combined with osteocalcin content at time point 4 weeks allowed to discuss osteogenic differentiation of human MSC. Increased ALP levels are predominately observed at the maturation phase of the cell matrix [51, 52] although ALP on its own is not a completely reliable marker for bone formation [53]. A comparison of ALP activities (Figure 4-7) revealed no significantly distinguishable results between the non-osteogenic control and the scaffolds in osteogenic medium. Therefore osteocalcin, which is among the most specific markers for osteoblast maturation [54] was quantified using an ELISA assay (Figure 4-7). No osteocalcin was detected for the control sample which corroborated the strong influence on osteogenic differentiation of the medium. Scaffold samples cultured under investigated conditions showed significant ( $p < 0.0001$ ) higher osteocalcin levels but were generally in the same range.

## 4.5. Conclusions

Non-woven PLGA scaffolds with up to 40% (w/w) of aerosol-derived amorphous tricalcium phosphate nanoparticles were prepared by electrospinning. Human mesenchymal stem cells seeded on nanocomposite scaffolds showed no morphological changes and the *in vitro* proliferation was unaffected if compared to pure PLGA scaffolds. The osteogenic differentiation as expressed by ALP activity and osteocalcin content was comparable to pure PLGA scaffolds. The cotton-wool like compressibility and flexibility of the electrospun, high-mineral content biomaterial suggests applications of such materials for non-load bearing, complex shaped bone defects.

## 4.6. Acknowledgements

We wish to thank M. Günthert for assistance in confocal laser scanning microscopy. Financial support by the Gebert-Rüf Foundation project 048/04 is kindly acknowledged.

## 4.7. References

- [1] Greenwald A S, Boden S D, Goldberg V M, Khan Y, Laurencin C T and Rosier R N 2001 Bone-graft substitutes: Facts, fictions, and applications *J. Bone Joint Surg.-Am. Vol.* **83A** 98-103
- [2] Aro H T and Aho A J 1993 Clinical Use of Bone Allografts *Ann. Med.* **25** 403-12
- [3] Damien C J and Parsons J R 1991 Bone-Graft and Bone-Graft Substitutes - a Review of Current Technology and Applications *J. Appl. Biomater.* **2** 187-208
- [4] Hench L L 1998 Bioceramics *J. Am. Ceram. Soc.* **81** 1705-28
- [5] Suchanek W and Yoshimura M 1998 Processing and properties of hydroxyapatite-based biomaterials for use as hard tissue replacement implants *J. Mater. Res.* **13** 94-117
- [6] Bucholz R W, Carlton A and Holmes R E 1987 Hydroxyapatite and Tricalcium Phosphate Bone-Graft Substitutes *Orthop. Clin. North Am.* **18** 323-34
- [7] Dorozhkin S V and Epple M 2002 Biological and medical significance of calcium phosphates *Angew. Chem.-Int. Edit.* **41** 3130-46
- [8] Jarcho M 1981 Calcium-Phosphate Ceramics as Hard Tissue Prosthetics *Clin. Orthop. Rel. Res.* 259-78
- [9] LeGeros R Z 2002 Properties of osteoconductive biomaterials: Calcium phosphates *Clin. Orthop. Rel. Res.* 81-98
- [10] Eanes E D 1998 Amorphous Calcium Phosphate: Thermodynamic and Kinetic Considerations *Calcium Phosphates in Biological and Industrial Systems* ed Amjad Z (Boston, MA: Kluwer Academic Publ.) pp 21-40.

- 
- [11] Tung M S 1998 Calcium Phosphates: Structures, Composition, Solubility and Stability *Calcium Phosphates in Biological and Industrial Systems* ed Amjad Z (Boston, MA: Kluwer Academic Publ.) pp 1-20.
- [12] Wang M 2003 Developing bioactive composite materials for tissue replacement *Biomaterials* **24** 2133-51
- [13] Yaszemski M J, Payne R G, Hayes W C, Langer R and Mikos A G 1996 Evolution of bone transplantation: Molecular, cellular and tissue strategies to engineer human bone *Biomaterials* **17** 175-85
- [14] Donkerwolcke M, Burny F and Muster D 1998 Tissues and bone adhesives - historical aspects *Biomaterials* **19** 1461-66
- [15] Knaack D, Goad M E P, Aiolo M, Rey C, Tofghi A, Chakravarthy P and Lee D D 1998 Resorbable calcium phosphate bone substitute *J. Biomed. Mater. Res.* **43** 399-409
- [16] Oda H, Nakamura K, Matsushita T, Yamamoto S, Ishibashi H, Yamazaki T and Morimoto S 2006 Clinical use of a newly developed calcium phosphate cement (XSB-671D) *J. Orthop. Sci.* **11** 167-74
- [17] Song C X, Labhasetwar V, Murphy H, Qu X, Humphrey W R, Shebuski R J and Levy R J 1997 Formulation and characterization of biodegradable nanoparticles for intravascular local drug delivery *J. Control. Release* **43** 197-212
- [18] Huang Y C, Connell M, Park Y, Mooney D J and Rice K G 2003 Fabrication and in vitro testing of polymeric delivery system for condensed DNA *J. Biomed. Mater. Res. Part A* **67A** 1384-92
- [19] Pattison M A, Wurster S, Webster T J and Haberstroh K M 2005 Three-dimensional, nano-structured PLGA scaffolds for bladder tissue replacement applications *Biomaterials* **26** 2491-500
- [20] Bini T B, Gao S J, Tan T C, Wang S, Lim A, Hai L B and Ramakrishna S 2004 Electrospun poly(L-lactide-co-glycolide) biodegradable polymer nanofibre tubes for peripheral nerve regeneration *Nanotechnology* **15** 1459-64
- [21] Laurencin C T, Ambrosio A M A, Borden M D and Cooper J A 1999 Tissue engineering: Orthopedic applications *Annu. Rev. Biomed. Eng.* **1** 19-46
- [22] Ambrosio A M A, Sahota J S, Khan Y and Laurencin C T 2001 A novel amorphous calcium phosphate polymer ceramic for bone repair: 1. Synthesis and characterization *J. Biomed. Mater. Res.* **58** 295-301
- [23] Khan Y M, Katti D S and Laurencin C T 2004 Novel polymer-synthesized ceramic composite-based system for bone repair: An in vitro evaluation *J. Biomed. Mater. Res. Part A* **69A** 728-37
- [24] Kim S S, Park M S, Jeon O, Choi C Y and Kim B S 2006 Poly(lactide-co-glycolide)/hydroxyapatite composite scaffolds for bone tissue engineering *Biomaterials* **27** 1399-409
- [25] Loher S, Reboul V, Brunner T J, Simonet M, Dora C, Neuenschwander P and Stark W J 2006 Improved degradation and bioactivity of amorphous aerosol derived tricalcium phosphate nanoparticles in poly(lactide-co-glycolide) *Nanotechnology* **17** 2054-61
- [26] Ramay H R R and Zhang M 2004 Biphasic calcium phosphate nanocomposite porous scaffolds for load-bearing bone tissue engineering *Biomaterials* **25** 5171-80
- [27] Liu H N, Slamovich E B and Webster T J 2005 Increased osteoblast functions on nanophase titania dispersed in poly-lactic-co-glycolic acid composites *Nanotechnology* **16** S601-S08
- [28] Palin E, Liu H N and Webster T J 2005 Mimicking the nanofeatures of bone increases bone-forming cell adhesion and proliferation *Nanotechnology* **16** 1828-35
- [29] Hutmacher D W 2001 Scaffold design and fabrication technologies for engineering tissues - state of the art and future perspectives *J. Biomater. Sci.-Polym. Ed.* **12** 107-24
- [30] Zuo W W, Zhu M F, Yang W, Yu H, Chen Y M and Zhang Y 2005 Experimental study on relationship between jet instability and formation of beaded fibers during electrospinning *Polym. Eng. Sci.* **45** 704-09
- [31] Teo W E and Ramakrishna S 2006 A review on electrospinning design and nanofibre assemblies *Nanotechnology* **17** R89-R106



- [32] Stark W J, Pratsinis S E, Maciejewski M, Loher S and Baiker A 2005 *Flame synthesis of metal salt nanoparticles, in particular calcium and phosphate comprising nanoparticles* patent WO2005/087660 A1
- [33] Loher S, Stark W J, Maciejewski M, Baiker A, Pratsinis S E, Reichardt D, Maspero F, Krumeich F and Gunther D 2005 Fluoro-apatite and calcium phosphate nanoparticles by flame synthesis *Chem. Mat.* **17** 36-42
- [34] Madler L, Kammler H K, Mueller R and Pratsinis S E 2002 Controlled synthesis of nanostructured particles by flame spray pyrolysis *J. Aerosol. Sci.* **33** 369-89
- [35] Stark W J, Schneider O D, Loher S, Brunner T J, Simonet M, Grass R N and Schmidlin P R 2006 *Implant material* PCT patent application
- [36] Meyer J L and Eanes E D 1978 Thermodynamic Analysis of Secondary Transition in Spontaneous Precipitation of Calcium-Phosphate *Calcified Tissue Research* **25** 209-16
- [37] Meyer J L and Eanes E D 1978 Thermodynamic Analysis of Amorphous to Crystalline Calcium-Phosphate Transformation *Calcified Tissue Research* **25** 59-68
- [38] Madler L, Stark W J and Pratsinis S E 2002 Rapid synthesis of stable ZnO quantum dots *Journal of Applied Physics* **92** 6537-40
- [39] Pratsinis S E 1998 Flame aerosol synthesis of ceramic powders *Prog. Energy Combust. Sci.* **24** 197-219
- [40] Limbach L K, Li Y C, Grass R N, Brunner T J, Hintermann M A, Muller M, Gunther D and Stark W J 2005 Oxide nanoparticle uptake in human lung fibroblasts: Effects of particle size, agglomeration, and diffusion at low concentrations *Environmental Science & Technology* **39** 9370-76
- [41] Staiger M, Bowen P, Ketterer J and Bohonek J 2002 Particle size distribution measurement and assessment of agglomeration of commercial nanosized ceramic particles *J. Dispersion Sci. Technol.* **23** 619-30
- [42] Kruis F E, Kusters K A, Pratsinis S E and Scarlett B 1993 A Simple-Model for the Evolution of the Characteristics of Aggregate Particles Undergoing Coagulation and Sintering *Aerosol Sci. Technol.* **19** 514-26
- [43] Reneker D H and Chun I 1996 Nanometre diameter fibres of polymer, produced by electrospinning *Nanotechnology* **7** 216-23
- [44] Larsen G, Spreitz R and Velarde-Ortiz R 2004 Use of coaxial gas jackets to stabilize Taylor cones of volatile solutions and to induce particle-to-fiber transitions *Adv. Mater.* **16** 166-69
- [45] Jilkaevkatesa A and Condrate R A 1998 The infrared and Raman spectra of beta- and alpha-tricalcium phosphate (Ca-3(PO4)(2)) *Spectr. Lett.* **31** 1619-34
- [46] Heidemann W, Jeschkeit S, Ruffieux K, Fischer J H, Wagner M, Kruger G, Wintermantel E and Gerlach K L 2001 Degradation of poly(D,L)lactide implants of calciumphosphates with or without addition in vivo *Biomaterials* **22** 2371-81
- [47] Skrtic D, Antonucci J M and Eanes E D 2003 Amorphous calcium phosphate-based bioactive polymeric composites for mineralized tissue regeneration *J. Res. Natl. Inst. Stand. Technol.* **108** 167-82
- [48] Kothapalli C R, Shaw M T and Wei M 2005 Biodegradable HA-PLA 3-D porous scaffolds: Effect of nano-sized filler content on scaffold properties *Acta Biomater.* **1** 653-62
- [49] Sun H L, Wu C T, Dai K R, Chang J and Tang T T 2006 Proliferation and osteoblastic differentiation of human bone marrow-derived stromal cells on akermanite-bioactive ceramics *Biomaterials* **27** 5651-57
- [50] Brunner T J, Wick P, Manser P, Spohn P, Grass R N, Limbach L K, Bruinink A and Stark W J 2006 In vitro cytotoxicity of oxide nanoparticles: Comparison to asbestos, silica, and the effect of particle solubility *Environmental Science & Technology* **40** 4374-81
- [51] Owen T A, et al. 1990 Progressive Development of the Rat Osteoblast Phenotype In vitro - Reciprocal Relationships in Expression of Genes Associated with Osteoblast Proliferation and Differentiation During Formation of the Bone Extracellular-Matrix *J. Cell. Physiol.* **143** 420-30

- [52] Ljunghall S and Lindh E 1989 Assessment of Bone Turnover with Biochemical Markers *J. Intern. Med.* **225** 219-20
- [53] Puleo D A 1997 Dependence of mesenchymal cell responses on duration of exposure to bone morphogenetic protein-2 in vitro *J. Cell. Physiol.* **173** 93-101
- [54] Holy C E, Fialkov J A, Davies J E and Shoichet M S 2003 Use of a biomimetic strategy to engineer bone *J. Biomed. Mater. Res. Part A* **65A** 447-53

## **5. Homogeneous, catalytic absorption of ethene by a modified Wacker process incorporated into a polymeric coating**

### **Abstract**

The present study investigates the ethene absorption capacity of a polymeric film material with a homogeneously incorporated modified Wacker catalyst (Catalytica process). An aqueous solution of poly(styrenesulfonic acid) and a catalytic system consisting of palladium chloride (catalyst) and a heteropolyanion (co-catalyst), more specifically  $\text{Na}_3\text{H}_3\text{PMo}_9\text{V}_3\text{O}_{40}$ , were solution-coated on a polyester carrier film and dried at ambient conditions. Different “catalyst to co-catalyst” ratios were evaluated for their performance in conversion of low ethene concentration (100 ppm) over an extended time period of three weeks and totally six loadings of 100 ppm ethene in synthetic air. The palladium content in the coating was kept constant at  $5 \text{ mg/m}^2$ . The ethene conversion was determined by gas chromatography using a flame ionization detector (GC-FID) and followed for up to 200 hours. While initially the catalytic films reached ethene levels of  $<5 \text{ ppm}$  within one day the activity drastically decreased after 3 weeks and six ethene loadings, where levels of  $<5 \text{ ppm}$  ethene were observed after about 5 days. The “catalyst to co-catalyst” ratio had only minor influence on the activity. Further an active coating was additionally covered with a polystyrene protection coating to prevent subsequent migration of the catalyst. The protected film converted roughly 50 ppm of ethene after 25 hours and three quarter of the initial  $\text{C}_2\text{H}_4$  concentration were absorbed after 60 hours. The high conversion rate suggests the use of such films for the packaging of ethene-sensitive fresh produce such as fruits, vegetables, or cut flowers.

Part of this chapter has been applied for as a PCT patent application (PCT/CH2007/000141).

## 5.1. Introduction

*Effect of ethene:* Control on the ripening process of fresh cut fruit, vegetables and flowers is a major issue when dealing with the time it takes from the harvest to the consumption implying distribution and storage at the distributor, seller and customer. Ethene is a key player in the growing process of many fruit, vegetables and flowers. More specifically, ethene accelerates respiration which results in maturity and senescence, softening and ripening of plants. It is therefore considered as a phytohormone being effective at parts-per-million to parts-per-billion concentrations [1, 2]. It has been observed that accumulation of ethene can even cause yellowing of green vegetables (e.g. broccoli) or specific post-harvest disorders leading to a quality loss and shortened shelf-life. Controlling the ethene concentration or its influence on the plant growth is crucial in today's quality management of any plant dealing industry. There are two major concepts to avoid ethene related ripening and senescence which will be elucidated in the following.

*Ethene receptor blocking:* Much research has focused on the blocking of ethene receptors in plants which would substantially slow down or stop the ripening process [3, 4]. The use of 1-methylcyclopropene (1-MCP) [5, 6] and its derivatives [7] is today commercially applied mostly to prolong the shelf-life of apple fruits in large storage rooms [8]. While this method shows great potential in centralized product storage it is limited in terms of application on the customer level. Further limitations of the process include possible genotoxic impurities, such as monohaloalkenes [9], the poor binding to the receptor and hence low efficiency at low temperatures [3], and the uncertainty regarding ethene recovery after 1-MCP treatment [10] since the blocking of the receptors seems to be irreversible.

*Prevention of accumulation of ethene:* Another approach is to avoid accumulation of plant-released ethene by either passive or active methods. Where "passive" means that no chemical reaction is involved in the ethene removing process. All passive solutions once in use are limited in terms of ethene adsorbing capacity and hence are inactive after a certain time period or an unusual burst of ethene until desorption mostly done by heating.

### **5.1.1. Passive methods**

Passive removal can be achieved either simply by sufficient ventilation or by introducing an adsorbing material. Latter might be in the form of sachets or incorporated into the packaging material. Most of existing investigations imply zeolites either of hydrophobic [11, 12] or hydrophilic [13] character. Incorporation of the zeolites and other inorganic materials (e.g. Ohya stone, cristobalite, orniophtilolite) in plastics ([14], realized in WO8900960) allows the use of the materials for packaging of ethene-sensitive produce. The problems associated with the zeolite approach are manifold: Hydrophilic zeolites loose their adsorption capacity with increasing humidity and even release already adsorbed ethene in case of water condensation in produce packs [15]. Further the adsorption isotherms at relevant ethene concentrations (e.g. 100 ppm) are rather poor which highly increases the amount of material needed. In addition the packaging materials containing zeolites have a hazy appearance attributed to scattering of the micrometer particles, which negatively affects consumer acceptance.

Other commercial applications in the form of packaging films use earth-type scavengers such as ground coral (US5084337), crysburite ceramic [16], Japanese Oya stone (Evert-Fresh bags, Evert-Fresh Corporation) or mixtures of minerals (US4847145). Apart of being not transparent, the claimed ethene adsorption capacity generally relies on shelf-life experiments and often lacks relevant experimental data. It is believed that the putative adsorption is in fact the result of an enhanced permeability of the mineral containing plastics.

### **5.1.2. Active methods**

Active removal of ethene implies a chemical reaction and can be subdivided into two processes. The first method describing a non-catalytic reaction is inactive after the reagent is consumed whereas the second process involves a catalytic absorption of ethene.

*Non-catalytic methods:* The most predominant non-catalytic approach for the removal of ethene is using oxidizing agents (e.g. potassium permanganate  $\text{KMnO}_4$ ). The permanganate is generally immobilized on any of several minerals (e.g. zeolites, silica and titania) having a high surface area ([17], US5314852, WO0154496, WO0130658, US5955004, WO9523517, US5075117). The products are available in the form of sachets for packages, blankets that can be placed in produce-holding rooms, and polymeric films or paper board with incorporated or entrapped activated minerals all showing an extension of shelf-life for different fresh produce

[18]. A further consumptive approach uses a compound having a hydrosilyl group and a hydrosilylation catalyst selected from group VIII metals which is carried on a porous inorganic material (EP0635219). In this case ethene reacts with the hydrosilyl group via hydrosilylation and therefore is limited to the amount of hydrosilyl groups present. Another solution for non-catalytic absorptions is composed of electron-deficient dienes or trienes (e.g. tetrazine) in an ethene-permeable, hydrophobic, polymeric substrate in the form of a film ([19], realized in WO9104292, WO2004076545, US5334623).

*Catalytic methods:* Commercial ethene scrubbers [Isocell Italia SPA] are available for fruit cool stores which transport the ethene containing air from the storage room to a heated reaction zone ( $\sim 270^{\circ}\text{C}$ ) using a supported platinum catalyst for the oxidation. Another possibility might be the sorption of ethene at room temperature (or at lower temperatures) followed by desorption and catalytic oxidation at higher temperatures. However such indirect oxidation processes include transportation of contaminated air or sorption material and a separated heating step, which is energy consuming. Further these methods are reasonable for large storage rooms of distributors but would be difficult to implement on the level of the seller (storage area or vending shelf) or even the consumer. For the latter it would be most convenient to directly oxidize the ethene at the vicinity of the ethene-sensitive product for example by the packaging material. The concept of active packaging implies that the catalyst is active at storage temperatures which normally range from  $0^{\circ}\text{C}$  to room temperature. Unfortunately most of the reactions (i.e. oxidation of VOC) under discussion occur above  $200^{\circ}\text{C}$  [20]. Only little is reported on catalysts active at temperatures below  $50^{\circ}\text{C}$  [20-22].

One catalytic approach is based on the use of an alcohol extract from plants, particularly raw bamboo, which may be used for the manufacturing of wrapping or packaging material (US20040210099). The authors assume that the enzyme ethene monooxygenase is responsible for the ethene absorption activity of the extract. Two investigations disclose palladium compounds, in particular palladium (II) chloride deposited on carbon black (US5015282) or activated carbon (US5436067). Latter covers also the process to fabricate a sheet consisting of a synthetic binder and  $\text{PdCl}_2/\text{carbon}$  for the use in low temperature removal of ethene. However the catalytic property of both materials is not fully clarified since it has been observed that palladium salts oxidize ethene to acetaldehyde while being reduced to  $\text{Pd}^0$  [23, 24]. The reoxidation of  $\text{Pd}^0$  to  $\text{Pd}^{\text{II}}$  without a co-catalyst is unlikely to happen.

Moreover the experiments lack relevant reference data and sheets containing carbon materials are not transparent but have a deep black appearance. The reoxidation of metallic Pd can be achieved including a co-catalyst. A heterogeneous approach was investigated making use of  $\text{H}_2\text{PdCl}_4$  adsorbed on  $\text{Al}_2\text{O}_3$  or  $\text{TiO}_2$  pre-coated with  $\text{V}_2\text{O}_5$ , which was active at mild conditions (1 atm, 293-353 K) [25].

Present industrial oxidation of ethene relies on the use of  $\text{CuCl}_2$  as reoxidation catalyst specific for the Wacker process [26, 27]. In conventional Wacker processes with palladium salt and  $\text{CuCl}_2$  high chlorine concentrations are needed which favors the formation of chlorinated byproducts. An alternative process had been proposed using palladium salt and heteropolyacids comprising vanadium (WO9113853, WO9113854) to circumvent this drawback. These investigations cover exclusively reactions of olefins in catalytic aqueous solutions at elevated olefin partial pressures.

## 5.2. Materials and Methods

### 5.2.1. Catalytic solution and film preparation

Catalytic solutions with different  $\text{Pd}^{\text{II}}$  concentrations were obtained by dissolving corresponding amounts of  $\text{PdCl}_2$  (99.9%, ABCR Chemicals) in a 0.3 M  $\text{Na}_3\text{H}_3\text{PMo}_9\text{V}_3\text{O}_{40}$  aqueous solution prepared following the procedure outlined in patent WO 91/13681. For film preparation the palladium content was chosen constant such that a palladium to dry polymer weight ratio of  $2.5 \times 10^{-4}$  was obtained. Corresponding amounts of catalytic solution were added to 5.0 g of poly(styrenesulfonic acid) solution (PSSA, 18wt% in  $\text{H}_2\text{O}$ , Sigma-Aldrich) and mixed thoroughly. The weight ratio of the heteropolyanion to dry PSSA (HPA/PSSA) was 0.12, 0.25, and 0.49, respectively. The resulting mixture was coated using an automatic film applicator (ZAA 2300, Zehntner GmbH) equipped with a 50  $\mu\text{m}$  doctor roller and dried at room temperature. An amorphous PET film (40  $\mu\text{m}$ ) was used as a substrate. A film containing no catalytic solution was prepared from the PSSA solution and used as a reference.

In one follow-up experiment the catalytic coating (HPA/PSSA=0.25) was subsequently coated with a 10  $\mu\text{m}$  polystyrene (BASF) film from a 20wt% solution in toluene.

### 5.2.2. Characterization methods

Ethene absorption experiments were done in closed 500 ml Erlenmeyer flasks at room temperature 23°C and 1 atm. In a first set of experiments the catalytic properties of the system palladium chloride / heteropolyanion (HPA, namely  $\text{Na}_3\text{H}_3\text{PMo}_9\text{V}_3\text{O}_{40}$ ) was investigated. 10 ml of the catalytic solution with different palladium concentrations (0, 0.1, 0.25, 2.5 mM  $\text{PdCl}_2$ ) and 0.3 M  $\text{Na}_3\text{H}_3\text{PMo}_9\text{V}_3\text{O}_{40}$  was tested for the conversion of 1000 ppm ethene (>99%, Fluka) in synthetic air. The solution was stirred at 1000 rpm with a magnetic stirrer to minimize mass transfer limitation.

In a second set of experiments, the coated films (0.9 g PSSA, ca. 400 cm<sup>2</sup>) were put in 500 ml Erlenmeyer flasks, sealed with a septum and flushed for 4 minutes at a flow of 5000 ml/min with 100 ppm ethene in synthetic air (PanGas). In a typical experiment a set of catalytic films were tested together with the reference. For all ethene conversion experiments gas samples were withdrawn at specific time point with a gas-tight 500 µl syringe. First the syringe was flushed one time with the sample gas mixture and afterwards 100 µl were injected into a GC-FID (TraceGC, ThermoQuest) equipped with a wide bore capillary column (PoraPLOT Q, Chrompack). The split ratio was set to 25 and the carrier gas flow was kept constant at 10 ml/min applying isothermal oven conditions (40 °C). Observed chromatograms all showed one distinct peak which could be attributed to ethene using a standard ethene sample (>99%, Fluka). Ethene concentration is expressed as the peak area.

## 5.3. Results and Discussions

### 5.3.1. Activity of the aqueous catalytic solution

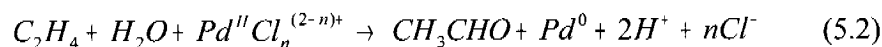
The catalytic performance of the system was first investigated in aqueous solutions. A relatively high concentration of ethene (1000 ppm) was chosen as to evaluate the turnover of palladium. Turnover meaning the number of cycles palladium has been reduced to  $\text{Pd}^0$  and reoxidized to the active  $\text{Pd}^{\text{II}}$ . The oxidation of ethene to acetaldehyde



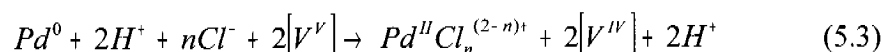
in our case can be subdivided into three reactions [28]:



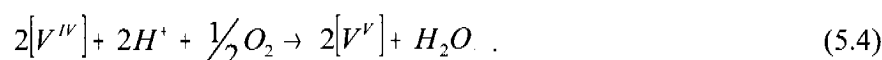
*Oxidation of ethene and reduction of Pd<sup>II</sup> to Pd<sup>0</sup>*



*Reoxidation of Pd<sup>0</sup> to Pd<sup>II</sup> and reduction of [V<sup>V</sup>] to [V<sup>IV</sup>]*



*Reoxidation of [V<sup>IV</sup>] to [V<sup>V</sup>]*



The conversion of ethene for 2.5 and 0.5 mM Pd proceeds very similar (Figure 5-1) leading to a reduction of ethene concentration <10 ppm after about 20 hours. This indicates that the rate determining step is either the reoxidation of Pd<sup>0</sup> (Eq. 5.3) or of [V<sup>IV</sup>] (Eq. 5.4) or most likely of all we encounter mass transfer limitation. For 0.1 mM Pd the reaction clearly slows down and a ethene concentration of <10 ppm is reached after about 45 hours. Limitation due to mass transfer for this conditions can therefore be excluded and one of the reactions Eq. 5.2 to 5.4 is rate determining. Although the solution without palladium chloride is active a reduction to <10 ppm ethene was not reached within the time tested and a final concentration of around 250 ppm was observed after 48 hours. Assuming first order kinetics for the overall reaction the rate constant [h<sup>-1</sup>] can be calculated (Table 5-1) by linear fitting of the data when  $-\ln(c_{\text{Ethene}} - c_{0,\text{Ethene}})$  is plotted against time (Figure 5-2), where  $c_{\text{Ethene}}$  is the ethene concentration at a specific time and  $c_{0,\text{Ethene}}$  is the initial ethene concentration. In the case of 0.1 mM Pd the palladium has done 21 cycles indicating its catalytic activity in the oxidation of ethene.

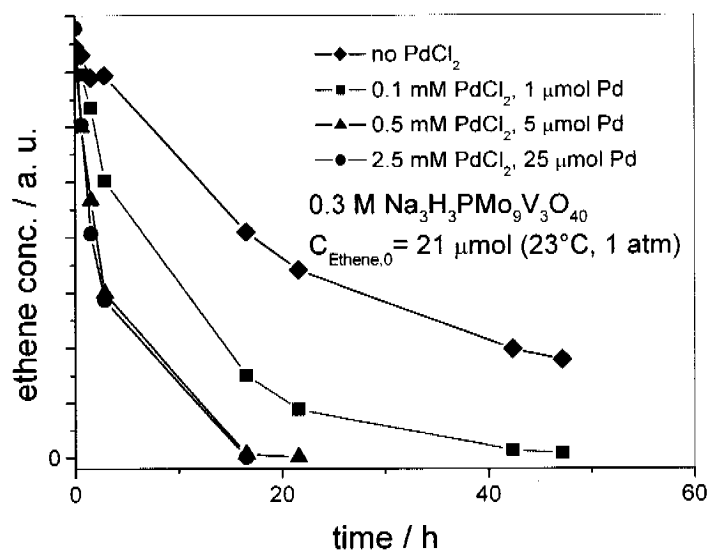


**Figure 5-1.** Ethene concentration as a function of time for different aqueous catalytic solutions. The palladium chloride concentration has been varied from 0 to 2.5 mM and the co-catalyst concentration was held at 0.3 M.

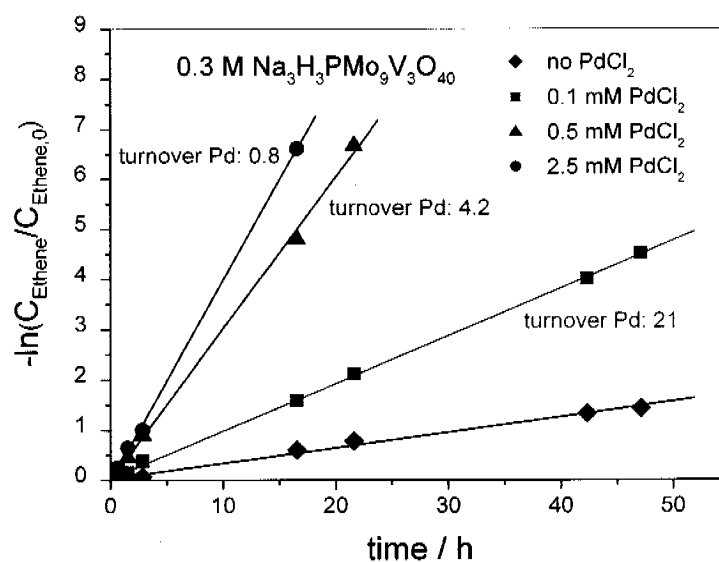


**Figure 5-2.** Logarithmic plot of the normalized ethene concentration versus time. Linear regression was used for data fitting assuming first order kinetics. The reaction rate constant is given as the corresponding slope of the linear fitting line.

**Table 5-1** Calculated reaction rate constants assuming first order kinetics.

Sample	PdCl <sub>2</sub> concentration / [mM]	Reaction rate constant / [h <sup>-1</sup> ]
no PdCl <sub>2</sub> 0.3 M Na <sub>3</sub> H <sub>3</sub> PMo <sub>9</sub> V <sub>3</sub> O <sub>40</sub>	0	0.031
0.1 mM PdCl <sub>2</sub> 0.3 M Na <sub>3</sub> H <sub>3</sub> PMo <sub>9</sub> V <sub>3</sub> O <sub>40</sub>	0.1	0.095
0.5 mM PdCl <sub>2</sub> 0.3 M Na <sub>3</sub> H <sub>3</sub> PMo <sub>9</sub> V <sub>3</sub> O <sub>40</sub>	0.5	0.302
2.5 mM PdCl <sub>2</sub> 0.3 M Na <sub>3</sub> H <sub>3</sub> PMo <sub>9</sub> V <sub>3</sub> O <sub>40</sub>	2.5	0.400

### 5.3.2. Activity of the film material

Addition of the different catalytic solutions (PdCl<sub>2</sub>/Na<sub>3</sub>H<sub>3</sub>PMo<sub>9</sub>V<sub>3</sub>O<sub>40</sub>) to an aqueous poly(styrenesulfonic acid) solution resulted in stable homogeneous mixtures. This mixtures were applied on a carrier film using a doctor blade coater. After ambient curing smooth, translucent polymer films of deep yellow color resulted. The reference film was prepared from the pure aqueous PSSA solution and showed high translucence and a slightly yellow color. PSSA was used to maintain acidic conditions needed for optimal activity [28]. In a first run of 100 ppm ethene loading all three films with different HPA content but the same palladium loading (5 mg/m<sup>2</sup>) showed similar reactivity (Figure 5-3). Although the film with the highest HPA concentration (HPA/PSSA=0.49) clearly exhibits the best performance. After 25 hours the ethene concentration reached values below of around 8 ppm, 4 ppm and 3 ppm for HPA/PSSA= 0.12, 0.25, and 0.49, respectively. For the reference film the concentration was still in the range of 90 ppm. It has to be noted that approximately 2 μmol of ethene was initially present in the flask which corresponds roughly to the amount of Pd present in the 400 cm<sup>2</sup> film. Therefore, theoretically, the catalytic activity of the film would not have been proofed. A second run (100 ppm ethene) was conducted after 25 hours and the reaction was followed until <10 ppm ethene was reached.

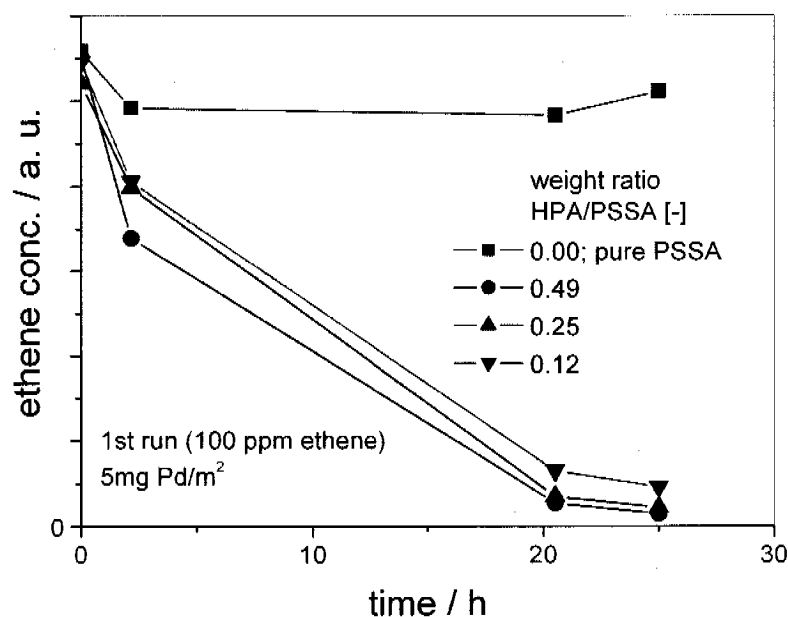


**Figure 5-3.** Ethene content as a function of time for a first loading of the reaction flask with 100 ppm ethene and for poly(styrenesulfonic acid) (PSSA) films containing catalytic solutions with 5 mg Pd/m<sup>2</sup> and different heteropolyanion (HPA; specifically Na<sub>3</sub>H<sub>3</sub>PMo<sub>9</sub>V<sub>3</sub>O<sub>40</sub>) concentrations.

The third loading 4 days after the first run clearly showed a decreased activity if compared to the first run and the concentration fell below 10 ppm for all catalytic films after 43 hours (Figure 5-4). This observation allows for the exclusion of a diffusion limiting step. Again the film with the highest HPA concentration (HPA/PSSA=0.49) performed best with around 3 ppm followed by HPA/PSSA=0.25 with ~4 ppm and HPA/PSSA=0.12 with ~7 ppm at 46 hours. The trend of better performance of high HPA/PSSA concentrated films is especially pronounced at a later stage of the reaction at time points >20 hours. Up to this point the palladium has been reactivated at least twice.

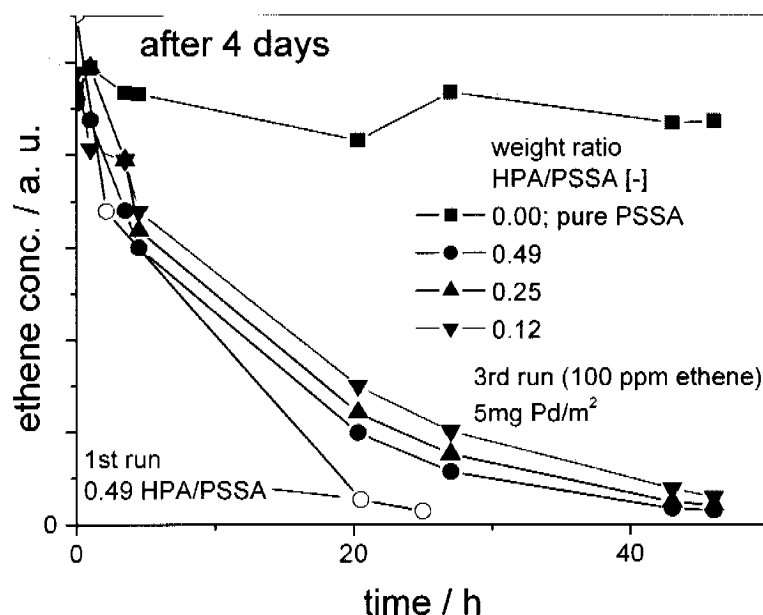


**Figure 5-4.** Third loading of the reaction flask with 100 ppm ethene after 4 days of first experiment. The catalytic activity of the films decreased and concentrations below 10 ppm are observed after 45 hours.

After 3 weeks the performance was measured in a sixth ethene loading where a further decrease of the activity was observed (Figure 5-5). At 130 hours after filling the ethene concentration was in the range of 2-3 ppm for all catalytic films and even fall below 1 ppm when measured after about 200 hours. At this time the reference sample still contained about 60 ppm ethene. The steady ethene decrease might be attributed to diffusion through the septum or minute activity of the PSSA. The continuous drop in activity for the repeated runs clearly indicates that the rate limiting step can be attributed to the chemical reaction and further that a change of the catalytic system occurs. In the first run, theoretically, all ethene might have been reacted without the need of reoxidation of  $\text{Pd}^0$  since similar amounts of ethene and palladium(II) are present in the experiment. But since the high loaded HPA films performed better both either the reoxidation of  $\text{Pd}^0$  (Eq. 5.3) or the oxidation of  $[\text{V}^{\text{IV}}]$  to  $[\text{V}^{\text{V}}]$  (Eq. 5.4) might play the key role. A further significant decrease in activity for the sixth run compared to the third indicates that the catalytic system in the present formulation is not

stable. One possible explanation is the poisoning effect sulfur (in PSSA) might have on the palladium catalyst.

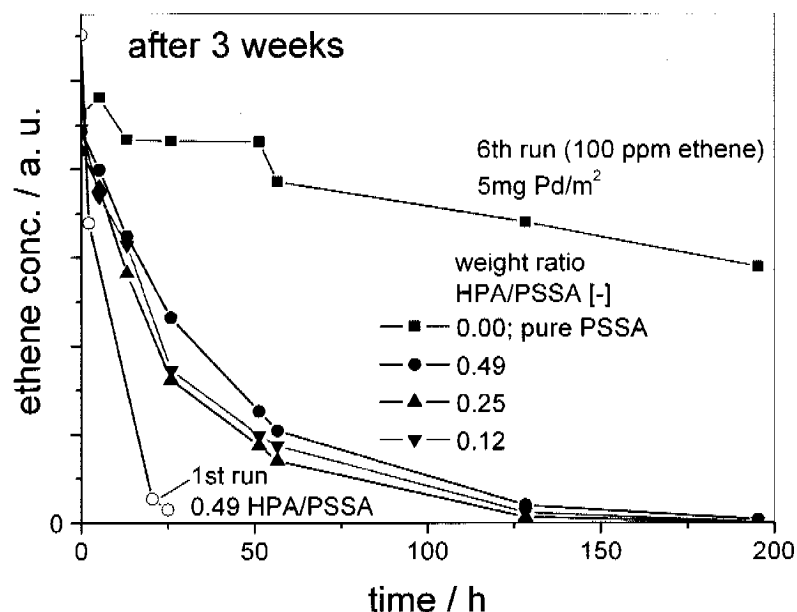


**Figure 5-5.** Third loading of the reaction flask with 100 ppm ethene after 4 days of first experiment. The catalytic activity of the films decreased and concentrations below 10 ppm are observed after 45 hours.

In a follow-up experiment an active film (HPA/PSSA=0.25) was subsequently covered by a polystyrene protection coating as to prevent migration of the catalyst to the packaged product. In a first run with 100 ppm ethene the protected film clearly showed a decreased activity if compared to the unprotected active coating (Figure 5-6). Half of the initial ethene concentration was converted after 25 hours and a quarter was left after around 60 hours which is comparable to the activity of the six times loaded unprotected films (Figure 5-5). There are two possible effects which might influence the activity of a protected film. First the ethene has to diffuse through the protective coating in this case polystyrene before it comes into contact with the active film material. Second the material of the protective cover either in its wet form or as a dry coating influences the catalyst in the layer underneath. In our case the toluene might have negatively affected the catalyst system especially the palladium component and therefore diminished the activity.

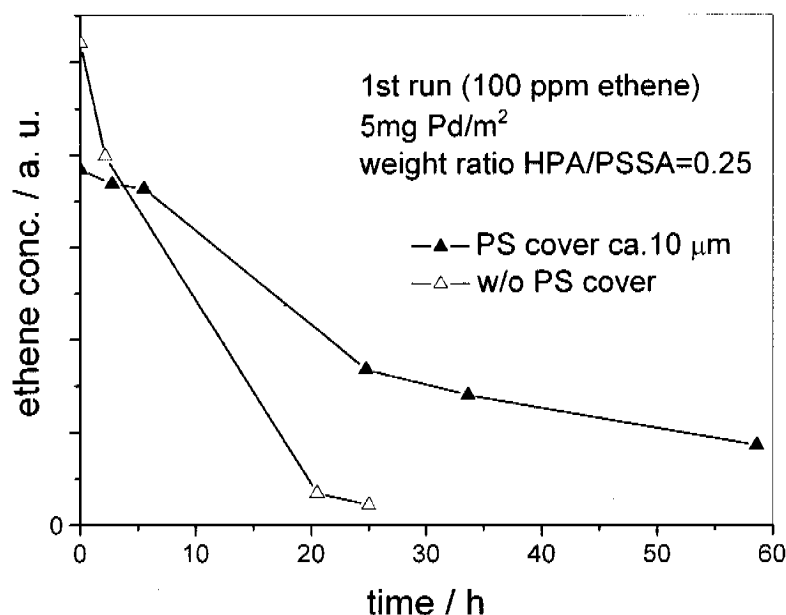


**Figure 5-6.** Comparison of a catalytic film with and without a 10µm polystyrene (PS) cover coating. Weight ratio of heteropolyanion (HPA) to polymer is held at 0.25.

## 5.4. Conclusions

A modified Wacker process consisting of an aqueous solution of palladium (II) chloride and a heteropolyanion (phosphomolybdovanadate,  $\text{Na}_3\text{H}_3\text{PMo}_9\text{V}_3\text{O}_{40}$ ) was successfully incorporated into a poly(styrenesulfonic acid) film. The solution-coated, translucent coatings with different  $\text{Na}_3\text{H}_3\text{PMo}_9\text{V}_3\text{O}_{40}$  concentrations and constant  $\text{PdCl}_2$  loading (5 mg/m<sup>2</sup>, constraint for price) were investigated for the homogeneous catalytic oxidation of ethene at concentrations  $\leq 100$  ppm at room temperature and ambient pressure. While the initial 95% conversion of ethene was observed after 25 hours the activity drastically decreased after six loadings of 100 ppm ethene over a time period of three weeks. At that time the catalytic films was still able to reach a level of  $< 5$  ppm  $\text{C}_2\text{H}_4$  within 130 hours. The performance decrease over time could be attributed to an unstable catalyst system in the poly(styrenesulfonic acid) matrix.

An active film covered with a polystyrene coating showed a 50% conversion after 25 hours. The application of a protective polystyrene coating onto the active film material avoids

migration of the catalyst system to the packaged product. The present active film material suggests the use for packaging of ethene-sensitive fresh produce such as fruits, vegetables and flowers.

## 5.5. Acknowledgements

Financial support by the Swiss Commission for Technology and Innovation, CTI project 7021.2.

## 5.6. References

- [1] Abeles F B, Morgan P W and Saltveit M E 1992 *Ethylene in plant biology*. (San Diego: Academic Press)
- [2] Saltveit M E 1999 Effect of ethylene on quality of fresh fruits and vegetables *Postharvest Biol. Technol.* **15** 279-92
- [3] Sisler E C and Serek M 1997 Inhibitors of ethylene responses in plants at the receptor level: Recent developments *Physiol. Plant.* **100** 577-82
- [4] Sisler E C and Serek M 2003 Compounds interacting with the ethylene receptor in plants *Plant Biol.* **5** 473-80
- [5] Daly J and Kourelis B 1999 *Complexes and delivery methods for the safe and convenient storage, transport and application of compounds for inhibiting the ethylene response in plants* patent EP1597968
- [6] Sisler E C and Blankenship S M 1994 *Method of counteracting an ethylene response in plants* patent WO9533377
- [7] Sisler E C 2000 *Methods of blocking an ethylene response in plants using cyclopropene derivatives* patent WO0137663
- [8] Watkins C B 2006 The use of 1-methylcyclopropene (1-MCP) on fruits and vegetables *Biotechnol. Adv.* **24** 389-409
- [9] Anonymous. Conclusion regarding the peer review of the pesticide risk assessment of the active substance 1-methylcyclopropene: European Food Safety Authority; 2005.
- [10] Jeong J and Huber D J 2004 Suppression of avocado (*Persea americana* Mill.) fruit softening and changes in cell wall matrix polysaccharides and enzyme activities: Differential responses to 1-MCP and delayed ethylene application *J. Am. Soc. Hortic. Sci.* **129** 752-59
- [11] Kooijman P and Anthon C 1995 *Reducing concentration of unwanted component, esp. ethylene, in atmosphere in enclosable chamber* patent NL1000595
- [12] Shigemi O and Tokutarou M 1991 *Low-temperature storage case* patent EP0417811
- [13] Sextl E, Heindl F, Gaitzsch T and Full R 1999 *Process for the adsorption of ethylene* patent EP1106233
- [14] Sextl E, Maier H J and Mueller M 2000 *Plastics for absorption of volatile organic compounds* patent EP1170327
- [15] Yamashita H 2000 Introduction to active food packaging technologies *Innovations in food packaging* ed Han J H (Amsterdam: Elsevier Academic Press) pp 121-43
- [16] Joyce D C 1988 Evaluation of a Ceramic-Impregnated Plastic Film as a Postharvest Wrap *Hortscience* **23** 1088-88
- [17] Klätte F 1992 *Chemically impregnated zeolite and method for chemically impregnating and coating zeolite* patent US5278112



- [18] Chamara D, Illeperuma K, Galappatty P T and Sarananda K H 2000 Modified atmosphere packaging of 'Kolikutu' bananas at low temperature *Journal of Horticultural Science & Biotechnology* **75** 92-96
- [19] Holland R V 1990 *Absorbent material and uses thereof* patent WO9104292
- [20] Spivey J J 1987 Complete Catalytic-Oxidation of Volatile Organics *Industrial & Engineering Chemistry Research* **26** 2165-80
- [21] Gonzalez R D and Nagai M 1985 Oxidation of Ethanol on Silica Supported Noble-Metal and Bimetallic Catalysts *Applied Catalysis* **18** 57-70
- [22] McCabe R W and Mitchell P J 1986 Exhaust-Catalyst Development for Methanol-Fueled Vehicles .1. a Comparative-Study of Methanol Oxidation over Alumina-Supported Catalysts Containing Group-9, Group-10, and Group-11 Metals *Applied Catalysis* **27** 83-98
- [23] Phillips F C 1894 *Am. Chem. J.* **16** 255-77
- [24] Phillips F C 1894 *Z. Anorg. Chem.* **6** 213-28
- [25] Vanderheide E, Zwinkels M, Gerritsen A and Scholten J 1992 Oxidation of Ethylene to Acetaldehyde over a Heterogenized Surface-Vanadate Wacker Catalyst in the Absence of Gaseous Oxygen *Appl. Catal. A-Gen.* **86** 181-98
- [26] Smidt J, Hafner W, Jira R, Sedlmeier J, Sieber R, Ruttinger R and Kojer H 1959 Catalytic Reactions of Olefines on Platinum Metal Compounds *Angew. Chem.-Int. Edit.* **71** 176-82
- [27] Smidt J, Sedlmeier J, Hafner W, Sieber R, Sabel A and Jira R 1962 The Oxidation of Olefins with Palladium Chloride Catalysts *Angew. Chem.-Int. Edit.* **1** 80-88
- [28] Gate J H, Hamm D R and Mahajan S 1993 Palladium and Phosphomolybdovanadate catalysed olefin oxidation to carbonyls *Polyoxometalates* eds Pope M T and Müller A (Dordrecht [etc.]: Kluwer Academic) pp 281-305.



## 6. Silver-doped tricalcium phosphate nanoparticles as highly efficient antimicrobial agents in hydrophobic polymers

### Abstract

Silver-doped tricalcium phosphate (Ag-TCP) with silver contents ranging from 1wt% to 10wt% and silver-doped silica (Ag-SiO<sub>2</sub>) containing 1wt% and 5wt% silver were prepared by flame spray synthesis. The characteristics of the powders were compared to pure tricalcium phosphate and currently used antimicrobial agents. The morphology and the phase composition of the powders was accessed by electron microscopy, nitrogen adsorption, X-ray disc centrifugation and X-ray powder diffraction. While all flame-made powders and one reference material were composed of a nanoparticulate support carrying finely dispersed, <10 nm metallic silver particles the most widely used commercial material consisted of large, >1 µm particles containing no detectable amounts of metallic silver.

As to access the antimicrobial efficacy of a hydrophobic polymer by ASTM E2149-01 and ASTM E2180-01 the materials were incorporated into a silicone elastomer film. All films containing 20wt% of flame-made Ag-TCP showed a 4- to 6-log reduction of Gram-negative *E.coli* in both tests. Films containing flame-made Ag-SiO<sub>2</sub> showed only a 2- to 4-log reduction and were at least 10 fold less efficient as corresponding films with Ag-TCP. *In a direct comparison of Ag-TCP films and both commercial products the efficiency of the phosphate containing carrier clearly excelled by a factor of 100 to 1000.* The Ag-TCP film further exhibited high efficacy (4-log to 6-log reduction) against *P.aeruginosa* and *C.albicans*. The exceptional antimicrobial activity of Ag-TCP films suggest the use of such materials for the coating of surfaces in sanitary and hospital facilities and for the packaging of food and pharmaceuticals.

Part of this chapter has been applied for as a PCT patent application.

## 6.1. Introduction

Silver has been used for decades as a disinfectant predominately in the form of ionic silver solutions (e.g.  $\text{AgNO}_3$  solution). Although the activity of silver is not fully understood it enjoys a widespread application in different forms (ionic and metallic) and physical appearance (in solution or as a solid).

### 6.1.1. Release systems using ionic silver

Present commercial systems (US4938958) apply an antibiotic resin comprising 0.05-80wt% of ion-exchanged (e.g. silver ions) zeolites. In WO0030697 an antibiotic coating is described, comprising a hydrophilic polymer with dispersed antibiotic ceramic particles such as ion-exchanged zeolites, hydroxyapatite, and zirconium phosphate. Sugiura A. et al. (US5296238) and Ohsumi S. et al. (US5441717) have investigated micro-biocides composed of a phosphate salt of a tetravalent metal element, specifically Zr, Ti, and Sn, which carries effective amounts of antibacterial, antifungal or antialgal ions such as Ag, Cu, Zn, and the like. Silver containing hydroxyapatite materials were evaluated by Sakuma S. et al. (US5009898) as an antimicrobial powder comprising hydroxyapatite containing absorbed silver ions. Barry J. E. and Trogolo J A (WO0018577) have done investigations on a high-pressure laminate with antimicrobial properties attributed to inorganic antibiotic particles such as silver-exchanged zeolites, hydroxyapatite, zirconium phosphate, and/or silver salts. Terry R. (WO0143788) investigated a polymer containing silver salt colloids and its use as a medical device.

Delivering the silver from an ionic form is problematic in terms of its relatively fast release and hence the danger of a burst of ionic silver which exceeds the cytotoxic threshold. This is especially true for systems consisting of silver salts such as silver nitrate, silver acetate, or the like. If the release is fast the duration of activity is limited. As a result the silver content must be chosen high which unfortunately increases the risk of an undesired cytotoxic effect of the material. The white color of most of the silver substituted materials has been considered an advantage compared to the metallic rather grayish or brownish powders. Unfortunately, if no so-called photo stabilizer is used many of the ionic delivery systems tend to discolor and appear brownish upon exposure to light. This discoloration may take place at the customer's resulting in disaffection with the product. Most of the above mentioned ionic silver systems use a carrier which can be considered as persistent, meaning not degradable in

a biologic environment (biodegradable) within a reasonable time. Biodegradable carriers mentioned above include for example hydroxyapatite as described in US5009898.

### **6.1.2. Release systems using metallic silver**

The release of silver ions from metallic silver is a slow process but sufficient in certain circumstances to develop an antimicrobial activity. Using metallic silver allows for a virtually never ending supply of silver ions although limited through its solubility a cytotoxic burst is unlikely to happen in environments relevant to its later use. Without doubt, the release of silver ions from metallic silver is strongly dependent on the surface of the metal and therefore the size of the particles.

#### **6.1.2.1. Materials having no carrier**

Bechert T. and Steinbruecke P. (EP1621217) have developed an antimicrobial metallic silver material with primary particle mean diameter between 10 to 100 nm and the incorporation of the antimicrobial material in a polymer matrix. Wagener M. and Hartwig A. (WO03024494) prepared an antimicrobial adhesive and coating material with metallic silver particles with low (<5ppm) Ag, Na, and K ion content and a particle size below 100 nm, preferably in the range of 5-50 nm. Both above mentioned work uses silver particles obtained by an inefficient evaporation/condensation process in vacuum rendering the silver nanoparticles a costly material.

#### **6.1.2.2. Materials with inorganic carrier**

Zeng F. Y. (CN1792508) has investigated an antimicrobial material comprising silver nanoparticles deposited on TiO<sub>2</sub>, SiO<sub>2</sub>, ZrO<sub>2</sub> obtained by a sol-gel method. Baret G. (WO2005120441) has done work on cerium oxide, yttrium oxide or calcium titanate with dispersed silver sub-particles on the surface having a size between 20-200 nm and suggested the use in cosmetics. Nonniger R. and Schichter M. (US2005182152) have used a material for antimicrobial purposes with a core-shell structure, comprising an inorganic material having a particle size <100 nm and the shell being formed by at least one substance having an antimicrobial action (e.g. Ag, Cu). Cichos C. and Guggenbichler J. P. (WO2006092155) did work on a material comprising 0.1%-50% metallic silver deposited on BaSO<sub>4</sub> or equivalent inert material or micro cellulose for the external application in pharmaceuticals or cosmetics. Atsumi K. et al. (US5151122) have investigated a calcium containing phosphate, calcium

carbonate, calcium silicate or zeolite with metallic silver, zinc, and/or copper by a wet impregnation technique and subsequent high temperature treatment ( $>800^{\circ}\text{C}$ ) or reduction of the precipitated metallic salt with hydrogen. Guggenbichler J. P. and Cichos C. (WO2004024205) evaluated the treatment of a metallic colloid with a polymer or an inorganic material composed of barium sulfate, calcium sulfate, strontium sulfate, titanium dioxide, aluminum oxide, silica, zeolite, calcium fluoride, mica, talc, hydroxyapatite, kaolin and/or micro cellulose with additional deposition of a soluble or slightly soluble salt of an antimicrobial metal (such as silver, zinc, copper, cerium, zirconium, bismuth, platinum and/or gold). Pratt A. S. and Smith P. R. (EP0190504) have done investigations on an antimicrobial composition comprising an antimicrobial metal such as silver and a hydratable or hydrated oxide component and its dispersion in a polymeric material.

*Physical properties of the metallic particles:* The use of metallic silver as a particle alone or supported on an inorganic material allows for dispersion of the particulate material in a polymeric substrate. A low water content of the particles is desired in case of dispersing them in hydrophobic polymers or pre-polymers to obtain best possible results in terms of dispersibility. Low water content is also advantageous in terms of thermal post treatment of the polymer which would result in the release of water vapor or bubble formation in the used polymeric material. Most of the inorganic supports discussed above are obtained by a wet chemistry process which generally entails large  $>10\%(\text{w/w})$  of water in the resulting inorganic powder.

The use of metallic silver generally entails a darkening of the treated product. However a subsequent discoloration at the customer's can be avoided.

The size of the metallic silver particles limits the dissolution and the release of ionic silver. Therefore it is desired to have small particles of metallic silver present in the antimicrobial material. Most discussed work describe antimicrobial materials with metallic silver particle sizes above 5 nm (e.g. EP1621217, WO03024494, WO2005120441). However present methods for the preparation of colloidal silver allow obtaining silver particles below 5 nm although this process is inefficient requiring large amounts of solvents and surfactants.

Using a carrier for the metallic nanoparticles has the advantage of keeping them separated and the amount of active material (in this case silver) in a later polymeric formulation can be easily adjusted. Dispersibility of the powder in the polymer or pre-

polymer is also facilitated when using a support material. The size of the used support material in many of the patented materials lies above 1  $\mu\text{m}$  rendering the obtained antimicrobial polymer opaque or at least limited in terms of transparency because of the intense light scattering of particles  $>200\text{ nm}$ . A favored carrier therefore would have particle sizes below 200 nm.

*Ecological advantages of degradable supports.* Most of the mentioned patents describing inorganic/metallic silver materials use oxidic materials, sulfates, or persistent phosphates such as  $\text{Zr}_3(\text{PO}_4)_4$ . The use of non-persistent support materials is ecologically advantageous and furthermore minimizes the threat of the material to humans [1, 2]. To obtain the best possible result in terms of transparency and dispersibility a nanoparticulate form of the support material is desired. However it has been shown that nanoparticulate materials enter cells and may have a toxic effect. In case of persistent materials the damage is unsure and may not be evaluated within a reasonable time.

*Active silver release on demand.* As a matter of fact the growth of most unwanted occurring microorganisms on the surface of commodity products is often nutrition limited. Using a non-persistent support which provides nutrition ions such as phosphates but which also carries a highly active antimicrobial (e.g. silver in a nanoparticulate form) could function as a Trojan horse. Such a release-on-demand proceeds as follows: While the inorganic support material at the vicinity of the surface of a polymeric coating or bulk material is slowly taken up by a microorganism the deadly agent (in this case silver nanoparticles) would also be taken up. The silver nanoparticles which crossed the wall of the microorganism now function as a silver ion supply right at the most vulnerable location being most efficient. Silver nanoparticles in the bulk material still release silver ions to the environment resulting in a twofold attack to microorganisms in contact with the antimicrobial material.

## 6.2. Materials and Methods

### 6.2.1. Polymeric coating preparation

Silver tricalcium phosphate nanoparticles (Ag-TCP) and silver silica (Ag-SiO<sub>2</sub>) were prepared by flame spray pyrolysis [6]. The silver precursor was obtained by dissolving silver acetate in 2-ethylhexanoic acid (puriss.  $\geq 99\%$ , Fluka). Calcium hydroxide (Riedel de Haen, Ph. Eur.) dissolved in 2-ethylhexanoic acid (puriss.  $\geq 99\%$ , Fluka) and tributyl phosphate (puriss.  $\geq 99\%$ , Fluka) were used as calcium and phosphate sources, respectively [5, 7] while hexamethyldisiloxane (HMDSO,  $>98\%$ , Lancaster Synthesis GmbH) was used as silica precursor. The correspondingly mixed liquid was diluted to a final metal concentration of 0.75 M with toluene (puriss p.a., Ph. Eur.,  $\geq 99.7\%$ , Riedel de Haen) and fed through a capillary (diameter 0.4 mm) into a methane/oxygen flame at a rate of 5 ml min<sup>-1</sup>. Oxygen (5 L min<sup>-1</sup>, 99.8%, Pan Gas) was used to disperse the liquid leaving the capillary and resulted in a burning spray of about 10 cm height [5]. A more detailed view on the nanoparticle formation may be found in [8].

The as-formed particles were collected on a glass fibre filter (Whatman GF/A, 25.7 cm diameter), placed on a cylinder mounted above the flame, by the aid of a vacuum pump (Busch Seco SV 1040 C). After removal of the product from the filter the particles were sieved (450  $\mu\text{m}$  mesh) and 1.0 g powder was dispersed in 16.0 g 2-propanol (Ph. Eur., Fluka). Dispersion was done using an ultra sonic mini flow cell (Dmini, Hielscher, 5 bar water pressure, power 250 W, frequency 24 kHz). The flow rate was adjusted with a peristaltic pump (REGLO Digital MS-2/6, Ismatec) to 2 ml/min. Subsequently, 4.0 g of a thermoplastic silicone elastomer (Geniomer200, Wacker Silicone) was dissolved in the dispersion by mixing at room temperature. The obtained mixture was applied (50  $\mu\text{m}$  wet coating if not otherwise stated) on a 36  $\mu\text{m}$  PET film using an automatic film applicator coater (ZAA 2300, Zehntner Testing Instruments) equipped with a spiral doctor blade. The applied film was cured at ambient condition resulting in a 10  $\mu\text{m}$  thick, dry coating containing 20wt% of the flame-made powder. In addition to in-house prepared powders two commercially available products, namely HeiQ-Silver (HeiQ, Switzerland) and Ionpure40 (Ishizuka Glass Co. L.t.d., Japan), were also investigated. HeiQ-Silver is a flame-made nanoparticulate silver-doped silica containing 25wt% silver, predominately in metallic form deposited on a silica matrix. Ionpure40 consists of silver ions incorporated into a glass matrix with a particle size  $<4 \mu\text{m}$ .



In the case of HeiQ-Silver 0.2 g of powder were used with 4.0 g polymer as to keep the silver content in the final coating at 1wt%. For Ionpure40 20wt% were used with 4.0 g polymer. The dispersion and coating procedure was done as mentioned above.

### 6.2.2. Characterization methods

Hydrodynamic particle size distributions of the Ag-TCP powders were measured on an X-ray disc centrifuge (BI-XDC, Brookhaven Instruments) [2, 9] using 3 % (wt/vol) of powder in absolute ethanol (Fluka) and the mean particle diameter was denoted as  $d_{XRD}$ . Prior to analysis the powder was dispersed by ultrasonication (UP400S, 24 kHz, Hielscher GmbH) at 200 W for 5 min. To determine the silver content the powders were digested in concentrated nitric acid and analyzed by flame atomic absorption spectrometry (AAS) on a Varian SpectraAA 220FS (slit width 0.5 nm, lamp current 4.0 mA) applying an air (13.5 L min<sup>-1</sup>, PanGas)/acetylene (2.1 L min<sup>-1</sup>, PanGas) flame and measuring absorption at a wavelength of 328.1 nm. Transmission electron microscopy (TEM) images were recorded on a CM30 ST (Philips, LaB6 cathode, operated at 300 kV, point resolution ~4 Å). Particles were deposited onto a carbon foil supported on a copper grid. Scanning transmission electron microscopy (STEM) images were obtained with a high-angle annular dark-field (HAADF) detector (Z contrast). Silver particle size distribution were determined by measuring at least 300 particles from scanning transmission electron microscopy images. Due to limiting resolution the smallest particles detectable were ~1nm. X-ray powder diffraction (XRD) patterns were recorded on a Stoe STADI-P2 (Ge monochromator, CuK<sub>α</sub> radiation, PSD detector, step mode, step size of 0.3°, ambient conditions). Antimicrobial activity of powder and film samples was determined by ASTM E2180-01 and ASTM E2149-01 at a temperature of 25°C. All values for reduction of colony forming units per milliliter (CFU/ml) are based on the “bacteria only” reference for powder samples and on the reference film (Geniomer200) for film samples. Further the comparison to the corresponding reference has been determined at the given contact time.

## 6.3. Results and Discussion

### 6.3.1. Powder characteristics

Flame synthesis is known as a most versatile tool for the production of nanoparticulate oxides and metal salt materials. Such materials can easily be doped with noble metals in a single step yielding support nanoparticles comprising finely dispersed noble metal. Synthesis of silver-doped tricalcium phosphate materials nicely depicts the result of single-step doping in the flame (Figure 6-1).

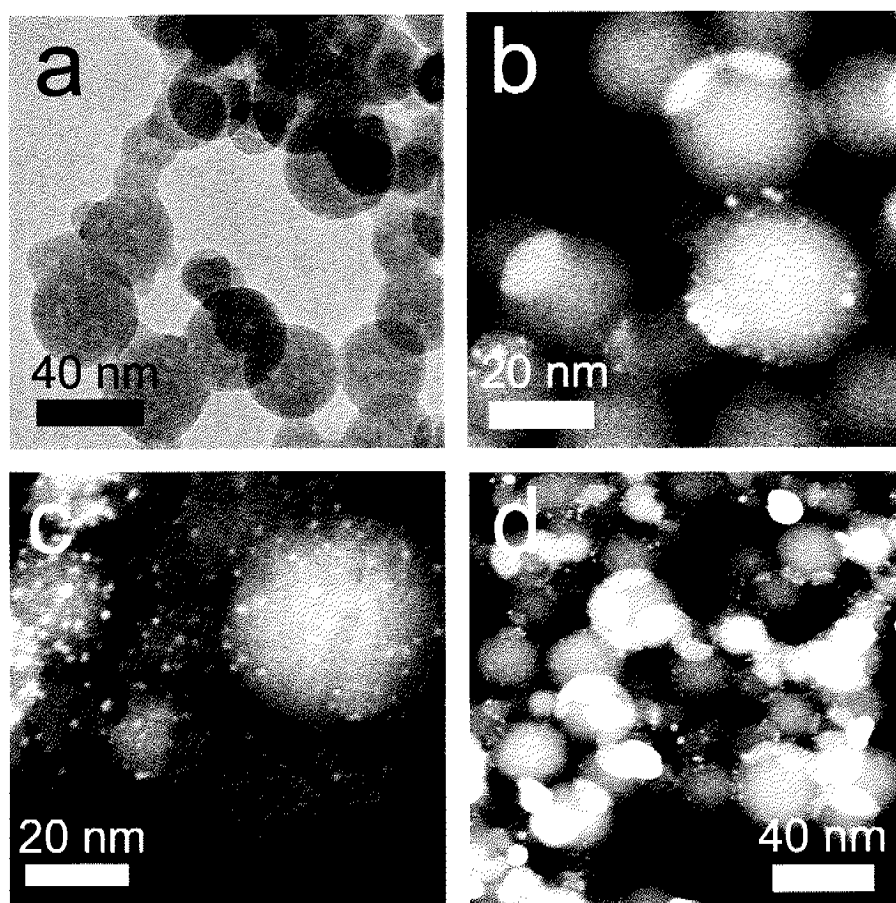


**Figure 6-1.** Transmission (a) and scanning transmission electron (b, c, d) images of pure TCP (a), 1 Ag-TCP (b), 5 Ag-TCP (c), and 10 Ag-TCP (d) showing a primary particle size of TCP in the range of 20-50 nm. Silver-doped samples (b, c, d) contain finely dispersed Ag particles (bright spots) with a smallest diameter of around 2-4 nm. Increasing the content of silver resulted in the formation of larger Ag clusters with a size around 10 nm (d).

While the pure tricalcium phosphate (TCP, Figure 6-1a) showed no distinct electron density gradients all silver-doped TCP samples (Figure 6-1b, c, d) carry small silver nanoparticles (bright spots) which was verified by energy dispersive X-ray measurements. A very dense, yet highly dispersed coverage with silver was observed for 5Ag-TCP (Figure 6-1c). The increase to 10wt% silver (sample 10Ag-TCP) resulted in the formation of relatively large Ag clusters with a size of  $>10$  nm (Figure 6-1d).

The primary particle size of the TCP ranging from 20-50 nm seems unaffected by the incorporation of silver in the system. This observation by electron microscopy is in line with the specific surface areas (Table 6-1) between  $71.6 \text{ m}^2 \text{ g}^{-1}$  and  $78.0 \text{ m}^2 \text{ g}^{-1}$  for pure TCP and silver containing TCP (1Ag-TCP to 10Ag-TCP). A comparison of the hydrodynamic diameter between sample 1Ag-TCP and 5Ag-TCP (Figure 6-2) further corroborates the similarity in morphology. Both samples exhibited a particle size in the range of 15-200 nm resembling a log-normal distribution as generally observed for flame-made powders.

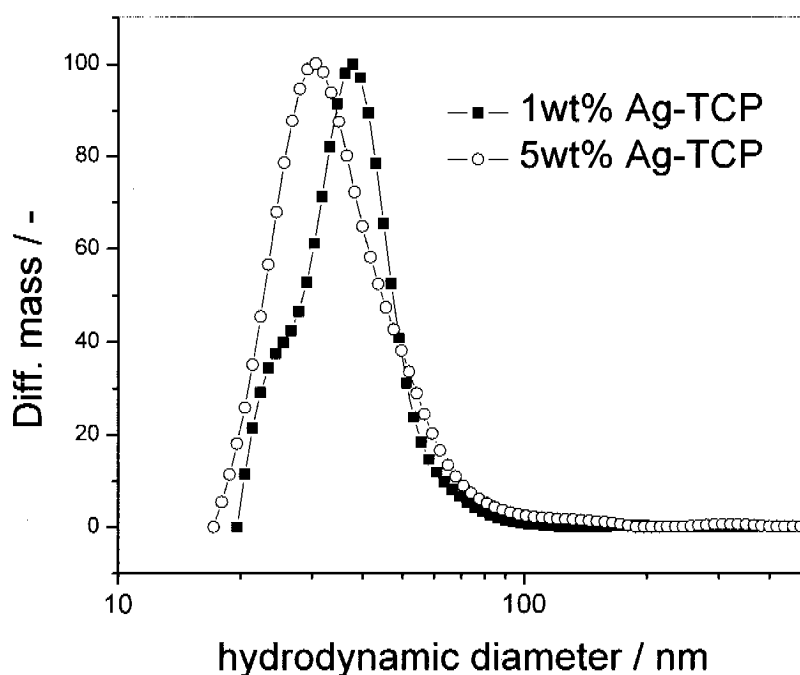


**Figure 6-2.** Hydrodynamic particle size distribution as determined by X-ray disc centrifugation. Both samples (1 Ag-TCP and 5 Ag-TCP) exhibit a very similar log-normal size distribution between 15-200 nm.

Silver silica samples (1Ag-SiO<sub>2</sub> and 5Ag-SiO<sub>2</sub>) show a very similar morphology although the primary particle size of the carrier, silica, tends to lower values which can be attributed to the higher melting point compared to TCP. An increase in melting point generally entails a decreased sintering ability of the agglomerates in the hot region of the flame and therefore yielding smaller primary particles and hence a higher specific surface area (Table 6-1).

**Table 6-1** Silver content as determined by atom absorption spectroscopy, specific surface area measured by nitrogen adsorption and antimicrobial activity accessed by ASTM E2149-01 using *E.coli* C43 (working bacterial concentration  $1 \times 10^5$  CFU/ml)

powder sample	Ag content <sup>a</sup> / wt%	SSA <sub>BET</sub> <sup>b</sup> / m <sup>2</sup> g <sup>-1</sup>	reduction after 2h compared to test without particles / %
TCP	0.004	78.0	54.06
1Ag-TCP	0.92	71.6	-
2Ag-TCP	1.88	72.6	-
3Ag-TCP	2.82	75.5	-
5Ag-TCP	5.19	75.8	99.98
7.5Ag-TCP	8.21	74.7	-
10Ag-TCP	10.7	74.8	-
1Ag-SiO <sub>2</sub>	1.09	271	-
5Ag-SiO <sub>2</sub>	4.33	357	-
HeiQ-Silver	18.0 (25.0 <sup>c</sup> )	110	-
Ionpure40	1.88	0.50	-

<sup>a</sup> error  $\pm 10\%$

<sup>b</sup> specific surface area, error  $\pm 3\%$

<sup>c</sup> as specified by the manufacturer

Scanning transmission electron micrographs of silver-doped silica (Figure 6-3a, b) depicted the very similar morphology to silver-doped TCP. Most of the silver particles (bright spots) are present in a nanoparticulate form of  $<10$  nm and deposited on the amorphous silica matrix. Transmission electron microscopy of the flame-made HeiQ-Silver sample (Figure 6-3c) revealed nanoparticulate silver on a silica carrier which underlined its origin (flame synthesis). Silver particles of around 5 nm and smaller are finely dispersed on the silica matrix and the high specific surface area of  $110 \text{ m}^2 \text{ g}^{-1}$  (Table 6-1) is in line with the primary particle size of 20-50 nm as observed by TEM (Figure 6-3c). Ionpure40 (Figure 6-3d) showed large particles and the absence of electron density gradients which corroborated the

specification of the manufacturer (ionic silver). The small specific surface area (Table 6-1) of  $0.5 \text{ m}^2 \text{ g}^{-1}$  further underlined the enormous difference in particle size to flame synthesized powders.

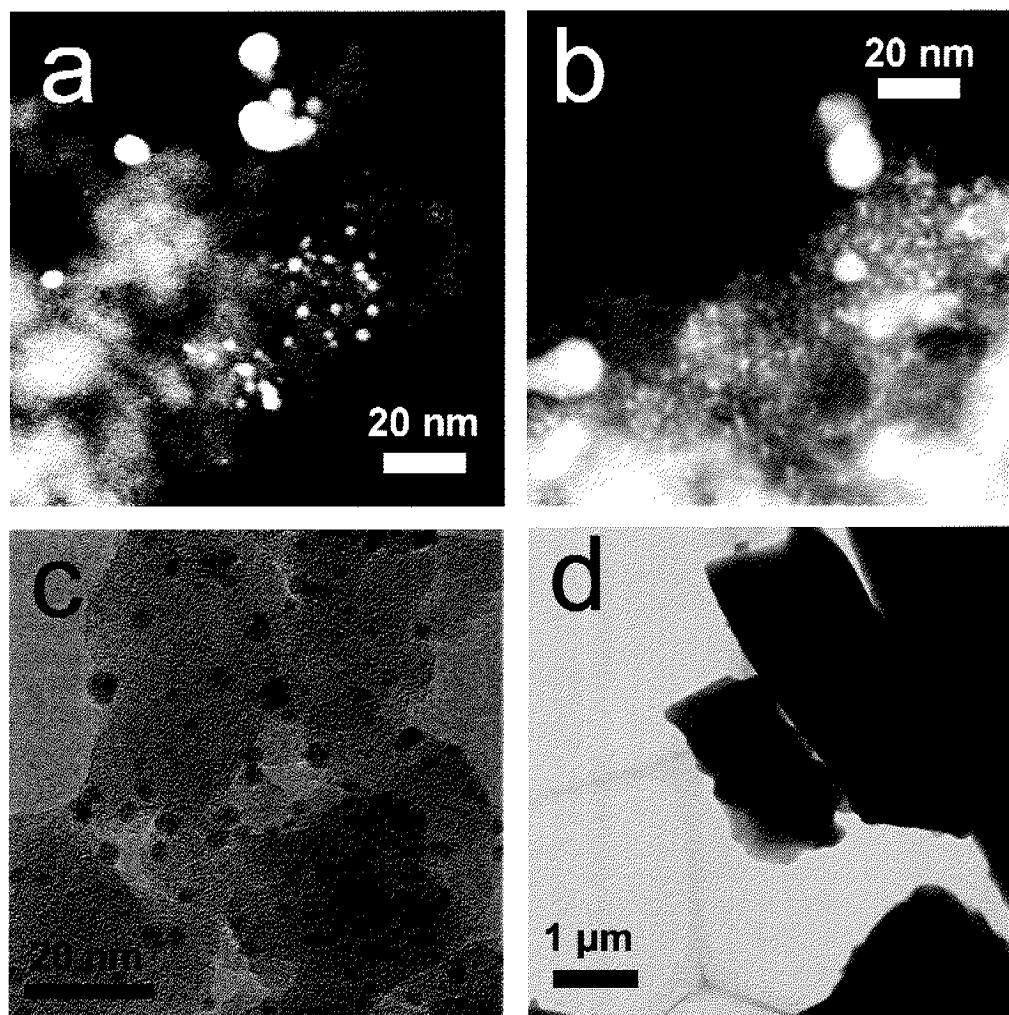


**Figure 6-3.** Scanning transmission electron images of 1Ag-SiO<sub>2</sub> (a) and 5Ag-SiO<sub>2</sub> (b) prepared in-house by flame synthesis. Finely dispersed silver nanoparticles are deposited on the silica matrix. Transmission electron images of HeiQ-Silver (c) depicted silver nanoparticles in the range of 5 nm carried on silica particles. The transmission electron micrograph of Ionpure40 (d) showed large,  $>1 \mu\text{m}$  particles and no indication of metallic silver was observed.

Atom absorption spectroscopy confirmed the robustness of the flame process in terms of silver content (Table 6-1). Except for sample 5Ag-SiO<sub>2</sub> all values were within the error of measurement. This discrepancy for the silica sample might be attributed to the incomplete dissolution of silica in nitric acid. It can be assumed that only silver which is not captured within the silica matrix is included in the measurement. The dissolution of the HeiQ-Silver sample also seemed to be insufficient since only 18wt% Ag were detected in our measurements. Unfortunately, the manufacturer of Ionpure40 did not specify the glass composition nor the silver content. Therefore the content of around 2wt% silver has to be handled with care.

*Silver particle size distribution.* The silver particle number size distribution was determined for flame-made Ag-TCP and Ag-SiO<sub>2</sub> (Figure 6-4). Most of the silver particles exhibited a diameter of <10 nm for all samples. While the 1wt% containing samples (1Ag-TCP and 1Ag-SiO<sub>2</sub>) showed a very similar size distribution the powders with 5wt% silver clearly revealed a trend to smaller particles for the TCP carrier. Most of the silver for 5Ag-TCP was present as nanoparticles smaller than 2 nm.

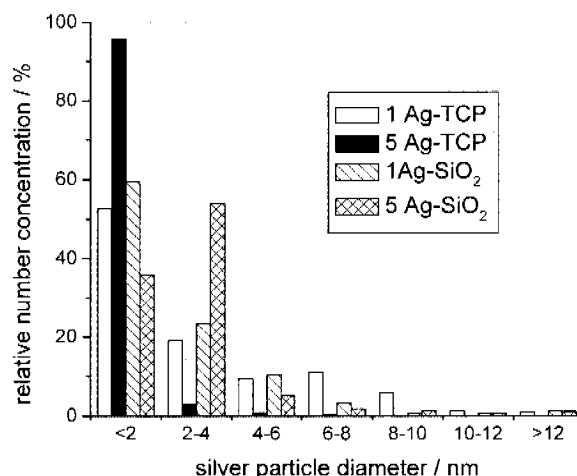


**Figure 6-4.** Counted relative number concentration of the silver particle size for Ag-TCP (1 Ag-TCP and 5 Ag-TCP) and Ag-SiO<sub>2</sub> powders (1 Ag-SiO<sub>2</sub> and 5Ag-SiO<sub>2</sub>). For low (1wt%) silver content the size of the silver particles are very similar whereas for high (5wt%) silver content a shift to smaller particles for TCP was observed. The size of the silver particles stays predominantly below 4 nm for all samples.

The size of the silver has a direct influence on the available silver surface and therefore the solubility which further determines the antimicrobial activity. Hence small silver particles excel over larger ones in term of silver ion release.

*Support and silver phase composition.* The phase composition of the powder was investigated by X-ray powder diffraction to further elaborate the presence of silver (Figure 6-5). For Ag-TCP samples no distinct silver peaks were observed for contents up to 5wt% silver which is in line with the silver particle size distribution of Ag-TCP samples (Figure 6-4). TCP samples containing 7.5wt% and 10wt% Ag clearly showed broad peaks specific for silver. The trend to larger particles for a silica carrier compared to a TCP support (Figure 6-4) was also observed by X-ray diffraction. Sample 5Ag-SiO<sub>2</sub> already had a distinct signal characteristic for metallic silver. No peaks were observed for Ionpure40 which corroborated the presence of ionic silver and the glassy matrix as specified by the manufacturer. The commercial high loaded silver-silica, HeiQ-Silver, in contrast showed distinct metallic silver peaks. It has to be noted that the signal of the HeiQ-Silver sample in Figure 6-5 was divided by a factor of five. This observation indicated the presence of far larger >100 nm silver particles than observed by TEM (Figure 6-3).

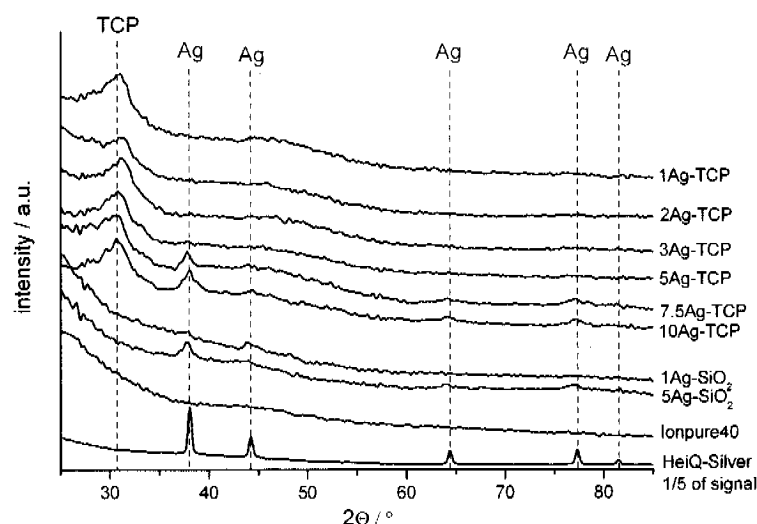


**Figure 6-5.** X-ray powder diffraction patterns of different flame-made Ag-TCP and Ag-SiO<sub>2</sub> samples in comparison to commercially available HeiQ-Silver and Ionpure40.

In a first antimicrobial test the activity of two flame-made particle samples (TCP and 5 Ag-TCP) was investigated by ASTM E2149-01 (Table 6-1) using a contact time of 2 hours with *E.coli* C43 (working bacterial concentration  $1 \times 10^5$  CFU/ml). 5 mg of powder was immersed in 8 ml of buffered working bacterial solution. The silver containing sample 5Ag-TCP showed a strong, nearly 4-log reduction after only two hours of exposure to the material. The pure TCP had only minor influence on the growth of the *E.coli* yielding half the CFU/ml compared to the reference.

### 6.3.2. Film characteristics

Since transparency is a market-defining factor for packaging materials or coatings in general, the UV-Vis spectra of different Ag-TCP films were recorded (Figure 6-6). Both 1Ag-TCP and 5Ag-TCP films showed high transmission of  $>50\%$  at wavelengths above 350 nm. Generally, the transmission decreases for increased silver content. An increasingly brownish coloration is observed optically by eye and also by UV-Vis measurements. This is expressed by the evolution of a distinct peak around 440 nm for films with 7.5Ag-TCP and 10Ag-TCP.

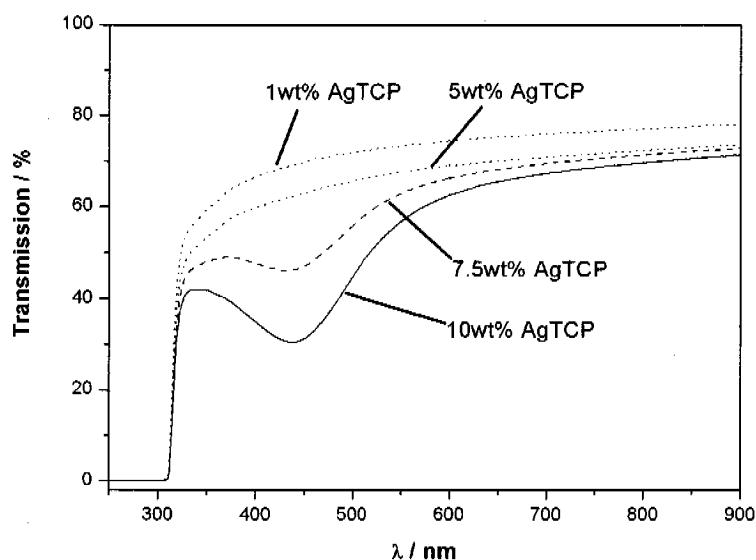


**Figure 6-6.** UV-Vis spectra of different Ag-TCP containing films with a thickness of  $\approx 10 \mu\text{m}$  showing high transmission in the visible range.



*Antimicrobial properties.* The same antimicrobial test as for the powders was conducted with two films containing 20wt% of the powder applying a contact time of 26 hours (Table 6-2). An area of 6 cm<sup>2</sup> film (corresponding to ≈15 mg powder for 10 μm coatings) was immersed in 8 ml of working bacterial solution. The film containing 5Ag-TCP powder showed a 6-log reduction which is exceptionally high for film materials. The film containing TCP only had no significant influence on bacterial growth (reduction approx. 26%).

**Table 6-2** *Antimicrobial activity as determined by ASTM E2149-01 using E.coli C43 (working bacterial concentration 1×10<sup>6</sup> CFU/ml)*

film sample	reduction after 26 h compared to the reference film/ %
TCP film	25.99
5Ag-TCP film	99.99993

In a third set of experiments different coatings were tested for their efficiency against *E.coli*, American Type Culture Collection (ATCC) No. 8739 with both testing methods ASTM E2149-01 and E2180-01 (Table 6-3). For ASTM E2149-01 two contact time points of 2h and 24h were chosen as to access short and long term effects. The film containing only TCP powder showed no change in bacteria concentration for both time points. The film containing 5Ag-TCP showed nearly a 6-log reduction after 24h whereas at time point 2h the reduction was not significantly changed. This suggests that the mechanism is not instantaneous but rather proceeds via a slow and steady bacteria destruction keeping in mind that for the reference film a 3-log CFU/ml increase was observed in the 24 hours experiment. Hence, the antimicrobial material has not only to struggle with the initial bacteria but also has to prevail over the bacteria's growth. For the static contact test ASTM E2180-01 the bacteria concentration for film sample containing TCP increased by a factor of ten compared to the reference. Again the addition of 5Ag-TCP to the film entailed a 5-log reduction.

**Table 6-3** Antimicrobial efficiency of different films as determined by a dynamic contact test (ASTM E2149-01) and a static test for hydrophilic materials (ASTM E2180-01)

film sample	reduction / % ASTM E2149-01, <i>E.coli</i> ATCC 8739		reduction / % ASTM E2180-01, <i>E.coli</i> ATCC 8739
	Contact time:	2h	24h
TCP film		14.29	-4.55
5Ag-TCP film		69.81	99.9998

Further investigation on film materials containing different Ag-TCP and Ag-SiO<sub>2</sub> samples were conducted by ASTM E2180-01. More specifically, *E.coli* (ATCC 8739) was used and tested with films containing 1 to 10 wt% silver-doped TCP and 1 and 5 wt% silica powders (Table 6-4). All silver-TCP films showed a significant activity resulting in a 3 to 6-log reduction. There is no trend in quality of performance as a function of silver content in the TCP powders. The high silver-loaded silica (5Ag-SiO<sub>2</sub>) reduced the *E.coli* by a factor of 10'000 (4-log reduction). Only around a ten fold reduction was observed for 1Ag-SiO<sub>2</sub> films. Although the morphology in terms of primary particle size and silver particle size of both 1Ag-TCP and 1Ag-SiO<sub>2</sub> are very similar the antimicrobial performance of 1Ag-TCP excels. One possible explanation might be the better bioavailability of the silver in Ag-TCP powders. While the silica matrix can not be affected by a biological environment the TCP support can be degraded. In case of silica the activity would be limited to the mere solubility of the silver particles. The high surface area of the finely dispersed silver nanoparticles enables reaching effective silver ion concentrations despite the low solubility of silver in water. In case of a non-persistent matrix (e.g. TCP) the microbes in the vicinity might also take up metal silver by degradation or dissolution of the TCP support.

If such a Trojan horse effect takes place a further advantage of such a mechanism might be the application of Ag-TCP in environments with high sulfur concentration. For systems with persistent carriers, silver ions would be literally disposed while forming silver-sulfur compounds such as silver sulfide which are even less water soluble than silver metal. As a result the silver concentration would decrease to ineffective or insufficiently effective concentrations.

**Table 6-4** Antimicrobial activity of different film materials against *E.coli* in ASTM E2180-01.

film sample	reduction / %	
	ASTM E2180-01, <i>E.coli</i> ATCC 8739, 24h	log reduction / -
1Ag-TCP film	99.993	4
2Ag-TCP film	99.9998	6
3Ag-TCP film	99.9998	6
5Ag-TCP film	99.998	5
7.5Ag-TCP film	99.9998	6
10Ag-TCP film	99.998	5
1Ag-SiO <sub>2</sub> -film	92	1
5Ag-SiO <sub>2</sub> -film	99.990	4

In a further set of antimicrobial experiments films containing the commercial products were compared to flame synthesized 5Ag-TCP (Table 6-5). The silver content in the coating was set to 1wt% for HeiQ-Silver and 5Ag-TCP samples where as Ionpure40 was incorporated at a weight ratio of 20% in the film. The test was conducted in duplicate by ASTM E2180-01 using *E.coli* (ATCC 8739) and a working bacterial concentration of  $3 \times 10^6$  CFU/ml. The coating containing TCP were far more efficient as reflected by averaged 5-log reduction film sample 5Ag-TCP. A maximal 2-log reduction was achieved by film sample HeiQ-Silver while the Ionpure40 film only reduced the bacteria up to 97%. The exceptionally high performance of Ag-TCP could be either attributed to the smaller silver particle size or the phosphate containing, degradable support material.

**Table 6-5** Antimicrobial activity of commercially available agents compared to present flame-made Ag-TCP against *E.coli* in ASTM E2180-01.

film sample	reduction / %	
	ASTM E2180-01, <i>E.coli</i> ATCC 8739, 24h	
	1. experiment	2. experiment
HeiQ-Silver film (10 µm dry)	99.4	97.3
Ionpure40 film (10 µm dry)	97.1	94.3
5Ag-TCP film (10 µm dry)	99.998	99.9996
5Ag-TCP film (2 µm dry)	99.96	99.94

In addition to the 10  $\mu\text{m}$  thick coatings a film having a thickness of only 2  $\mu\text{m}$  containing the same weight percentage of 5Ag-TCP (20wt% in dry film) was tested (Table 6-5). The application of a thinner coating is interesting in terms of final cost of the film since the amount of the antimicrobial agent is directly proportional to the coating thickness. The five times thinner coating reduced *E.coli* by a factor of up to 2500 compared to a factor of around 100'000 for the thick coating. The total amount of antimicrobial agent present seemed to be a very crucial parameter. Obviously, not only the surface located Ag-TCP plays an important role but also the silver in the bulk of the polymeric coating has major influence on the activity.

*Efficacy against pathogenic microorganisms.* The efficiency of the TCP containing films was further investigated for different, commonly occurring microorganisms (Table 6-6). The film containing 5Ag-TCP showed efficacy against *P.aeruginosa* and *C.albicans* with an exceptional 6 to 7-log reduction and a 4-log reduction, respectively. Both microbes were not influenced in contact with the TCP film (4% increase for *P.aeruginosa* and 18% reduction for *C.albicans*). Again the role of the silver as the active, deadly agent is confirmed.

**Table 6-6** Antimicrobial activity of Ag-TCP containing film materials against different microorganisms. Gram-negative (*P.aeruginosa*), Gram-positive (*S.aureus*) bacteria as well as for a yeast-like fungi (*C.albicans*) and fungi spores (*A.niger*) were tested.

microorganism	reduction / % ASTM E2180-01, 24h	
	TCP film	5Ag-TCP film
<i>P.aeruginosa</i> ATCC 9027	-4.00	99.99996
<i>S.aureus</i> ATCC 6538	-50.25	64.00
<i>C.albicans</i> ATCC 10231	17.45	99.994
<i>A.niger</i> spores ATCC 16404	36.36	13.05

The Gram-positive *S.aureus* was not significantly reduced (64%) by the silver containing film and only a slightly increased growth was observed for TCP films. *A.niger* in spore form was not reduced to reasonable degrees by either of the films (36% reduction for TCP film, 13% reduction for 5Ag-TCP film). So far, a high (3 to 7-log reduction) antimicrobial activity was observed for 5Ag-TCP containing films especially against Gram-

negative bacteria (*E.coli*, *P.aeruginosa*) and a yeast-like fungus (*C.albicans*). Microbes with a more robust defense mechanism such as Gram-positive *S.aureus* and the spore form of *A.niger* were far less affected.

## 6.4. Conclusions

Flame spray synthesis of silver-doped tricalcium phosphate (Ag-TCP) and silver-doped silica (Ag-SiO<sub>2</sub>) resulted in nanoparticles composed of <10 nm metallic silver particles deposited on the tricalcium phosphate or silica matrix, respectively. The incorporation of such materials in a hydrophobic silicone polymer resulted in highly efficient antimicrobial coatings. The Ag-TCP containing coatings excelled in efficacy against *E.coli* by a factor of 10-1000 compared to polymer/Ag-SiO<sub>2</sub> films. A comparison to commercially available silver-silica (HeiQ-Silver) and a silver ion containing glass powder (Ionpure40) further revealed the advantageous effect of Ag-TCP. HeiQ-Silver was 100-5000 less efficient against *E.coli* than Ag-TCP and Ionpure40 was even excelled by a factor of 1000-5000. The unprecedented efficacy of polymer/Ag-TCP coatings against *E.coli* might be attributed to the small silver particle size and the phosphate containing, degradable support material. It is suggested that the nutrition limiting bacteria might use TCP as a phosphate source but simultaneously taking up deadly silver particles. In addition the polymer/Ag-TCP films also showed high efficacy against Gram-negative *P.aeruginosa* and *C.albicans*. This observations suggest the use of Ag-TCP as a highly efficient antimicrobial agent in polymeric coatings for the use in sanitary, hospital facilities and the packaging of food and pharmaceuticals.

## 6.5. Acknowledgements

Financial support by the Swiss Commission for Technology and Innovation, CTI project 7021.2 is kindly acknowledged.

## 6.6. References

- [1] Brunner T J, Wick P, Manser P, Spohn P, Grass R N, Limbach L K, Bruinink A and Stark W J 2006 In vitro cytotoxicity of oxide nanoparticles: Comparison to asbestos, silica, and the effect of particle solubility *Environmental Science & Technology* **40** 4374-81
- [2] Limbach L K, Li Y C, Grass R N, Brunner T J, Hintermann M A, Muller M, Gunther D and Stark W J 2005 Oxide nanoparticle uptake in human lung fibroblasts: Effects of particle size, agglomeration, and diffusion at low concentrations *Environmental Science & Technology* **39** 9370-76
- [3] Brunner T J, Bohner M, Dora C, Gerber C and Stark W J 2007 Comparison of amorphous TCP nanoparticles to micron-sized alpha-TCP as starting material for calcium phosphate cements *J Biomed Mater Res B* accepted
- [4] Loher S, Reboul V, Brunner T J, Simonet M, Dora C, Neuenschwander P and Stark W J 2006 Improved degradation and bioactivity of amorphous aerosol derived tricalcium phosphate nanoparticles in poly(lactide-co-glycolide) *Nanotechnology* **17** 2054-61
- [5] Loher S, Stark W J, Maciejewski M, Baiker A, Pratsinis S E, Reichardt D, Maspero F, Krumeich F and Gunther D 2005 Fluoro-apatite and calcium phosphate nanoparticles by flame synthesis *Chem. Mat.* **17** 36-42
- [6] Madler L, Kammler H K, Mueller R and Pratsinis S E 2002 Controlled synthesis of nanostructured particles by flame spray pyrolysis *J. Aerosol. Sci.* **33** 369-89
- [7] Stark W J, Pratsinis S E, Maciejewski M, Loher S and Baiker A 2005 *Flame synthesis of metal salt nanoparticles, in particular calcium and phosphate comprising nanoparticles* patent WO2005/087660 A1
- [8] Pratsinis S E 1998 Flame aerosol synthesis of ceramic powders *Prog. Energy Combust. Sci.* **24** 197-219
- [9] Staiger M, Bowen P, Ketterer J and Bohonek J 2002 Particle size distribution measurement and assessment of agglomeration of commercial nanosized ceramic particles *J. Dispersion Sci. Technol.* **23** 619-30

## 7. Research Recommendations & Outlook

This work has provided a basis for the introduction of complex physical properties derived from fluid dynamics and has shown how chemical functionality can be implemented into existing polymer processing, especially polymer films.

### 7.1. Further application fields of micro-structured coatings

The availability of micro-structured coatings on a large scale opens possibilities for the use in other technically most important applications. Further investigation could be done to evaluate self-cleaning properties of such micro-patterned surfaces. It has been observed that micron-sized patterning, if suitable, implies a self-cleaning effect [1, 2]. Further, the so-called lotus effect [3-5] has been previously attributed to a combination of surface hydrophobicity and geometric features in the nanometer and micrometer scale.

Investigations on the surface morphology of the present structured coatings by confocal profilometry (CP) and atomic force microscopy (AFM) revealed not only the presence of micro-sized structures (CP image, Figure 7-1) but also features in the nanometer range (AFM image, Figure 7-2). These nano-features arise most likely from the incorporated silica particles. More distinct nano-structuring could be achieved by the implementation of larger amounts of silica or silica with altered morphology as commercially available. Care has to be taken to keep similar rheological properties since structuring and preservation of the structure during the roll coating process is determined by the polymer precursor rheology. The self-cleaning properties of such modified coatings could be accessed by the measurement of the water contact angle. A successful development of a self-cleaning coating would be most relevant to industry. While current methods to introduce self-cleaning or superhydrophobic surface properties are limited in terms of availability or cost of the materials the present method would allow for low-cost large area production.

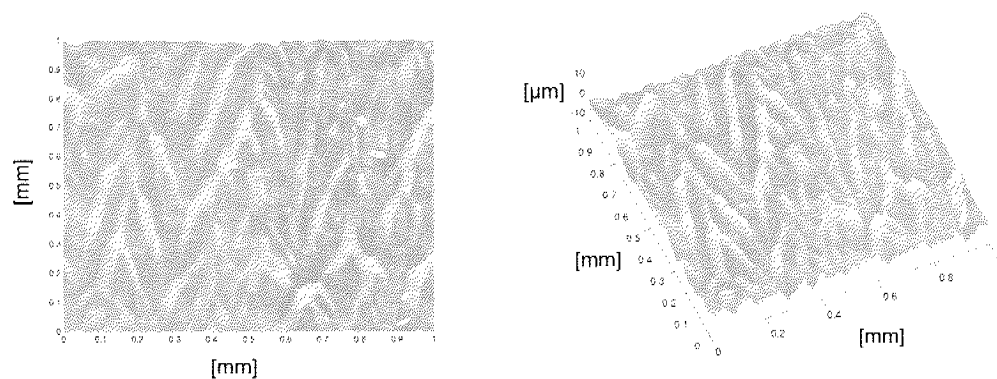


**Figure 7-1.** Profilometry of a micro-structured silica/poly(dimethylsiloxane) coating.

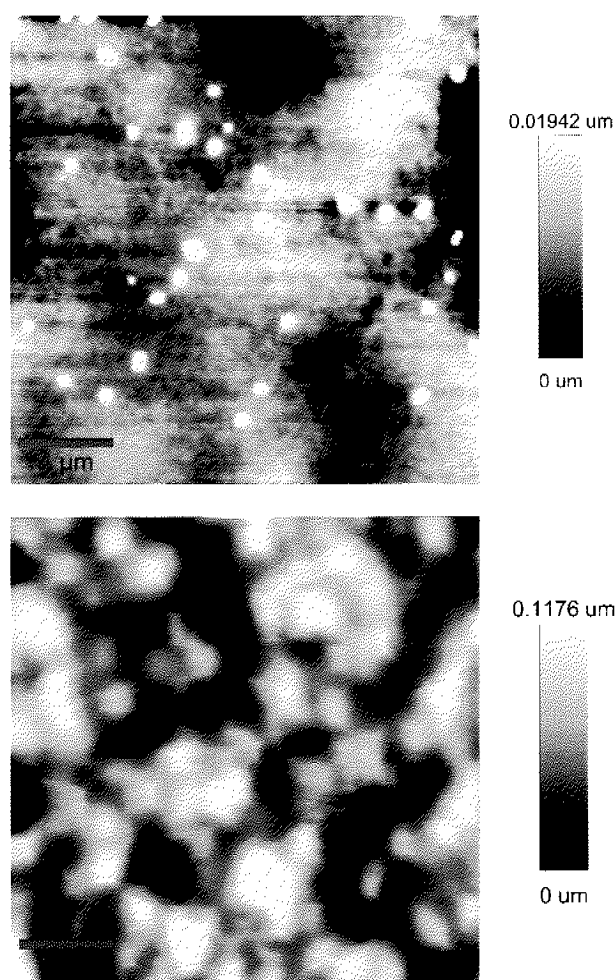


**Figure 7-2.** Atomic force microscopy images of smooth reference poly(dimethylsiloxane) (top) and nano-featured silica/ poly(dimethylsiloxane) composite (bottom).



A second field of application for discussed micro-structured surfaces covers the reduction of the coefficient of friction. Structures as observed for instance on the skin of a shark reduce near wall drag forces and might result in a drag reduction of up to 9% [6-8]. The readily available micro-structured films could be used for fluid dynamical experiments on laboratory models or even on a large scale set-up.

- [1] Furstner R, Barthlott W, Neinhuis C and Walzel P 2005 Wetting and self-cleaning properties of artificial superhydrophobic surfaces *Langmuir* **21** 956-61
- [2] Otten A and Herminghaus S 2004 How plants keep dry: A physicist's point of view *Langmuir* **20** 2405-08
- [3] Barthlott W and Neinhuis C 1997 Purity of the sacred lotus, or escape from contamination in biological surfaces *Planta* **202** 1-8
- [4] Onda T, Shibuichi S, Satoh N and Tsujii K 1996 Super-water-repellent fractal surfaces *Langmuir* **12** 2125-27
- [5] Neinhuis C and Barthlott W 1997 Characterization and distribution of water-repellent, self-cleaning plant surfaces *Ann. Bot.* **79** 667-77
- [6] Bechert D W and Bartenwerfer M 1989 The Viscous-Flow on Surfaces with Longitudinal Ribs *Journal of Fluid Mechanics* **206** 105-29
- [7] Bechert D W, Bruse M and Hage W 2000 Experiments with three-dimensional riblets as an idealized model of shark skin *Exp. Fluids* **28** 403-12
- [8] Bechert D W, Bruse M, Hage W and Meyer R 2000 Fluid mechanics of biological surfaces and their technological application *Naturwissenschaften* **87** 157-71

## 7.2. Flame-made calcium phosphates for the preparation of polymeric nanocomposite biomaterials

The use of calcium phosphate nanoparticles in degradable polymers has proven very useful in terms of biomineralization. Besides rigid film materials (chapter 3) or flexible cotton wool-like composites (chapter 4) other morphologies such as foams could be evaluated. The versatility of the flame spray synthesis would also allow incorporating other physiological cations, such as magnesium or zinc, into the calcium phosphate lattice. It has previously been postulated that such materials may be able to induce bone formation [1, 2].

The implantation of bone substitute materials often entails post-infections and inflammations which inhibit the recovery or even give rise to a second surgery for removal of the implant [3]. Such infections are very painful and costly for the patient. In dentistry, many indications, such as a pocket after tooth extraction, require the regeneration of bone [4]. In chapter 4 a cotton wool-like nanocomposite is discussed which might be used for such

regeneration. The enhanced biomineralization could accelerate bone formation and therefore shorten recovery time. However, the risk of an infection in oral operation sites is very high as the wound is continuously subjected to the environment and bacterial contamination. Using a silver-doped calcium phosphate in combination with a degradable polymer might be helpful to tackle the demanding task.

The incorporation of silver-doped calcium phosphate nanoparticles in degradable polymers would allow for a combination of biomineralization and antimicrobial efficacy. Fine-tuning of silver content would help avoiding cytotoxic effects while still providing the desired antimicrobial properties.

- [1] Ito A, et al. 2002 Zinc-releasing calcium phosphate for stimulating bone formation *Mater. Sci. Eng. C-Biomimetic Supramol. Syst.* **22** 21-25
- [2] Sun H L, Wu C T, Dai K R, Chang J and Tang T T 2006 Proliferation and osteoblastic differentiation of human bone marrow-derived stromal cells on akermanite-bioactive ceramics *Biomaterials* **27** 5651-57
- [3] Halpern L R and Dodson T B 2007 Does prophylactic administration of systemic antibiotics prevent postoperative inflammatory complications after third molar surgery? *J. Oral Maxillofac. Surg.* **65** 177-85
- [4] Thoma K, Pajarola G F, Gratz K W and Schmidlin P R 2006 Bioabsorbable root analogue for closure of oroantral communications after tooth extraction: A prospective case-cohort study *Oral Surg. Oral Med. Oral Pathol. Oral Radiol. Endod.* **101** 558-64

## Curriculum Vitae

### Stefan Loher

Functional Materials Laboratory  
Wolfgang Pauli Strasse 10  
ETH Hönggerberg, HCI E 113  
CH-8093 Zurich  
Switzerland  
Tel: ++41 44 633 62 57  
stefan.loher@chem.ethz.ch

private address:  
Agerstenweg 8  
CH-9462 Montlingen  
Switzerland

---

#### Personal Data

Date of Birth	10.07.1979
Place of Birth	Oberriet - Montlingen SG, Switzerland
Nationality	Swiss
Marital Status	Single Male

---

#### Publications

1. Loher S, Stark W J, Maciejewski M, Baiker A, Pratsinis S E, Reichardt D, Maspero F, Krumeich F and Gunther D 2005 Fluoro-apatite and calcium phosphate nanoparticles by flame synthesis **Chem. Mater.** 17 36-42
2. Loher S, Reboul V, Brunner T J, Simonet M, Dora C, Neuenschwander P and Stark W J 2006 Improved degradation and bioactivity of amorphous aerosol derived tricalcium phosphate nanoparticles in poly(lactide-co-glycolide) **Nanotechnology** 17 2054-61
3. Loher S, Stark W J, Maienfisch T, Bokorny S and Grimm W 2006 Rapid production of micropatterned surfaces using a fluid dynamical instability **Polym. Eng. Sci.** 46 1541-47
4. Huber M, Stark W J, Loher S, Maciejewski M, Krumeich F and Baiker A 2005 Flame synthesis of calcium carbonate nanoparticles **Chem. Commun.** 5 648-50
5. Osterwalder N, Loher S, Grass R N, Brunner T J, Limbach L K, Halim S C and Stark W J 2007 Preparation of nano-gypsum from anhydrite nanoparticles: Strongly increased Vickers hardness and formation of calcium sulfate nano-needles **J. Nanopart. Res.** 9 275-81
6. Luechinger N A, Loher S, Athanassiou E K, Grass R N and Stark W J 2007 Highly sensitive optical detection of humidity based on liquid condensation on nano-particulate metal films **Langmuir** 23 3473-77
7. Hotz N, Stutz M J, Loher S, Stark W J, Poulidakos D 2007 Syngas production from butane using a flame-made Rh/Ce<sub>0.5</sub>Zr<sub>0.5</sub>O<sub>2</sub> catalyst *accepted for publication in* **Appl. Catal. B-Environ.**
8. Schneider O D, Loher S, Brunner T J, Uebersax L, Simonet M, Grass R N, Merkle H P and Stark W J 2007 Cotton wool-like nanocomposite biomaterials: *In vitro* bioactivity and osteogenic differentiation of human mesenchymal stem cells, *accepted for publication in* **J. Biomed. Mater. Res. Part B**

## Patents

1. Stark W J, Pratsinis S E, Maciejewski M, Loher S and Baiker A 2005 *Flame synthesis of metal salt nanoparticles, in particular calcium and phosphate comprising nanoparticles* patent WO2005/087660 A1
  2. Loher S and Stark W J 2005 *Method for the application of a structured coating upon a smooth surface* PCT patent application
  3. Stark W J, Schneider O D, Loher S, Brunner T J, Simonet M, Grass R N and Schmidlin P R 2006 *Implant material* PCT patent application
  4. Loher S and Stark W J 2007 *Catalytically active coatings for the absorption of gaseous reactants* PCT patent application
  5. Loher S, Stark W J, Schneider O D and Bokorny S 2007 *Antimicrobial material* PCT patent application
- 

## Education

- PhD in Chemical- and Bioengineering, ETH Zurich, Switzerland** 04.04 – 04.07
- “Physical and chemical functionalization of polymers” advisor Prof. W. J. Stark, 3 patents, 1 commercial product
- Master of Science in Mechanical Engineering, ETH Zurich, Switzerland** 10.99 – 02.04
- *Master thesis:* Fluoroapatite and calcium phosphate nanoparticles by flame synthesis, published in *Chemistry of Materials*, patent application.
  - *Semester theses:*
    - Flame-made zirconia/silica nanoparticles and their catalytic performance in glycol synthesis
    - Introduction and validation of a dynamic hydrogen reference electrode in a direct methanol fuel cell
  - Major subjects:
    - Mechanical process engineering and particle technology
    - Renewable energies
  - Optional subjects: Accounting for Managers, Profitability and Solvency I and II, Introduction in Spanish language and culture I, Ecodesign
- 

## Teaching

- Lecture „Chemical engineering“, professorship W. J. Stark** 2004-2005
- Teaching assistant, summer 2004 and 2005.
- Supervised Master theses:**
- Oliver Schneider (Chemical engineering): Cotton wool-like biomaterials 03.06-06.06
  - Valentine Reboul (Chemistry, Paris): Bioactivity of degradable polymers with ultra-fine calcium phosphate fillers 07.04-04.05
- Supervised Semester theses:**
- Norman Luechinger (Materials science): Carbon/copper nanoparticles and the application in conductive paints, nanofluids and in polymers for the application in humidity sensing 10.06-11.06
  - Stephanie Streather (Chemical engineering): Influence of silica and titania doped silica on mechanical properties of polyurethane 02.05

- Samuel Halim (Materials science): Nanoparticle synthesis of ceria based oxides for fuel cell applications 02.04-04.04

#### Student supervision (scientific assistant)

- Oliver Schneider (Chemical engineering): Electrospinning of nanocomposites and polymer-based compositions with antimicrobial effect 12.06-04.07
- Norman Luechinger (Materials science): Carbon/copper nanoparticles in swellable polymers 10.06-11.06
- Roland Fuhrer (Chemical engineering): Nanoporous polymers 04.06-07.06
- Stephanie Streather (Chemical engineering): Titania/silica nanoparticles in polar polymers 03.05-06.05
- Matthias Huber (Chemical engineering): Flame synthesis of calcium carbonate nanoparticles 03.04-05.04

#### Internships

- Jansen AG, 9463 Oberriet, Switzerland: Basics of mechanical metal processing 11.99-12.99
- ETH Zurich, 8092 Zurich: Scientific assistant, Flame synthesis of nanoparticles 07.02-08.02
- National Technical University of Athens, Greece: „Experimental, numerical and theoretical investigation on pressurized pulverized coal combustion“ 09.02-10.02

#### Conference Presentations and Proceedings

1. Loher S, Brunner T J and Stark W J *Fluoro-apatite and Calcium Phosphate Nanoparticles by Flame Spray Synthesis* (poster), Swiss Society for Biomedical Engineering Annual Meeting 2005, Sept 1-2, EPFL Lausanne.
2. Brunner T J, Loher S and Stark W J *Fluoro-apatite and Calcium Phosphate Nanoparticles by Flame Spray Synthesis* (poster), 1<sup>st</sup> Empa PhD Symposium, 2005, Oct 20, Empa Dubendorf, Switzerland
3. Loher S, Huber M and Stark W J *Biodegradable, nanoparticulate polymer fillers*, AIChE Annual Meeting 2005, Oct 30 –Nov 4, Cincinnati, OH, USA
4. Brunner T J, Loher S and Stark W J *Tricalcium Phosphate and Fluoroapatite Nanoparticles for Medical Implants*, AIChE Annual Meeting 2005, Oct 30 –Nov 4, Cincinnati, OH, USA
5. Brunner T J, Loher S and Stark W J *Nanoparticulate Biomaterials by Flame Synthesis*, GRIBOI-16th Interdisciplinary Research Conference on Biomaterials 2006, March 16-18, Berne, Switzerland
6. Loher S and Stark W J, *Rapid production of micro-structured surfaces using a fluid dynamical instability*, 1<sup>st</sup> European Chemistry Congress, 2006, Aug. 27-31, Budapest, Hungary
7. Loher S and Stark W J, *High-speed micro-patterning of polymer films driven by a fluid dynamical instability* (poster), SCS Fall Meeting 2006, Sept. 13, Zurich, Switzerland
8. Loher S and Stark W J, *High-speed microstructuring of polymer films driven by a fluid dynamical instability*, AIChE Annual Meeting 2006, Nov. 12-17, San Francisco, CA, USA
9. Loher S, Schneider O D, Schmidlin P R and Stark W J, *Electrospinning of novel tricalcium phosphate /poly(lactide-co-glycolide) nanocomposites for repair of bone defects*, AIChE Annual Meeting 2006, San Francisco, Nov. 12-17, CA, USA

10. Osterwalder N, Loher S, Grass R N, Brunner T J, Halim S C, Limbach L K and Stark W J, *Preparation of Nano-Gypsum from Anhydrite Nanoparticles: Strongly Increased Vickers Hardness and Formation of Calcium Sulfate Nano-Needles*, AIChE Annual Meeting 2006, San Francisco, Nov. 12-17, CA, USA
  11. Loher S, Maienfisch T, Grimm W, Bokorny S and Stark W J, *High-speed micro-patterning of polymer films driven by a fluid dynamical instability*, Partec 2007, March 27-29, Nuremberg, Germany
  12. Brunner T J, Loher S, Grass R N and Stark W J, *Nanoparticulate Biomaterials by Flame Synthesis*, Partec 2007, March 27-29, Nuremberg, Germany
  13. Osterwalder N, Loher S, Grass R N, Brunner T J, Halim S C, Limbach L K and Stark W J, *Preparation of Nano-Gypsum from Anhydrite Nanoparticles: Strongly Increased Vickers Hardness and Formation of Calcium Sulfate Nano-Needles* (poster), Partec 2007, March 27-29, Nuremberg, Germany
  14. Luechinger N A, Loher S, Athanassiou E K, Grass R N and Stark W J, *Optical humidity sensing on polymer/metal nanoparticle hybrid films* (poster), Partec 2007, March 27-29, Nuremberg, Germany
  15. Schneider O D, Loher S, Brunner T J, Uebersax L, Simonet M, Grass R N, Merkle H P and Stark W J *In vitro bioactivity and osteogenic differentiation of human mesenchymal stem cells* (poster), Partec 2007, March 27-29, Nuremberg, Germany
- 

## **Related Skills:**

### **Software**

General	Microsoft Office, Matlab
Design	Unigraphics (CAD)
Programming language	C (basic knowledge)

### **Languages**

German	native language
English	fluent
French	basic knowledge
Spanish	basic knowledge